Synthesis, Characterization and Process Parameter Optimization of Alumina Ceramic (Al_2O_3) Nanoparticles

Moges Kiros Meresa

A Thesis Submitted to Department of Mechanical Engineering,

College of Mechanical, Chemical and Materials Engineering.

Presented in Partial Fulfillment of the Requirement for the Degree of Master's in Manufacturing Engineering

School of Post Graduate Studies

Adama Science and Technology University

June, 2025

Adama, Ethiopia

Synthesis, Characterization and Process Parameter Optimization of Alumina Ceramic (Al_2O_3) Nanoparticles

Moges Kiros Meresa

Advisor:

Dr. Esmael Adem

A Thesis Submitted to Department of Mechanical Engineering,

College of Mechanical, Chemical and Materials Engineering.

Presented in Partial Fulfillment of the Requirement for the Degree of Master's in Manufacturing Engineering

School of Post Graduate Studies

Adama Science and Technology University

June, 2025

Adama, Ethiopia

DECLARATION

I hereby declare that this Master's Thesis entitled "synthesis, characterization, and process parameter optimization for alumina ceramic (Al_2O_3) nanoparticles" is my original work. That is, it has not been submitted for the award of any academic degree, diploma, or certificate in any other university. All sources of materials that were used for this thesis have been duly acknowledged through citation.

Name of the student	Signature	Date

Recommendation

I, the advisor of this thesis, hereby certify that I have read the revised version of the thesis entitled “synthesis, characterization, and process parameter optimization of alumina ceramic **(Al_2O_3)** nanoparticles” prepared under my guidance by Moges Kiros Meresa submitted in partial fulfillment of the requirements for the degree of Mater’s of Science in Manufacturing Engineering. Therefore, I recommend the submission of revised version of the thesis to the department following the applicable procedures.

_____ _____ _____

Major Advisor Signature Date

Originality Declaration Form for Students

This form must be completed and signed for all works submitted to the University for Examination.

Name of Student	Moges Kiros Meresa
ID No .	PGR/35839/16
Department	Mechanical Engineering
College	CoMCME
Course title	M.Sc. Thesis
Tittle of the work	Synthesis, Characterization and Process Parameter Optimization of Alumina Ceramic (Al_2O_3) Nanoparticles
Date of submission	21/5/2025

Declarations

1. I understand what plagiarism is and I am aware of the university's policy in this regard.
2. I declare that this Synthesis, Characterization and Process Parameter Optimization of Alumina Ceramic (Al_2O_3) Nanoparticles research project is my original work and has not been submitted elsewhere for examination or award of a degree or publication. Wherever other's work or my own work has been utilized, it has been duly acknowledged and referenced in compliance with the university's requirements.
3. I have not sought or used the service of any professional agencies to produce this work.
4. I have not permitted, nor will permit, anyone to plagiarize my work with the intention of presenting it as their own.
5. I am aware that making any false claims regarding this work will lead to disciplinary action in accordance with the university's anti-Plagiarism Guidance's.

Signature _____

Date _____

Approval Page of M.Sc. Thesis

I the advisor of the thesis entitled "synthesis, characterization, and process parameter optimization for alumina ceramic (Al_2O_3) nanoparticles" and developed by Moges Kiros Meresa; hereby certify that the recommendation and suggestions made by the board of examiners are appropriately incorporated into the final version of the thesis.

Major Advisor	Signature	Date

We, the undersigned, members of the Board of Reviewers of the thesis open defense by Moges Kiros Meresa have read and evaluated the thesis proposal entitled "synthesis, characterization, and process parameter optimization for alumina ceramic (Al_2O_3) nanoparticles" and assessed the understanding of the candidate about the research. This is, therefore, to certify that the thesis is accepted and we recommend the implementation of the proposal.

Chairperson	Signature	Date
Internal Examiner	Signature	Date
Desalegn Wogaso (PhD)		.
External Examiner	Signature	Date

Final approval and acceptance of the thesis is contingent upon submission of its final copy to the School of Postgraduate Studies (SPGS) through the Department Graduate Council (DGC) and College Graduate Committee (CGC).

Department Head	Signature	Date
College Dean	Signature	Date
School of Postgraduate Studies, Dean	Signature	Date

ACKNOWLEDGMENT

First and foremost, I would like to express my deepest gratitude to the Almighty God for the limitless blessing throughout the process of doing this thesis. Following that, I am eternally grateful to my advisor, Dr. Esmael Adem for their priceless support and mentorship. His insightful guidance, and constructive criticism have been instrumental in shaping the thesis. I would like to extend my heartfelt thanks to my respected friends for their unwavering encouragement and support. Finally, I am deeply indebted to all those who have contributed in any way both directly or indirectly to the completion of this research work. Despite their contributions small, it has been essential in making it came to complete. All in all, I am truly blessed to have such supportive network of individuals in this journey, since their contribution have made this work possible and I am eternally grateful and respectful for their unlimited support.

Table of contents

Contents page

This research is funded by Adama Science and Technology University under the grant number ASTU/SM-R/1097/25 .....**Error! Bookmark not defined.**

LIST OF TABLES

Table Page

LIST OF FIGURES

FUGERE PAGE

List of Acronyms and Abbreviations

AFM=Atomic force microscopy

ANOVA= Analysis of variance

ANPs= alumina nanoparticles

BET=Brunaner Emmett teller

DOE=Design of experiment

EDS= Energy dispersive x-ray spectroscopy

FESEM=Field emission scanning electron microscope

FTIR=Fourier transformation infrared

FWHM= Full width half maximum

HAP= Hydroxyapatite

NPs =Nanoparticles

PEG=Polyethylene glycol

PLCR=Permanent linear change in refractory

PSDS=Particle size distribution

SAED=Selected area electron diffraction

SEM= scanning electron microscopy

SSA=Specific surface area

SSR=Solid state reaction

TAB=Triethylammonium bromide

TGA= Thermogravimetry Analysis

UV= Ultraviolet

XRD =X ray diffraction

XRPD=X-ray powder diffraction

Abstract

Nanoparticles, especially alumina ceramics, are widely used due to their versatile applications, but there is still limited understanding of how various processing parameters together influence its properties. This research investigated that the effect of process parameters and their combined interplay on the thermal stability and crystallite size of alumina ceramic. Aluminum oxide (alumina) was synthesized using the well-known bottom-up technique Sol-gel method. An L_9 orthogonal array was used to design the experiment. Optimization of the three process parameters in their three levels with single and multi-response analyses was conducted. XRD characterization revealed phase and crystallite size details, TGA provided the mass loss of the nine samples and its morphology and elemental composition by SEM and EDS. The different phases obtained from XRD results were α, Θ, δ, and γ with their corresponding crystallite size (20.6nm,6.5nm, 5.8nm, 8nm, 6.9nm, 5.2nm, 26.5nm, 8.6nm, and 6.5nm) respectively for all nine samples. The TGA characterization also delivered a significant insight about to thermal stability of each sample through its mass loss (5.70%, 5.40%, 4.90%, 6.00%, 5.50%, 5.00%, 6.53%, 5.60%, and 5.30% respectively*). And, the SEM results also validate the significant difference of the particle size. the elemental composition was identified as aluminum and oxygen with no significant impurities. The optimized results which are obtained from the characterization showed a very promising results to see the optimal synthesis process and studied the complex interplay of different process parameters. Confirmation experiment was done. However, further validation through confirmation experiment and consideration of additional process parameters is highly recommended for a better result by improving the synthesis process.*

Keywords: *Alumina nanoparticles, Characterization, Sol-gel method, SEM, XRD, TGA, optimization*

CHAPTER ONE

INTRODUCTION

1.1Background

Metals are widely regarded as the most important categories of engineering materials, but it's worth noting that ceramic materials are actually more abundant and commonly used. The significance of ceramics in engineering stems from their natural abundance and distinct mechanical and physical properties, that differ by far from those of metals. A ceramic material is an inorganic compound composed of a metal (or semimetal) and one or more nonmetals. Key examples of ceramic materials include silica (silicon dioxide, SiO2), a primary component in most glass products; alumina (aluminum oxide, Al2O3), which has applications ranging from abrasives and high temperature to artificial bones.

(Madfa et al., 2014).Among the target spun materials, alumina (Al_2O_3) has received great attention once it is an important engineering material with high strength and elastic modulus, chemical stability and low thermal conductivity. Alumina has several polymorphs namely α, γ, θ, η, δ, χ, κ, and β-Al2 O3 and the alpha phase is the most thermodynamically stable based on (Mota et al., 2019).

According to (Rogojan et al., 2011) various techniques are currently used to produce and synthesize nanoparticles, including the sol-gel method (a solution-based approach), vapor phase deposition, mechanical alloying (involving collisions with high-energy pellets), solid-state reactions, hydrothermal methods, plasma techniques, and electrochemical methods, among others. While all these methods can produce large quantities of nanomaterials, the sol-gel method is particularly popular and widely used in industrial applications. This method stands out due to its ability to produce high-quality nanoparticles of uniform size on an industrial scale. Additionally, the sol-gel method can simultaneously produce two or more types of nanoparticles, allowing for the synthesis of alloy products in a single step by combining metal (or metal oxide) precursors in specific ratios. Moreover, the sol-gel method enables the production of highly homogeneous composites with exceptional purity (99.99%).

Additionally, the sol-gel process is one of the bottom-up synthesis technique, where the final products are created through a series of irreversible or one directional chemical reactions as Bokov et al., (2021) studied.

Despite the fact that extensive studies have been done on the synthesis of alumina nanoparticles, there remains a significant gap in understanding how multiple process parameters collectively affect the morphology, thermal stability, and overall properties of the resulting ceramic nanoparticles. Current limitations include a narrow focus, single or limited objectives, and a lack of optimization, as well as the absence of comprehensive modeling or design of experiments. These factors hinder the effective and efficient production of alumina nanoparticles with desired properties. Addressing these limitations through multi-parameter, multi-objective optimization, combined with a thorough design of experiments and statistical analysis, greatly enhanced the synthesis process as per the study by Krishnan et al., (2018) and Rogojan et al., (2011)

Based on (Rogojan et al., 2011) using the sol gel method of synthesis, the alumina nanoparticle was synthesized based on the design of experiment of Taguchi L9 orthogonal array. Based on the design of experiment nine samples is synthesized and characterized then investigated the effect of process parameter on the morphology of each sample, the phase of alumina ceramic of each sample, the effect of process parameter on the thermal stability of each sample, and determined the new compound formed as the result of the process in each sample as well as the dominating factor of the process parameter and recommended the optimum process parameters. **Morphological analysis:** The morphology of the synthesized nanoparticle from each experimental combination was analyzed using SEM to determine particle size, shape, and distribution. **Thermal stability analysis:** This analysis was conducted to determine the thermal stability of the nanoparticles using TGA to assess their weight loss and decomposition behavior at elevated temperatures for each sample. **Structural analysis**: In this analysis, crystal structure, constituent element, and phase of the nanoparticles of each sample will be analyzed using XRD according to Leng and Wiley (n.d., 2008)

1.2 Problem statement

Nanoparticles have emerged as crucial components in various field. The ongoing research and development are expected to further expand the scope and the impact by harnessing the potential of nanoparticle. Despite extensive research on alumina ceramics synthesis, a significant gap exists in understanding the general impact of multiple process parameters on the morphology (particle size and shape), thermal stability (mass loss and the decomposition process), and other properties of the resulting ceramic nanoparticles. As a consequence, the current research has different limitations in different aspects. Limited scope: Most studies focus on a single process parameter i.e. either in calcination temperature, comparing the different synthesize method, or different precursor material by neglecting the complexity and combined effect of multiple variables as per the study by Krishnan et al., (2018) and Rogojan et al., (2011). Single and/or narrow objective and lack of optimization: the existing studies primarily comparing for a narrow and/or single outcome, but overlooking the potential for multi objective optimization to achieve a balance between desirable properties. Lack of comprehensive modeling or design of experiment: Such design of experiment represents the complex interaction between process parameters and their impact an alumina by identifying the dominating parameter on its property. Therefore, this limitation had hindered the effectiveness and efficiency of synthesis alumina nanoparticle with the desired property. So, addressing this limitation through multi parameter, multi objective optimization, coupled with comprehensive design of experiment and statical analysis provided the potential to significantly optimize the alumina nanoparticle synthesis.

1.3 Objective

1.3.1 General objective;

- To synthesize, characterize, and optimize the process parameters (precursor materials, calcination temperature, and time) of alumina ceramic (Al_2O_3) nanoparticles

1.3.2 Specific objective;

1. To investigate the effect of precursor materials, calcination temperature, and calcination time on the morphology (crystallite size and shape) of each sample of alumina ceramic nanoparticles

2. To investigate the effect of precursor materials, calcination temperature, and calcination time on the thermal stability (mass loss) of each sample of alumina ceramic nanoparticles
3. Optimization of the process parameters to investigate the combined effect and the dominant factor on crystallite size and thermal analysis of alumina ceramic

1.4 Significance of the study

This study played an important role in filling the gab that is found from the literature review. The current research on alumina nanoparticle synthesis primarily focuses on isolated factors like calcination temperature or synthesis method by neglecting the complex interplay of various process parameters. This limited understanding had hindered the general optimization and prevented us from fully grasping how different parameters impact the final properties of alumina ceramic. By addressing this gap, it significantly improved the efficiency and effectiveness of the synthesis of nanoparticles and lead to a deeper understanding of combined effects of process parameters on the properties of alumina nanoparticles. By implementing a Taguchi design of experiment this study provided an opportunity to efficiently and effectively investigate the influence of multiple process parameters on the properties of synthesized alumina nanoparticle leading to a robust and optimized synthesis process. As well as, interpretation of the outcomes of the experiment contributed to a deeper understanding of the alumina nanoparticles synthesis process and lead to the development of a robust and efficient strategy for producing high quality materials with tailored properties.

1.5 Delimitation and limitations

Studies has focused heavily on synthesis and characterization of nanoparticles in order to achieve optimum property possible. However, the review highlighted a significant research gap regarding the optimization in synthesis and characterization of alumina. As a result, this research delimited by focusing on the systematic investigation of multiple process parameters and multiple objective optimizations of key sol-gel process parameters influencing the morphology, thermal stability and overall properties of alumina nanoparticles. While acknowledging the broad scope of alumina ceramics research, this study specifically concentrated on the combined effect of type of precursor, calcination time, and calcination temperature within the Sol-gel method.

It's acknowledged that other potentially influential factors, such as the pH level, the stirring speed and time, drying temperature and time, solvent type, and different synthesis routes. However, for the sake of achieving a manageable scope and in-depth analysis these are excluded. Furthermore, the properties under investigation were basically bound to particle size, particle shape, phase of the synthesized particles, particle distribution and weight loss with this both particle size and weight loss are used for optimization as a response. Finally, the research utilized a design of experiments (DoE) methodology and systematically explored the combined interplay of the parameters on the propriety of alumina on the selected properties and this focused approach addressed the identified gab in the existing literature. While computational modeling may complement the experimental findings, it was not the primary focus of this study. The synthesis process was challenging due to insufficient equipment and materials. This limitation is expected to have an effect on the properties of the synthesized nanoparticles and its purity. Besides of the synthesis process, the characterization was also challenging to get in time and all the equipment in need wasn't available.

1.6 Scope

In this particular research the alumina ceramic nanoparticle was synthesized, characterized and optimized the process parameter according to the design of experiment using Sol gel method. The process parameters considered in this thesis are; precursor material, calcination temperature and calcination time with three level of each parameter. The properties that selected and investigated in this study was; Morphological analysis: The morphology of the synthesized nanoparticles was analyzed using SEM. The thermal stability of the nanoparticles analyzed using TGA to assess their weight loss at elevated temperatures for each sample, and in the crystallite size, constituent element, and phase of the nanoparticles of each sample was analyzed using XRD. The data that obtained from the experiment was analyzed in order to optimize the process parameter.

1.7 organization of the study

This research is structured to provide a comprehensive investigation on synthesis, characterization, and process parameter optimization of alumina nanoparticles in to five distinct chapters, the study begins with an introduction that establishes the research context which outlines the background, problem of the statement, objective, significance of the study, delimitation and limitations, and the scope of the study. The second chapter presented a literature review to assess the existing knowledge and identify the gap in the current understanding of the research topic. Chapter three deals with the materials and the methodology employed which describes the synthesis process, techniques of characterization, optimization method and interpretation. In the fourth chapter, the findings and discussion present the result obtained from the analysis, interpreting their significance and implication in relation to the research objective and the previous studies. This structured approach ensures a logical progression of ideas which is supported by scientific approach and insightful exploration of the complex interplay of process parameter on the final property of alumina ceramic. Finaly, Conclusion from the findings and recommendation for future study also incorporated.

CHAPTER TWO

LITERATURE REVIEW

2.1. Introduction

A review of previous studies on alumina ceramics was essential for understanding various synthesis methods, such as sol-gel and hydrothermal techniques, along with their strengths and limitations. It guided the selection of suitable methods based on factors like purity, microstructure, and cost, while identifying research gaps for further investigation. This knowledge helped refine experimental design, optimize process parameters, and improve characterization methods, ultimately contributing to more efficient synthesis and advancement in the field.

2.2 Method of synthesis

2.2.1 Sol-gel Method of synthesis and Characterization

Krishnan et al., (2018) synthesized aluminum oxide nano particle by using both the sol-gel technique and solid-state reaction (SSR) method. This study focuses on synthesizing nano cones by varying the carbon content. It compares two low-cost, scalable methods for fabricating alumina nanoparticles: the sol-gel method and the SSR method. Initially, the sol-gel method is used to synthesize nano alumina, followed by the use of the SSR method for the same purpose. The synthesized samples are characterized by X-ray diffraction to identify different phases and transitions during the process. The average crystalline size of the nano alumina is found to be 45 nm using the sol-gel method and 43 nm using the SSR method. The surface morphology of the samples is analyzed using scanning electron microscopy, and a rough estimate of the crystal size is provided.

Niero et al., (2022) aimed to produce nano α-alumina through an inorganic sol–gel process, followed by calcination at 1,200 °C. The sol–gel method involves partial precipitation of the solution, which forms a gel by controlling the concentration of the solvent phase, thereby enabling control over particle morphology, size, and surface area. In this study, the inorganic sol–gel method was utilized to synthesize nano α-alumina, with sodium hydroxide acting as a precipitating agent and aluminum salts as precursors to obtain aluminum hydroxide, which then converted into nano α-alumina after calcination.

Bhattacharyya & Behera, (2017) aimed in creating alumina nanoparticles involved utilizing an aluminum salt combined with a plant extract, following a methodology similar to previous studies. The X-ray diffraction (XRD) analysis confirmed the creation of hexagonal phase alumina nanoparticles, with an average particle size of 61 nm. Scanning electron microscope (SEM) images revealed that the nanoparticles exhibited diameters ranging between 35 and 55 nm, showcasing a mix of spherical and rod-like shapes, often forming aggregates. Furthermore, UV-Vis spectrophotometer measurements indicated a surface plasmon resonance (SPR) of the nanoparticles at a wavelength of approximately 300 nm.

Milani et al., (2020) focused on the synthesis of alumina sol through an inorganic route using cost-effective starting materials, such as aluminum nitride, deionized water, ammonia, and nitric acid. The synthesized sol exhibited stability for approximately a month at 25 °C, but tended to gel at temperatures exceeding 60 °C due to water loss. The synthesized sol, derived from inexpensive starting materials, displayed clarity, homogeneity, and stability for over a month. However, it transitioned into a soft gel at 60 °C. The study also investigated various properties of the obtained sol, including pH, particle size distribution, solid content, phase analysis, existing bounds, and thermal behavior.

Farahmandjou et al., (2016) has presented a comprehensive review of the sol-gel method as a widely used, cost-effective, and versatile chemical technique for synthesizing nanomaterials, particularly metal oxide nanoparticles. It described how sol-gel processing involved hydrolysis and condensation reactions of metal precursors, leading to the formation of a wet gel, which was subsequently dried into various products like aerogels, xerogels, and dense ceramics. The study highlighted the advantages of the sol-gel method, including low-temperature synthesis, high purity, and control over the material's structure and composition. It also detailed various applications of sol-gel-derived nanomaterials in optics, electronics, energy, catalysis, coatings, and biomedical fields. The paper further explored the properties and synthesis techniques of aerogels, classifying them into inorganic, organic, carbon, and hybrid types, and emphasized their high porosity, low density, and thermal insulation capabilities.

Kam et al., (2021) synthesized gamma-alumina nanoparticles (γANPs) through an affordable process using natural bauxites. The γANPs were characterized using several techniques, including X-ray powder diffraction (XRPD), Fourier-transform infrared spectroscopy (FTIR),

Brunauer-Emmett-Teller (BET) theory, scanning electron microscopy (SEM), and atomic force microscopy (AFM). Furthermore, the γANPs were functionalized with CTAB, resulting in CTAB-modified γ-alumina nanoparticles (γANPs-CTAB), which were also characterized by XRPD and FTIR. These functionalized γANPs-CTAB were utilized as adsorbents for removing bisphenol-A (BPA) from water, with the adsorption process following pseudo-second-order kinetics and the Langmuir isotherm. The γANPs-CTAB were found to be effective in adsorbing BPA from water.

Singh & Sarkar, (2015) studied the successful synthesis and characterization using the sol-gel process. The sol-gel process is a chemical method primarily used for synthesizing various nanostructures, particularly metal oxide nanoparticles. The fundamental principle of the sol-gel method lies in producing a homogeneous sol from the precursors and converting it into a gel. The properties of the dried gel significantly depend on the drying method selected based on its intended application. The sol-gel process is versatile, allowing for the doping of materials with various additives to tailor physical, chemical, and optical properties. It is known for producing high-purity and homogeneous materials due to the molecular mixing of precursors. Furthermore, the process can be sensitive to reproducibility, making it a conventional and industrial method for synthesizing nanoparticles with different chemical compositions.

Danks et al., (2016) provided a comprehensive review of sol–gel chemistry, tracing its development from early hydrolysis and condensation reactions of metal alkoxides to more diverse and modern synthetic strategies. It described how sol–gel methods enabled the formation of metal oxides and other ceramics from solution-state precursors, offering advantages like homogeneity, structural control, and low processing temperatures. The study discussed various gel types, sol–gel precursors, and reaction mechanisms, including those involving hydrolysis-condensation, chelating agents, polymer networks, and biopolymer templates. It also explored advanced modifications such as the Pechini method and combustion synthesis, and emphasized the role of templating, processing conditions, and precursor chemistry in tuning material structure, porosity, and composition. Overall, the paper highlighted how sol–gel techniques evolved into a powerful and versatile tool for synthesizing a wide range of functional materials.

Adeniyi et al., (2019) have reviewed the use of alumina as precursors for the development of nanoparticles for water treatment was examined. It is clearly stated theta aluminum oxide (commonly called alumina) is the most commonly occurring oxide of aluminum and is represented by the chemical formula Al2O3. Aluminum is the most abundant metallic element and the third most abundant in the earth's crust after oxygen and silicon. Alumina in its natural form is corundum but can be made from bauxite which is rich in hydrated aluminum oxides. Alumina nanoparticles have been synthesized in a variety of ways and these includes precipitation and co-precipitation, sol-gel method, solution combustion and microwave synthesis.

Khazaei et al., (2016) highlighted that among the various phases of alumina, the γ and α phases are the most widely used in different industries. The study reports the successful synthesis of γ-Al2O3 porous nanoparticles using a simple aqueous sol-gel method with affordable materials. The structures and properties of the samples calcined at 800 ºC were examined using techniques such as X-ray diffraction (XRD), infrared spectroscopy (FTIR), scanning electron microscopy (SEM), thermogravimetric analysis (TG/DTA), and N2 adsorption/desorption. The γ-Al2O3 sample, which used polyethylene glycol as a surfactant, displayed an average crystallite size of 2.313 nm, an average particle size of 20 nm, a specific surface area (SSA) of 138.8 m^2/g, and a pore volume of around 0.166 cm^3/g.

Mavrič et al., (2019) prepared alumina sol from inorganic precursors, specifically aluminum nitrate nonahydrate (purity >98%) and liquor ammonia. Amorphous alumina has historically garnered attention in the forms of thin films or nanoparticles. However, attempts to increase its dimensions have led to destabilization of its amorphous structure and crystallization at relatively modest temperatures. Alumina exists in various crystallographic modifications with distinct properties, with α-Al2O3 (corundum) being the most prevalent form in nature. This phase is thermodynamically stable at room temperature.

The paper reported the successful synthesis and characterization of alumina (Al_2O_3) nanoparticles using the precipitation method, employing aluminum nitrate and methanol as precursors with sodium hydroxide added to maintain a pH of 10–11. The synthesized nanoparticles were calcined at 400°C and 600°C and then analyzed using X-ray diffraction (XRD), scanning electron microscopy (SEM), and dynamic light scattering.

The XRD analysis showed that crystallite size increased with calcination temperature, from 53 nm at 400°C to 72 nm at 600°C, indicating improved crystallinity. SEM images revealed a flower-like and needle-like morphology, with particle aggregation influenced by calcination temperature. Mechanical ball milling effectively reduced agglomeration. Microstrain and dislocation density analyses showed that lower temperatures resulted in more crystal defects. The study concluded that the precipitation method was a cost-effective and reproducible approach for producing Al_2O_3 nanoparticles with good chemical stability and low hygroscopicity. Bhoi et al., (2020)

The research by Wang & Lin, (2007) successful synthesis of alumina (Al_2O_3) nanoparticles using the sol-gel method and investigated their effectiveness in removing copper ions (Cu^{2+}) from aqueous solutions. Researchers used aluminum nitrate and citric acid with a C/N ratio of 0.5, forming a gel through heating and drying, followed by sintering at temperatures ranging from 600°C to 1200°C. XRD analysis showed that γ-alumina began forming at 800°C, transitioning into α-alumina at 1100°C and above, with crystallite sizes increasing from 11.5 nm to 49.1 nm. SEM and EDX analyses confirmed morphological changes and the removal of residual carbon at higher temperatures. Adsorption experiments revealed that copper ion removal efficiency improved with increased sintering temperature, reaching a maximum of 82.1% at 1200°C. The study concluded that removal efficiency was more influenced by particle size growth than by the specific alumina phase

2.2.2 Electrochemical method of synthesis and Characterization

Rabia et al., (2018) studied on the recent advancement of preparation and characterization of activated alumina particle (AAP) synthesized by the electrochemically process from aluminum and have gained serious attention inexpensive material that can be employed for water filtration due to its activated surface. XRD and SEM microscopy techniques are used to examine the material's microstructure. The study reviews recent advancements in the synthesis and characterization of activated alumina. As a result, excellent outcomes were observed, and the study outlined the optimal conditions for preparing activated alumina to achieve high yield. Additionally, a systematic characterization using SEM, FTIR, X-ray diffraction, and EDX was also summarized.

The paper by (Attil et al., 2024) emphasizing how hydrolysis and condensation of molecular precursors enabled the controlled formation of nanostructured oxides under mild conditions. It explained how vanadium oxide gels were prepared from vanadic acid solutions and exhibited lyotropic nematic behavior, forming anisotropic layers with enhanced electrochemical properties. The author also described how vanadium alkoxides yielded thermochromic VO_2 thin films with reversible metal-insulator transitions. Zirconium alkoxides, when modified with acetylacetone and hydrolyzed under specific conditions, produced monodispersed zirconia nanoparticles suitable for membrane applications. Furthermore, the study showed how the sol-gel process allowed the encapsulation of biomolecules and even whole protozoan cells in silica matrices without damaging their structure or antigenic properties, thus demonstrating potential for biosensing applications. Overall, the sol-gel method was presented as a versatile and gentle technique for fabricating functional inorganic and hybrid materials.

Rogojan et al., (2011) synthesized and characterized gamma-alumina nanoparticles using various methods and materials. The nanoparticles were produced through a cost-effective process using natural bauxites and were characterized by techniques such as X-ray powder diffraction (XRPD), Fourier-transform infrared spectroscopy (FTIR), Brunauer–Emmett–Teller (BET) theory, scanning electron microscopy (SEM), and atomic force microscopy (AFM). The functionalized γANPs-CTAB were employed as adsorbents for the removal of bisphenol-A (BPA) from water. These γANPs-CTAB materials proved to be effective in adsorbing BPA from water.

Pourmadadi et al., (2022) focused on enhancing the effectiveness of drug delivery systems, particularly through the use of alumina nanoparticles. This research reviews the different phases of alumina, the synthesis methods for producing biomedical-grade alumina tailored to specific biomedical engineering applications, and the properties of alumina nanoparticles (NPs). Additionally, the study examines existing literature on the use of alumina as a drug carrier and presents new strategies to improve the therapeutic efficacy of alumina-based nanocarriers. The growing use of alumina for drug delivery in recent years is attributed to its outstanding structural and chemical properties, such as thermal stability, mechanical strength, high surface area, tunable pore size, and modifiable surface.

Marlina Ginting & Bukit, (2015) investigated the electrochemical technique for producing alumina (α-Al2O3) from aluminum metal. The α-Al2O3 precursor was calcined at 110 °C for six hours and then analyzed using Fourier Transform Infrared (FTIR) spectroscopy, Particle Size Analysis (PSA), X-ray Diffraction (XRD), and Scanning Electron Microscopy (SEM). To study the transformation of the precursor into α-Al2O3, three samples were sintered at temperatures of 400, 800, and 1200 °C and analyzed. A key finding was the conversion of AlOH and β-Al(OH)3 into γ-Al2O3 at lower temperatures (400 to 800 °C), followed by the transformation of γ-Al2O3 into α-Al2O3 at 1200 °C. The overall results indicated that the electrochemical method is a promising alternative for producing nearly pure α-Al2O3 at a sintering temperature of 1200 °C.

2.2.3 Hydrothermal method of synthesis and Characterization

Mota et al., (2019) showed the successful production of alumina nanofiber after thermal treatment of solution blow spine hybrid fiber. The material used to synthesis aluminum nitrate nonahydrate and polyvinylpyrrolidone were used as inorganic and organic processors to form hybrid fibers and ethanol and distilled water were used as solvent for preparation of solution. The X-ray diffraction patterns presented all the characterization of the gamma and alpha phase of the alumina. In addition, the scanning election microscopy showed alumina nanofiber diameters varying between 200nm and 270nm for different temperature. The thermal treatment analysis presented mass loss that occurred during the process calcination.

Krishnan et al., (2018) successfully prepared alpha alumina structure via hydrothermal synthesis supported with sodium dodecyl sulfonate anionic surfactant. Aluminum nitrate nonahydrate was used and sodium dodecyl sulfonate was used as an anionic surfactant ammonia solution 35% was hydrolyzing agent. A precursor solution was prepared by dissolving alumina nitrate nonahydrate in deionized water and stirred at room temperature for an hour and surfactant solution were added to the precursor solutions. The characterization of the sample calcinated at 1200^{o}c was preformed using roman spectroscopy, X-ray diffraction analysis, Fourier transform infrared spectroscopy, thermogravimetric analysis, and scanning electron microscopy techniques with this the experimental result showed the pure alpha alumina were obtained with different morphology.

Kaur et al., (2020) synthesized alumina nanoparticles by thermal dehydration of aluminum oxide. Alumina exists in several transitional phase. The experimental method and characterization process is conducted very well. For this Aluminum metal powder was mixed with dilute hydrochloric acid to produce a clear solution of aluminum chloride. A hydrogen gas evolved out with fizzing sound, accompanied by the liberation of a lot of heat and then ammonium hydroxide solution was then added slowly to the solution of aluminum chloride and white gelatinous precipitation of aluminum hydroxide were obtained. Then the XRD pattern showed that the formation of different phase of aluminum under the effect of heat treatment and indicated a consistent picture the structural transformation in alumina nanoparticle with heat treatment.

Vignesh Raj et al., (2018) investigated the preparation of a nanocrystalline hydroxyapatite/alumina (HAp−Al2O3) composite using a custom-designed stir-type hydrothermal reactor. Phase identification and crystallite size analysis were performed using X-ray diffraction (XRD) with a CuK α radiation X'pert powder diffractometer from PAN Analytical (The Netherlands). The morphology and elemental composition of the synthesized samples were examined using high-resolution transmission electron microscopy (HRTEM) combined with energy-dispersive X-ray spectroscopy (EDS) from JEOL JEM 2100 (Germany). Elemental mapping of the composites was conducted using a field-emission scanning electron microscope (FESEM) from Bruker, Germany. The study found that increasing the reaction temperature enhances the formation of the nanocrystalline HAp−Al2O3 bio composite material.

The study Fatimah et al., (2022) detailed a method for calculating and interpreting crystallite size from X-Ray Diffraction (XRD) spectra, particularly utilizing the Scherrer method. It outlined a step-by-step approach to analyze XRD data, aiming to assist students and new users in comprehending XRD results. The research focused on explaining how to read XRD characterization results, specifically for calculating crystallite size by $D = \frac{K\lambda}{\beta COS\theta}$, and compared these findings with existing literature. The methodology involved qualitative analysis to determine the crystal phase and quantitative analysis to ascertain crystallite size, applying these techniques to samples of WO3 particles and barium hexaferrite particles.

Narayanan & Rakesh, (2018) produced aluminum oxide nanoparticles using aluminum nitrate and lemon extract, which is considered an environmentally friendly and non-toxic material. The mixture was then heated with microwaves at 600 W for 5 minutes, resulting in the observation of a peak at 271.50nm in the UV spectrum of the heated sample. This spectrum was compared with those of other research works to confirm the formation of alumina nanoparticles. Following this, the sample was centrifuged at 3500 rpm, leading to the formation of a sediment. The nanoparticles were characterized using UV Visible (UV-Vis) Spectroscopy, Dynamic Light Scattering, and a Zeta Analyzer, revealing an average size of 460nm. This synthesis method has demonstrated faster results than other methods due to the involvement of microwave heating. Moreover, the synthesized nanoparticles may possess potential antibacterial and antifungal properties, warranting further investigation.

Vignesh Raj et al., (2018) synthesized a nanocrystalline hydroxyapatite/alumina (HAp−Al2O3) composite using a specially designed stir-type hydrothermal reactor. The starting materials for the HAp−Al2O3 composite included analytical-grade calcium nitrate tetrahydrate (Ca(NO3)2·4H2O), diammonium hydrogen phosphate ((NH4)2HPO4), and aluminum nitrate (Al(NO3)3·9H2O). A 25% ammonia solution was incorporated to adjust the reaction's pH Thermogravimetric analysis indicated improved thermomechanical properties, with minimal weight loss at elevated temperatures. These findings support the development of biocompatible HAp−Al2O3 composite nanorods for biomedical applications.

Kaur et al., (2020) studied on detailed the synthesis and structural characterization of alumina (Al_2O_3) nanoparticles through thermal dehydration of aluminum hydroxide ($Al(OH)_3$). Researchers heat-treated the material in stages from 150°C to 1150°C, observing a sequential phase transformation from $Al(OH)_3$ to AlOOH (boehmite), then to γ-, δ-, θ-, and finally α-alumina. X-ray diffraction (XRD) confirmed the emergence of these distinct alumina phases at various temperatures.The concentration of α-alumina increased with temperature, reaching 84% at 1150°C, accompanied by a decline in θ- and δ-alumina. The study concluded that heat treatment influenced both phase composition and crystallite size, with α-alumina showing the largest crystallites. The consistency between XRD and NMR results validated the structural evolution and coordination environment of aluminum across different annealing temperatures.

2.2.4 Precipitation Method of synthesis and Characterization

Bhoi et al.,(2020) successfully prepared alumina nanoparticle from alumina nitrate precursor and methanol using the precipitation method. Aluminum nitrate, methanol, sodium hydroxide pellet and deionized water were used as starting precursor. The XRD pattern of the prepared sample all the visible peaks can be indexed as alumina can be related to the standard reference data. It was clearly observed that with increase in calcination temperature the crystallite size of the sample increase indicating the enhanced crystallinity and lattice strain in the crystalline structure largely affects the stability of the nanoparticles. The SEM result reveals that the alumina has a flower shape and needlelike structure. The calcination temperature had a greater influence on morphology of the formed nanoparticles. Besides macrostrain analysis has been performed which shows good chemical stability.

The study by Bhoi et al., (2020) focused on the synthesis and characterization of alumina (Al_2O_3) nanoparticles using a straightforward sol-gel method. Aluminum nitrate used as a precursor and ethanol as a solvent, maintaining a pH of 2–3 during synthesis and performing calcination at 500°C. They characterized the resulting nanoparticles using X-ray diffraction (XRD), scanning electron microscopy (SEM), transmission electron microscopy (TEM), and energy dispersive spectroscopy (EDS). The XRD analysis confirmed a phase transition from γ- to α-alumina at temperatures above 1000°C, revealing a rhombohedral structure. SEM and TEM images showed that the particles developed a sphere-like morphology with increased annealing temperature and exhibited an average size of about 28 nm with minimal agglomeration. EDS analysis confirmed the presence of only aluminum and oxygen, indicating the high purity of the synthesized nanoparticles.

Mirjavadi et al., (2018) synthesized nanoscale α-Al2O3 powders using a high-throughput impinging stream microreactor. The results showed that the powders produced had better dispersion and a more uniform particle size distribution compared to those made with the traditional parallel flow precipitation method. As a result of this uniform nucleation, homogeneous particles were produced. The study also thoroughly examined the effects of calcination temperature and time on the morphology, phase composition, and particle size of α-Al2O3. This research contributed to the development of ultrafine α-Al2O3 powders with a uniform size distribution, high crystallinity, and excellent thermal expansion properties.

Sadabadi et al., (2013) synthesized high-purity crystalline alpha alumina (α-Al2O3) platelet powder using a combustion synthesis method. The process involved utilizing aluminum nitrate as the aluminum source and urea as the oxidizer in an aqueous medium. Various analytical techniques were employed to characterize the synthesized alpha alumina powder. X-Ray diffractometer was used to study the crystalline phase, while Scanning Electron Microscopy (SEM) and Energy Dispersive X-ray Spectroscopy (EDAX) were utilized for morphological and chemical characterization of the nanoparticles. Further analysis of the crystalline structure was conducted using Transmission Electron Microscopy (TEM) and Selected Area Electron Diffraction (SAED). Additionally, the size distribution of the powder was investigated using a Particle Size Analyzer (PSA), and the thermal behavior of α-Al2O3 was evaluated through Thermal Gravimetric and Differential Thermal Analysis (TG/DTA).

2.2.5 Acid leaching method of synthesis and Characterization

Bhattacharyya & Behera, (2017) and Bhattacharyya & Behera, (2017) synthesized α-alumina powder with particle sizes smaller than 100 nm and a spherical shape from calcined kaolin using an acid leaching method. The process involved common transitional phases of alumina, such as gamma, delta, kappa, and theta, each with its own technological applications. The resulting amorphous white powders, obtained after precipitation, washing, and drying, were characterized using XRD, TG-DSC, and FTIR techniques. Furthermore, particle size distribution, specific surface area, and microstructural analysis of the powder calcined at 1200 °C were conducted to assess particle size, shape, and distribution. Pure-phase α-alumina, with particle sizes under 100 nm, was achieved at 1200 °C, and the addition of a surfactant during processing positively impacted the modification of particle size.

2.2.6 Application of alumina nanoparticles

The paper by (Adeniyi et al., 2019) provided a mini-review on the application of alumina nanoparticles for water treatment, highlighting their synthesis, availability, and effectiveness. It examined the natural occurrence of alumina in Nigeria and discussed various synthesis methods such as precipitation, sol-gel, solution combustion, and microwave techniques. The study reviewed numerous batch experiments which demonstrated that alumina nanoparticles typically exhibited monolayer adsorption behavior following pseudo-second order kinetics.

These nanoparticles effectively removed a wide range of water pollutants including heavy metals, dyes, and oils, showing high removal efficiencies despite variations in adsorption capacities. Overall, the study established alumina nanoparticles as promising adsorbents for wastewater treatment.

The study by (Souza & Braganc, 2017) investigated the extraction of humic acid (HA) from subbituminous coal and its application as a dispersant for ceramic powders. The extraction process was straightforward and suitable for laboratory-scale production. The HA was characterized through elemental analysis, FTIR, thermal analysis (TGA/DTA), zeta potential, turbidity, and SEM. Results showed that HA contained carboxylic and phenolic groups and exhibited polyelectrolyte behavior. Alkaline conditions enhanced its negative surface charge, and SEM analysis revealed an extended molecular structure at pH 11, favoring dispersion. Rheological tests on alumina suspensions confirmed that HA significantly reduced viscosity and improved fluidity, with optimal performance in alkaline pH (10–11). The absence of metal complexes ensured the availability of surface charges for effective dispersion. Overall, the study demonstrated that coal-derived HA could be a low-cost, efficient alternative to commercial dispersants in ceramic processing.

The study examined lime-based plasters modified with varying amounts of fine ceramic powder, a waste product from thermal insulation block production, to assess its suitability as a supplementary cementitious material. Researchers replaced lime with up to 80% ceramic powder and found that while overall porosity increased, capillary pore volume decreased, leading to improved hygric and thermal properties. Mechanical strength slightly declined with higher ceramic content but remained within acceptable limits. The plaster with 20% ceramic powder showed the best balance of physical, hygric, thermal, and mechanical properties, making it an effective and sustainable option. The study concluded that ceramic powder could positively enhance plaster performance while promoting waste material utilization based on Čáchová et al., (2016)

The paper by Giesche,(2007) provided a comprehensive overview of the preparation methods and applications of coated powders in ceramics and related fields. It discussed various techniques such as heterogeneous coagulation and nucleation in solution and gas phases, emphasizing their significance in achieving well-defined coated particulates.

The review highlighted practical examples, demonstrating how specific coating layers could influence essential properties such as homogeneous distribution, protection of core materials, and the design of controlled microstructures. The author illustrated that coated powders could enhance the performance of composite materials, influence optical, magnetic, and electrical properties, and mitigate undesirable reactions during processing, thereby establishing their critical role in advanced material systems.

Sigmund & Bell, (2000) had discussed various novel powder-processing methods for advanced ceramics, focusing on direct-casting techniques and solid freeform fabrication. It reviewed the fundamental principles of green body formation, distinguishing between physical and chemical gels based on the nature of gelation. An overview of dense suspensions' properties was provided, particularly regarding factors influencing maximum solids loading. Recent studies on direct measurements of interparticle forces in ceramic systems were highlighted and linked to rheological properties. The text emphasized the challenges faced in achieving high reliability in ceramics processing due to the brittleness of materials and the need for precise control over fine powders, leading to increased interest in innovative suspension handling and molding techniques.

2.2.7 Optimization Technique

The study by Wang & Lin, (2007) investigated the optimization of the fused deposition modeling (FDM) process in rapid prototyping (RP) by integrating the Taguchi method with Gray relational analysis.. They established that deposition orientation in the Z direction (DOZ) significantly affected both TS and DA, while layer thickness (LT) was critical for SR. By applying Gray relational analysis with entropy-based weighting and verifying results using the TOPSIS method, the study identified optimal parameter combinations that improved TS by 90.48%, DA by 99.36%, and SR by 62.27%. The integrated optimization approach effectively enhanced multiple quality attributes of FDM-printed parts, demonstrating its applicability for improving RP system performance.

This study by (Lin, 2012) an integrated approach that combined the Taguchi method, Grey Relational Analysis (GRA), and a Neural Network (NN) to optimize a novel Gas Metal Arc (GMA) welding process using activating flux. Initially, the Taguchi method was employed to identify optimal process parameters and construct a database.

GRA was then used to handle multiple performance characteristics—penetration depth, depth-to-width ratio, and fusion area—by converting them into a single grey relational grade. A neural network trained using the Levenberg-Marquardt back-propagation algorithm modeled the nonlinear relationship between process parameters and welding performance. Simulation results from the trained network identified optimal settings—welding voltage of 20 V, gas flow rate of 6 L/min, speed of 450 mm/min, and 100% MoO_3 flux—that improved the grey relational grade by 13.91% compared to Taguchi optimization alone. The study demonstrated that the proposed hybrid method effectively enhanced weld quality in the GMA process.

A study by Kuo et al., (2008) examined how simulation, while valuable for analyzing complex systems, lacked optimization capabilities—especially when multiple conflicting performance measures were involved. To address this, the authors proposed a method combining the Taguchi optimization technique with Grey Relational Analysis (GRA), effectively converting multi-response problems into a single-response format. They applied this method to a real-world case in an integrated circuit packaging company, aiming to improve throughput and cycle time of an ink-marking machine. The study showed that their approach performed comparably to other advanced methods in the literature, and the results demonstrated that the grey-based Taguchi method was both simple and effective for multi-response simulation optimization.

Based on Saeheaw, (2022) explored the use of a hybrid optimization technique that combined the CRITIC method (an objective weighting system) with Grey Relational Analysis (GRA) and the Taguchi method to optimize multiple quality outcomes in the Nd:YAG laser welding process. The researchers used a Taguchi L36 orthogonal array to experiment with six process parameters—beam diameter, laser power, flow rate, welding speed, laser offset, and pulse shape—aiming to maximize weld strength and minimize weld width. The CRITIC method was applied to assign objective weights to each response, and GRA was then used to convert the multi-objective optimization problem into a single performance index. Results showed that laser power and welding speed were the most influential parameters.

According to (Process, n.d.(2014) the optimization of welding parameters to enhance the mechanical properties and minimize defects in SA 516 Grade 70 steel welded by SMAW investigated. The study aimed to improve tensile strength, impact energy, hardness, and angular distortion using a hybrid method combining

Taguchi design, Grey Relational Analysis (GRA), and Principal Component Analysis (PCA). Experiments were structured using an L9 Taguchi orthogonal array, testing different levels of groove angle, preheat temperature, electrode diameter, and root gap. The results showed that preheat temperature and electrode diameter had the most significant effects on weld quality. The integrated GRA-PCA method allowed for simultaneous multi-response optimization, yielding improved mechanical properties and reduced distortion. Confirmation experiments validated the model, demonstrating substantial gains in weld strength and toughness, as well as a reduction in defects.

The paper focused on optimizing machining parameters in the turning process using Grey Relational Analysis (GRA) to enhance multiple performance outcomes simultaneously—namely material removal rate (MRR), tool life, and surface roughness (SR). Experiments were conducted on martensitic stainless steel (AISI 420) using a coated carbide tool (KC5010) under varying cutting speeds and feed rates, while the depth of cut was kept constant. A three-level two-factor factorial design with center points guided the experimental setup. GRA was employed to convert the multi-response problem into a single-objective optimization task through normalization, calculation of grey relational coefficients, and grey relational grades (GRGs). Results showed that the optimal machining parameters were a cutting speed of 100 m/min, feed rate of 0.16 mm/rev, and depth of cut of 0.2 mm. Among all parameters, cutting speed had the most significant influence on machining performance. The study demonstrated that GRA effectively identified the best combination of turning parameters for improved machining quality as per the study by (Mejid et al., 2023)

The paper presented by (Panda et al., 2016) a study on optimizing hard turning parameters during the machining of hardened AISI 52100 steel using a mixed ceramic insert under dry conditions. The authors employed Grey Relational Analysis (GRA) combined with the Taguchi method to simultaneously minimize flank wear and surface roughness—two critical quality metrics in hard machining. Experiments were conducted based on a Taguchi L16 orthogonal array, considering three key factors: cutting speed, feed rate, and depth of cut. A second-order regression model was developed and found to be more accurate than the first-order model. The analysis revealed that feed rate had the most significant impact on performance, followed by cutting speed and depth of cut. The optimal combination of process parameters was identified

as 0.1 mm depth of cut, 0.04 mm/rev feed rate, and 110 m/min cutting speed. This combination yielded significant improvements in machining performance, and the model predictions closely matched the experimental results. The study demonstrated that the proposed GRA-Taguchi approach was effective for multi-response optimization in hard turning operations.

According to the paper by (Yaqoob et al., 2024) investigated the optimization of high-speed orthogonal turning parameters for heat-treated AISI 4340 alloy steel using multi-layer coated carbide tools under dry conditions. A Taguchi L18 experimental design was employed to analyze the effects of tool type, cutting speed, feed rate, and depth of cut on surface roughness and tool life. Taguchi signal-to-noise (S/N) ratios and Grey Relational Analysis (GRA) were applied to identify optimal conditions. The results showed that the CVD-coated tool provided the highest tool life (14.75 minutes), while the PVD-coated tool resulted in the lowest surface roughness (0.276 μm). GRA revealed that the optimal machining setup was a CVD tool with a cutting speed of 300 m/min, feed rate of 0.05 mm/rev, and depth of cut of 0.1 mm. Among the input variables, feed rate had the most significant effect on both responses, followed by tool type. Confirmation tests validated the predicted results, showing a 14.57% improvement in Grey Relational Grade, demonstrating the effectiveness of GRA in multi-response optimization of hard turning processes.

2.3Research gap

The field of engineering focuses broadly on synthesis and characterization of nanoparticles in order to achieve optimum property possible. While a lot of studies have investigated the impact of process parameters on synthesis of alumina ceramic. A significant gab exists in synthesize process parameter needed to be considered. Most studies focus on calcination temperature or the method of synthesis to compare the result of the nanoparticle obtained from the two methods as well as using different precursor materials. This limited the ability to understand in depth the complex interactions and optimization of the process holistically. In addition, most of the existing studies primarily focused on optimizing a single outcome and neglecting the potential for multi-objective optimization to achieve a balance between different desirable outcomes.

Therefore, this literature review highlighted a significant research gap regarding the optimization in synthesis and characterization of alumina. Specifically, there was a need for research that investigate the a multiple process parameters and their combined impact on morphology and thermal stability of each sample, explores a wider range of parameter value to identify optimal conditions, conduct statistical analysis to draw reliable conclusions from experimental data, addresses multi-objective optimization to achieve a balance between different desirable outcomes, develop a comprehensive model that represents the complex interaction between process parameters and use optimization techniques.

So, addressing the research gap highlighted had the potential to significantly improved the efficiency and effectiveness of synthesis of alumina nanoparticles. This could lead to have a better understanding on the combined effect of the process parameter on the properties of alumina ceramic.

CHAPTER THREE

MATERIALS AND METHODS

3.1Materials

This research examined that how various process factors interact during the synthesis of alumina nanoparticles via the sol-gel method, addressing a gap in current understanding. The process begins by dissolving precursors in solvents (such as water, alcohol, organic liquids, or combinations) to create a uniform initial solution.

The materials used to synthesize alumina ceramic nanoparticles are: the precursor materials (Aluminum nitrate ($Al(NO_3)3.9H_2O$), Aluminum chloride ($AlCl_3$), and Aluminum sulfate($Al_2(SO4)_3$), Solvent (water) H_2O, and pH regulator (Sodium hydroxide) NaOH based on (Bokov et al., 2021). The properties of these materials are discussed in the Table 3.1 below.

Table 3.1 Materials and their properties (Callister & Wiley, n.d.2007)

Properties	Materials			
	Aluminum Nitrate ($Al(NO_3)3.9H_2O$)	Aluminum sulfate ($Al_2(SO4)_3$)	Aluminum Chloride ($AlCl_3$)	Sodium hydroxide NaOH
Molar mass	375.13g/mol	342.15g/mol	133.341g/mol	39.997g/mol
Appearance	White crystal	White crystalline solid	Colorless Crystal	White crystal
Density	1.72g/cm^3	2.672g/cm^3	2.48g/cm^3	1.515 g/mL
Melting point	73ºC	770ºC	180ºC	318 ºC
Solubility in water	Soluble in water	Soluble in water 31.2g/100ml(0ºC), 36.4g/100ml(20ºC), /	Soluble in water 439g/L (0ºC), 458g/L (20ºC),	Soluble in water 418g/L (0ºC

3.2 Methods

The methodology of this study was developed based on the review of previous studies which has been done so far. This included understanding the specific equipment and instruments used, the experimental producers followed, and the data analysis method employed. This clarity allowed to develop a robust and reliable methodology for the synthesis, characterization, and process parameter optimization by learning from their success and challenges.

A comprehensive research methodology was employed as shown in the Figure 3.1 below by taking in to account different aspects: Systematical investigation on the influence of wide range of process parameters beyond the commonly studied one by adopting a multi objective optimization framework to simultaneously optimize for multiple desirable properties was conducted. Then, characterization was done to thoroughly analyze the synthesized alumina nanoparticles and statically analyze the experimental data to identify significant relationship between process parameters and the material properties. By integrating these methodologies, this research provided a comprehensive understanding of the complex interaction of process parameter during alumina nanoparticle synthesis leading efficient synthesis strategy for producing high quality alumina ceramic with optimum property.

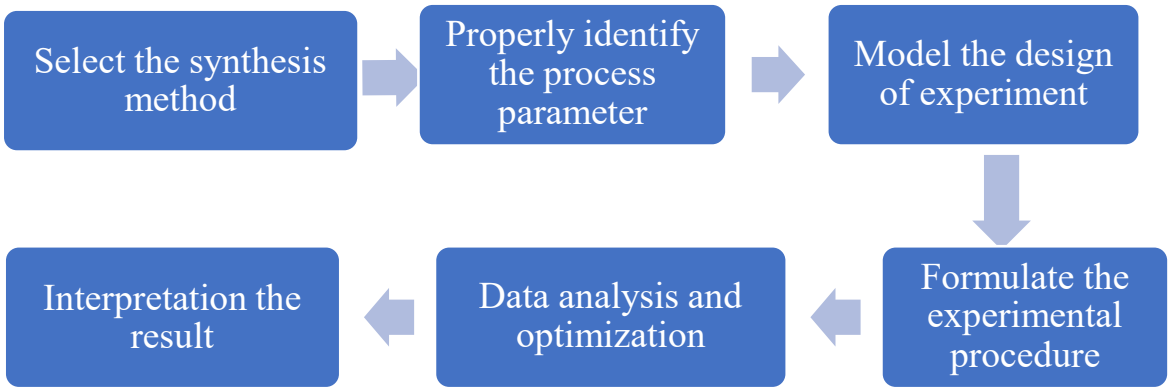

Figure 3.1: Schematic representation of the methodology

3.1.1 Method of synthesis

The sol-gel technique involves converting a 'sol'—a suspension of particles derived from metallic alkoxides or organometallic precursors—into a 'gel' through low-temperature polymerization. Subsequent steps include drying to remove the solvent from this wet gel, followed by a specific heat treatment. Advantages of this method include its adaptability, potential for high material purity, capability for creating specialized materials, and reduced energy consumption due to lower processing temperatures. It was anticipated that the resulting alumina powders possessed nanometric dimensions as.(Rogojan et al., 2011) studied.

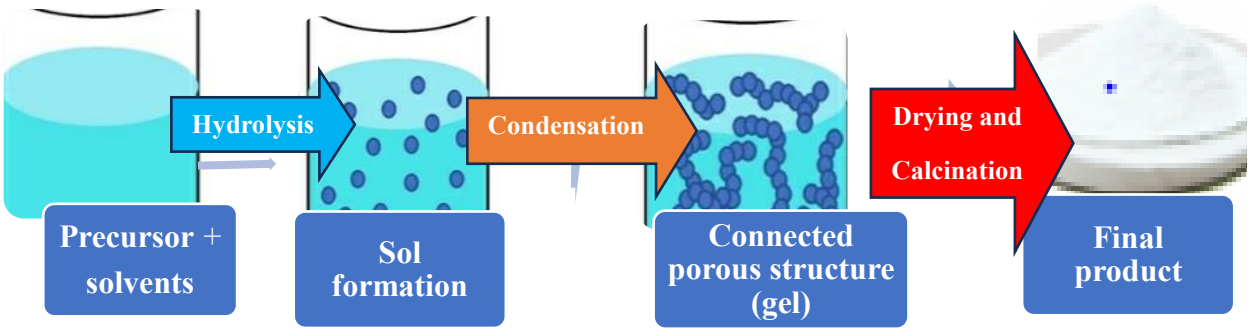

Figure 3.2: Schematic representation of Solgel method (Bokov et al., 2021)

As shown in the Figure 3.2 the sol-gel process is a wet chemical approach for synthesizing nanomaterials. It involves creating a stable colloidal solution, known as a "sol," which transforms into a gel-like structure. This structure ultimately solidifies through hydrolysis and condensation, enabling precise control over the chemical composition and size of the resulting nanoparticles. This technique is especially effective for producing high-purity and uniform metal oxide-based nanomaterials. The fundamental sol-gel process consists of several key steps as shown in figure 3.2 above: (1) the hydrolysis of the precursor, initiating the chemical reaction that leads to nanoparticle formation, (2) the nucleation and growth of these particles through condensation, (3) the introduction of an appropriate substance that causes gelling, and (4) the final stage where the material is dried and calcined to produce the completed sol-gel. (de Oliveira et al., 2015).

According to Bokov et al., (2021), the sol-gel method offered numerous advantages: it's simple, yields high-purity products efficiently, allows precise control over chemical composition for homogeneity, and enables the production of materials with modified physical traits like low thermal expansion and high optical clarity. Furthermore, it provides fine control over material structure by adjusting early-stage network formation variables* and combines low initial investment with high-quality output. The process itself occurs in a liquid state at relatively low temperatures (typically under 100°C) to form a solid product. By managing the parameters influencing the key hydrolysis and condensation reactions, materials with specific microstructures and surface chemistries can be created.

3.2.2Process parameter identification:

In order to achieve a comprehensive understanding of the synthesis process and optimize for desired properties, a wide range of process parameter was considered. The following parameters are selected as basic process parameter in order to optimize the properties of alumina nanoparticle in reference of the literature reviews.

3.2.2.1 Precursor type:

Precursor is the starting materials for the sol-gel process. Precursors should be soluble in the reaction media and they should be reactive enough to participate in the gel forming process. (Liu et al., 2023), (Spear, n.d.) (Mahdi SIAHPOOSH et al., 2016) have studied that the choice of precursor material in the sol-gel synthesis of alumina significantly impacts the final properties of the alumina product, including its particle size, morphology, phase composition, and overall reactivity, due to differences in the hydrolysis and condensation rates depending on the chemical nature of the precursor molecule, such as its ligands and solubility in the solvent.

The precursor material used to synthesize alumina nanoparticles significantly impacts their properties, including particle size, morphology, surface area, and crystal structure. Different aluminum precursors like aluminum chloride, aluminum nitrate, aluminum hydroxide, aluminum sulfate or aluminum alkoxides will result in different alumina phases. Romero Toledo et al.,(2018)determined that a small amount of impurity in precursor salt can modify the physical properties of alumina compared with conventional γ-alumina.

In this case three precursor material of Aluminum salts that are easily soluble in water are selected. i.e. the precursor materials aluminum nitrate, aluminum chloride, and aluminum sulfate are selected based on (Bokov et al., 2021).

3.2.2.2 Calcination temperature:

Calcination is a heat treatment process that removes organic components and stabilizes the nanoparticles, influencing their thermal stability and crystallinity. As (Bhoi et al., 2020) explained the calcination temperature has a notable effect on the stability and crystallinity of the nanoparticle.

Bin Mokaizh et al., (2021),Nampi et al., (2011), and(Su et al., (2023) studied that in the sol-gel synthesis of alumina ceramics, increasing the calcination temperature leads to a higher degree of crystallinity, larger crystallite size, and a phase transition from the less stable γ-alumina to the more stable α-alumina phase, which significantly impacts the final properties of the ceramic, including its density, hardness, and thermal stability; essentially, higher calcination temperatures result in a more fully developed and crystalline alumina structure. Based (Attil et al., 2024) on the calcination temperature recommended from 200^{o} c to 1200^{o} Three calcination temperature are, 800, ^{o}C, 1000 ^{o}C, and 1200^{o}C which are selected based on Rogojan et al., (2011). As Series, (2024) in the their study investigate that temperature has a significant effect on microscopic property of the materials. Nikiforov et al., (2023) has studied that the annealing temperature on the final properties of the material.

3.2.2.3Calcination time:

Bin Mokaizh et al., (2021) has investigated that increasing the calcination time generally leads to a higher degree of crystallinity, larger crystallite size, and a more complete transformation of the amorphous alumina gel into the desired crystalline phase (typically α-alumina), resulting in improved ceramic properties like density and strength. So based on Vural & Sari, (2019) the three levels of calcination time selected are 3 hour, 4 hours, and 6 hours. The systematical investigation the influence of these parameters of this research developed a comprehensive understanding of their individual and combined effect on the morphology, thermal stability, and overall properties of the synthesized alumina nanoparticles.

3.2.3Model the design of experiment (DoE):

Taguchi design of experiment for alumina nanoparticle synthesis. This method provided a robust framework for designing experiments and optimizing processes by systematically investigated the influence of multiple factor or process parameter on a desired response such as particle size, particle shape, and mass loss.

Identify control factor: Based on the previously identified process parameters, we can select the most influential factors for this study. Factor A: precursor material with three level i.e. Aluminum nitrate(A1), Aluminum sulfate (A2), and aluminum chloride (A3). Factor B: Calcination temperature with three level. B1, B2, and B3. Factor C: Calcination time with three level.C1, C2, and C3

The orthogonal Array: The suitable orthogonal array that accommodates the number of factors and levels is selected taking in to account the numbers of factors and their levels. In this case three factors with three level each. So, for three factors with three level each, the L_9 orthogonal array is suitable for its time and cost effective, robustness, and ease of explanation of the result. (Dar et al., 2018),(Ahmad Dar & Anuradha, 2018) (Maazinejad et al., 2020) investigated that the L9 orthogonal array design of experiment, often used in the Taguchi method, offers several advantages including: significantly reduced number of required experiments while still effectively evaluating multiple factors, allowing for efficient identification of the most impactful variables on a response, and providing a balanced approach to analyzing the effects of different factor levels with minimal experimental runs; making it cost-effective and time-saving compared to full factorial designs when dealing with multiple parameters at different levels.

Assign factor levels to array: Assign the levels of each factor to the corresponding columns of the orthogonal array. This ensures that all factor combinations help to be tested in a balanced efficient manner. **Conduct experiments**: The experiments performed according to the assigned factor combinations in the orthogonal array. **Analyze data:** Signal-to-Noise Ratio(S/N); the S/N ratio was calculated for each experiment based the desired response. The main response selected to optimize are, particle size, thermal stability, and particle shape. Analysis of Variance (ANOVA): ANOVA was conducted to determine the significance of each factor and their interaction on the response. Optimal Parameter Settings:

The optimal levels of each factor that maximize the S/N ratio and achieve the desired properties was identified. By implementing a Taguchi design of experiment this study investigated the influence of multiple process parameters on the properties of synthesized alumina nanoparticle which led to a robust and optimized synthesis process.

3.1.4 Formulate the experimental procedure

This experimental procedure for alumina nanoparticle synthesis and characterization outlines the step involved in synthesizing alumina nanoparticles using a Taguchi designed experiment and characterizing their properties.

3.1.4.1 Materials

- Aluminum precursors
- Deionized water
- Acids and/or bases for pH adjustment (NaOH)

3.1.4.2 Equipment

- Analytical precision balance
- Beaker, pH mater, Magnetic stirrer
- Forced convection drying oven
- Calcination furnace
- X-ray diffractometer (XRD)
- Thermogravimetric analyzer (TGA)

3.1.4.2 Experimental design

Experimental design is a field of knowledge and methods, developed through research, that equips investigators to run experiments resourcefully, interpret data accurately, and ensure their conclusions align with the study's primary aims.

Based on Krishnaiah & Shahabudeen, n.d.) utilized the L_9 orthogonal array to define the experimental runs based on the selected factors and levels as it is clearly stated in the modeling the design of experiment above. Each experiment will involve a specific combination of precursor type (A), calcination temperature(B), and calcination time(C) as shown in Table 3.2 below.

Design Summary

Taguchi Array	L9(3^3)
Factors:	3
Runs:	9

Table 3.2 Taguchi L9 design of experiment

	C1-T	C2	C3
	Precursor material	calcination temperature	calcination time
1	A1	800	3
2	A1	1000	4
3	A1	1200	6
4	A2	800	4
5	A2	1000	6
6	A2	1200	3
7	A3	800	6
8	A3	1000	3
9	A3	1200	4

3.1.4.3 Sol-Gel Synthesis procedure:

Step 1: precursor and solvent preparation; in this step the appropriate amount of precursor determined based on the recommended concentration of each experiment as shown in Figure 3.3 below and dissolved the precursor in deionized water to prepare the homogeneous solution. Young,(2002) recommended that the right proportion of solute (aluminum precursor like aluminum nitrate) and solvent (typically ethanol or water) in the sol-gel synthesis of alumina has a significant impact. The desired properties of final alumina product should be considered, such as particle size, porosity, and morphology.

The higher water content leads to faster hydrolysis and smaller particles, while a lower water content results in larger particles and slower gelation. The concentration was selected based on (Krishnan et al., 2018) the molarity as: $Molarity\ (M) = 0.125 mol/l$ and the mass of precursor material decided to be 15g the amount of solvent required calculated.

$$M = \frac{mole\ of\ solute}{litter\ of\ solution\ (v)} \quad \text{Eq. (3.1)}$$

$$mole\ of\ solute = \frac{mass\ of\ solute}{molar\ mass} = \frac{15g}{375.134g/mol} = 0.0399mol$$

Now, the amount of distilled water required calculated as;

$$Litter\ of\ solution\ (v) = \frac{mole\ of\ solute}{Molarity} = \frac{0.0399}{0.125} = 0.31988\text{L} = 320\text{mL}$$

Step 2: Sol and gel formation; After the concentration was determined, 320 mL of distilled water added to a bicker and then 15g of the precursor material added while stirring. In this step the precursor solution was stirred at a speed 600rpm and temperature of 80ºC for 2hours and then adjusted the pH of the solution to 3-4 by adding NaoH slowly and then measured using pH meter. After obtained the required level of pH, the solution got heat to the designated reaction temperature while stirring continuously then maintained the reaction temperature and stirring for the specified reaction time of 2hours.

As (Milani et al., 2020) studied pH significantly affects the particle size, morphology, and phase composition of the final alumina product, with lower pH values generally leading to smaller particles and a greater tendency towards the formation of the γ-alumina phase, while higher pH levels promote larger particles and the formation of the boehmite phase. pH level of 3-4 produced a particle size of 20nm to 40nm.A homogeneous solution was formed due to aluminum salts (aluminum nitrate nonahydrate, aluminum chloride, or aluminum sulphate) was fully dissolved in water and dissociated in to aluminum ions (Al^{+3}) and nitrate, sulfate, or chloride ions. Aluminum nitrate nonahydrate was used as precursor material for Sample one (S_1), Sample two (S_2), and Sample three (S_3). Aluminum sulfate was used as a precursor material for Sample four (S_4), Sample five (S_5), and Sample six (S_6). For the remaining three samples Aluminum chloride was used under the same Stirring parameter, the same concentration, and pH level of 4 as shown in Table 3.3. below. The hydrolysis equation of the three precursor materials is shown in the equation below.

Hydrolysis equation of aluminum nitrate nonahydrate

$$Al\ (NO3)_3.9H_2O\ (s) + H_2O\ (l) \rightarrow Al^{3+}\ (aq) + 3NO_3^-\ (aq) + 9H_2O\ (l) \quad \text{Eq.(3.2)}$$

Hydrolysis equation of aluminum sulfate

$$Al_2\ (SO_4)_3\ (s) + H_2O\ (l) \rightarrow 2Al^{3+}\ (aq) + 3SO4^{2-}\ (aq) \quad \text{Eq. (3.3)}$$

Hydrolysis equation of aluminum chloride

$$AlCl_3\ (s) + H_2O\ (l) \rightarrow Al^{3+}\ (aq) + 3Cl^-\ (aq) \quad \text{Eq.(3.4)}$$

Step 3: Washing and drying; In this step the precipitated gel was washed with the deionized water to remove impurities. By centrifuging again, the sample to collect the solid if any remain and then dry all the collected solids together in an oven or furnace at temperature of 1000° C for 24hours. As Bokov et al., (2021) and Dunn & Lan, (2020) studied washing and drying are crucial steps as they remove excess solvent and byproducts from the gel, allowing for the formation of a stable, well-defined structure with desired properties in the final product, significantly impacting the material's porosity, density, and mechanical strength; the drying process, especially, needs careful control to minimize maintain the desired property.

As per Rogojan et al., (2011) the drying temperature and time was specified to be 100ºC and 24hours respectively. When precursor solution started drying, the water started evaporating. It finally provided a solid form of the precursor material. After solid aluminum nitrate nonahydrate, aluminum sulfate, and aluminum chloride obtained, thermal decomposition happened by the applied temperature. First to lose the water of hydration and then breaking down the salts. A simplified reaction for the decomposition reaction is;

$$\mathrm{Al(NO3)3} \rightarrow \mathrm{Al2O3(s)} + 6\mathrm{NO2}(g) + 1.5O2(g) \qquad \text{Eq. (3.5)}$$

$$Al2(SO4)3.(s) \rightarrow Al2O3\ (s) + 3SO3(g) \qquad \text{Eq. (3.6)}$$

$$2AlCl3.H2O\ (s) \rightarrow Al2O3\ (S) + 6HCl(g) + 9H2O\ (l) \qquad \text{Eq. (3.7)}$$

Step 4: Calcination: The dried powder then calcined in a furnace at the designated temperature for the specified time based on each sample (800ºC, 1000ºC,1200ºC for 3hours,4hours, and 6hours) as it summarized in table 3.3 below and figure 3.3.

Then, the sample allowed to cool and maturate at room temperature before further analysis. This high temperature helped to completely decompose any remaining precursor material and promoted crystallization of alumina then lead to stable and defined aluminum structure. Shahraki et al., (2025),Yao et al., (2020), and Aldbea et al., (2025) have studied that calcination significantly affects the properties of alumina sol-gel by influencing its crystallinity, particle size, surface area, and phase transformation, with increasing calcination temperature generally leading to a more crystalline structure, larger particle size, reduced surface area, and a transition from the metastable gamma (γ) alumina phase to the stable alpha (α) alumina phase, impacting its suitability for different applications depending on the desired properties.

Table 3.3 Process parameters and their value

Process parameters kept constant during synthesis		**Samples**	**Precursor materials**	**Calcination Temperature (º C)**	**Calcination time (hrs.)**
Concentration	0.125M	**Sample 1**	Aluminum nitrate	800	3
Solvent	Distilled Water	**Sample 2**	Aluminum nitrate	1000	4
Stirring temperature	80ºC	**Sample 3**	Aluminum nitrate	1200	6
Stirring time	2hrs.	**Sample 4**	Aluminum sulfate	800	4
Stirring speed	600rpm	**Sample 5**	Aluminum sulfate	1000	6
pH level	4	**Sample 6**	Aluminum sulfate	1200	3
(Base used) pH adjuster	NaoH	**Sample 7**	Aluminum chloride	800	6
Drying temperature	100ºC	**Sample 8**	Aluminum chloride	1000	3
Drying time	24hrs	**Sample 9**	Aluminum chloride	1200	4

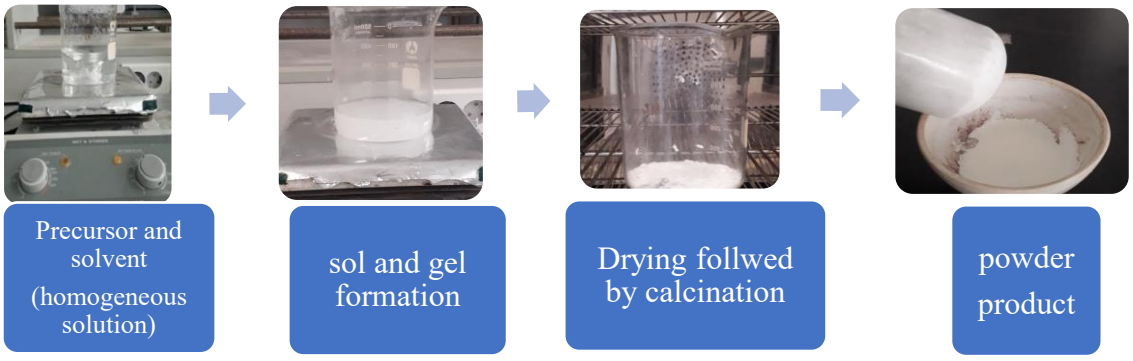

Figure 3.3 Sol-gel process synthesis method sequence

3.1.4.4 **Characterization of each sample:**

Structural analysis: X-ray diffraction (XRD) methods stand out for their ability to determine a material's crystal structure. Unlike techniques focusing on elemental composition, XRD identifies chemical compounds through their unique crystalline arrangement. This enables the differentiation of various compounds or phases, even those composed of the same elements. In this investigation, XRD was specifically used to analyze the crystalline size and phase of the nanoparticle samples. The measurement conditions used for the XRD characterization of all sample was:

X-ray tube:

- target= Cu
- voltage=40.0(KV)
- Current= 30.0(mA)

Slits:

- Divergent slit=1.00000(deg)
- Scatter slit=1.00000(deg)
- Receiving slit=0.30000(mm)

Scanning:

- Device axis=Theta -2Theta
- Scanning range=10.000-90.000
- Scanning mood=continuous scan
- Scan speed=4.0000(deg/min)
- Sampling pitch=0.0200(deg)
- Present time= 0.30(sec)

Morphological analysis: (Leng & Wiley, n.d.) (2008) described the morphology of the synthesized nanoparticle from each experimental combination will be analyzed using SEM to determine particle size, shape, and distribution. The scanning electron microscope (SEM)is the most widely used type of electron microscope.

It examines microscopic structure by scanning the surface of materials, similar to scanning confocal microscopes but with much higher resolution. **Thermal stability analysis:** This analysis was conducted to determine the thermal stability of the nanoparticles using TGA to assess their weight loss behavior at elevated temperatures for each sample. Thermal analysis (TA) is a group of analytical techniques that measure properties or property changes of materials as a function of temperature. Changes in materials properties with temperature are considered as thermal events. Possible thermal events of a solid was reviewed by increasing its temperature from absolute zero (zero Kelvin).

3.1.5 Data analysis and optimization:

Signal -to-Noise ratio (S/N): The S/N ratio was calculated for each experiment based on the desired response using Minitab software of Taguchi coupled coupled with Gray relational Analysis (GRA). Analysis of Variance (ANOVA): ANOVA was conducted to determine the significance of each factor and their interaction with their response. Optimal parameter settings: Identify the optimal level of each factor that maximize the S/N ratio and achieve the desired properties.

3.1.6 Interpreting the result:

After conducting the experiments and analyzing the data, the interpretation of the result was interpreted for better understanding the complex interplay of the process parameter and their impact on the properties of the synthesized alumina nanoparticles. The following breakdowns are the basic way to interpret the result.

3.1.6.1 Characterization data:

By analyzing the XRD data to determine the crystalline size and phase of the nanoparticles. Analyzing the SEM image to understand the particle size, shape and distributions. Analyzing the TGA data to assess the thermal stability of the nanoparticles basically mass loss of each sample.

3.1.6.2 Analysis of variance (ANOVA)

Significant factor: From ANOVA the factor that significantly influenced the desired response obtained and this highlighted the most important parameter to control for achieving the desired properties. Optimal level: This analysis provided a starting point for optimizing the synthesis process by properly determining the optimal levels of each factor that maximize the S/N ratio and achieve the desired properties.

3.1.6.3 Signal-to-Noise ratio (S/N)

A higher S/N ratio indicates that more robust process, but less susceptible to variations and the vice versa. Optimization: The optimal level of factors is those that maximize the S/N ratio indicating the most robust and efficient process settings.

CHAPTER FOUR

RESULTS AND DISCUSSIONS

4.1 Characterization results

The synthesized alumina nanoparticle was characterized using X-ray diffractometer (XRD), Thermogravimetric analyzer (TGA), and Scanning electron microscopy (SEM). The characterization result provided a crucial bridge between material synthesis/processing and understanding its properties and performance. These results obtained using the characterization and its optimization revealed key aspects of material's structure, composition, phase, the crystallite size, its thermal stability and other characteristics. Discussing these characterization findings is essential because it allowed us to validate the synthesis process, explain observed behaviors, ultimately their recommended application area.

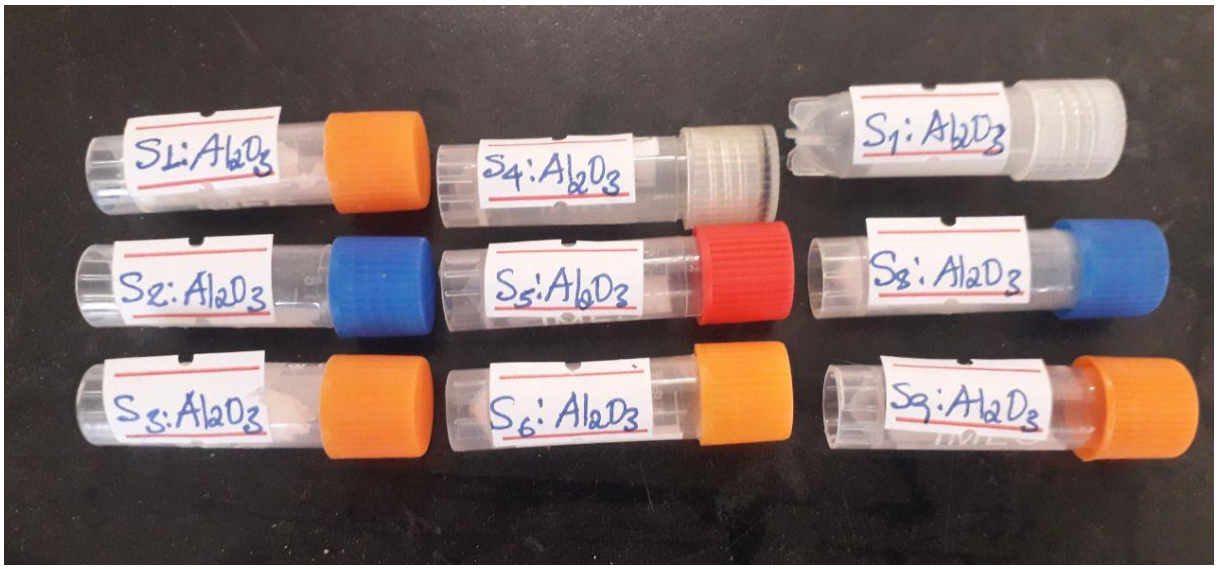

Figure 4.1 The synthesized samples

4.1.1 X-ray diffractometer (XRD) Results and analysis

X-ray diffraction (XRD), a powerful tool for analyzing crystalline structures, was used in this research to examine the synthesized alumina nanoparticles as shown in figure 4.1 above. This analysis provided crucial information about their phase composition, identified by comparing the XRD patterns to standard references, and their average crystalline size, estimated using the Scherrer equation based on peak broadening. Controlling these structural features (phase and size) is vital for optimizing alumina properties for specific uses.

Therefore, the XRD results were used to assess how effectively the synthesis method-controlled crystallite size and to correlate these structural details with the synthesis conditions. Comparing results across samples allowed for an evaluation of how different processing parameters influenced the final crystalline properties, demonstrating the level of control achieved. The findings or the XRD results presented and discussed below which provided a crucial information on a detailed structural characterization of the synthesized alumina nanoparticles and their relationship to the synthesis parameters. This study focused and analyzed the phase and the crystallite size of the synthesized nanoparticles using XRD.

The XRD result gave an information about the phase of the synthesized nanoparticle and its crystalline size as per the desired property needed to investigate. Based on (Kaur et al., 2020) in reference to Joint Committee on Powder Diffraction Standards (JCPDS) stated the angles (2Θ) at which different peaks are formed. XRD patterns which exhibit broad peaks centered at 36.9° (δ), 37.0º, 32.6°, 37.2°,45.7°,45.4°, 66.3°, 37.4°, 39.6°, 45.8°, 60.7°,61.0° and 66.7° are indexed to both γ and δ alumina phases. Some peaks exhibited a mixture of two phases at 31.9° (γ/δ), 45.8° (γ/δ), and 66.9° (γ/δ), 39.7° (γ/δ), 45.7° (γ/δ), 59.7° (α/ θ), 61.1° (α/ θ), 60.7° (γ) and 67.0° (γ/δ). Small peaks at 32.8°, 36.7°, 46.6°, 50.7°, 60.1° and 67.2° showed as the result of δ and θ phase of alumina. XRD peaks at 25.6°, 35.1°, 37.8°, 41.6°, 43.3°, 52.5°, 57.5°, 66.5° and 68.2° are forms due to the formation of α phase with small peaks appeared at 32.6°, 36.7°, 38.9°, 54.3°, 64.0° and 67.3° corresponding to θ phase.

Formation of different phase

As (Kaunisto et al., 2023) studied, the alumina transformation highly depends on different process parameters like precursor materials and the heating rate. γ-Alumina develops at relatively low temperatures, typically between 300 and 500 °C, and remains stable below 700–800 °C. As the temperature increases, it transitions into the δ and θ phases at approximately 800–900 °C and 900–1100 °C, respectively, before finally converting into the stable α phase at around 1150 °C.

4.1.1.1 XRD result and analysis for sample 1

In figure 4.2 the XRD pattern of sample 1 shows that it's crystalline structure and the main three peaks appeared at 67.5º, 66.8 º, and 31.5º which indicated that the presence of both Θ and δ and the crystallite sizes are, 11.2nm, 12.5nm, and 38.2nm respectively which is calculated using Scherrer equation. With this the average crystallite size is 20.6nm as shown in Table 4.1. All the nine samples were synthesized based on the design of experiment and sample 1 was synthesized using Aluminum nitrate nonahydrate as a precursor material and calcinate at temperature of 800ºC for about 3hours. Kept other (i.e. Concentration, solvent, stirring temperature, stirring time, stirring speed, pH level, pH level, drying temperature, and drying time) process parameters constant.

Despite the fact that the X-ray diffraction (XRD) provides a wealth of information about a material's structure and composition, including its crystal structure, phase, and properties like grain size or crystallite size and strain, this study only used the XRD result to analyze the crystallite size of the nanoparticle synthesized and its phase. The XRD provided an information about the phase of alumina nanoparticle under the first run of the experiment as Θ and δ basically due to these phases developed in the temperature range of 800ºC-900ºC. In this result impurities are observed that are formed during the process. These impurities expected to be formed due to the inefficacy of the synthesis process during the initial stage of the process at soliton formation. This is due to the purity of the distilled water itself, as result of its interaction with the environment. The other stage where impurity can be formed is, at the drying and calcination stage. During this stage of the process the sample could have been interacted with an element available in the oven (at the stage of drying) and furnace (at the stage of calcination) that are evaporated from the other sample. Some of them can also be inevitable byproduct of the process. The precursor materials also contributed for the impurity to exist, since it can be difficult to completely remove the nitrates during calcination and these ions can also decompose during calcination and leading to other contaminants. The processing equipment and environment also had an effect.

The basic strategies to minimize the impurities

The recommended strategies which are helpful to minimize the impurity and enhance the quality of the product are: high purity precursor materials, control the atmosphere, select the reaction vessel and crucible made inert materials (like quartz, platinum). Additionally, optimize calcination, and properly wash after gelation. By carefully considering these potential sources of impurities, the purity alumina synthesized by sol-gel method can be significantly improved.

Kaunisto et al., (2023) and Northwest et al., n.d.(2021) studied that theta alumina (θ-Al_2O_3) is a metastable form of alumina with various applications, particularly in catalysis and as a catalyst support. Its high surface area and specific physical and chemical properties make it suitable for adsorbing and catalytic processes. Additionally, it can be used as a substrate for metal catalysts in hydrogenation reactions, biomedical application, abrasive, high temperature application. Delta alumina, a metastable transition phase of aluminum oxide (Al_2O_3), finds applications in various fields including catalysis, adsorption, and as a catalyst support due to its unique properties like high surface area and specific surface energy. It's also used in the preparation of materials for biomedical applications, as a component in high-energy-density sodium-sulfur batteries, water purification, medical delivery, and medical device. Besides, the crystallite size (D) of the synthesized powder calculated using Scherrer equation as shown in equation 4.1 below.

$$D = \frac{K\lambda}{\beta COS\theta} \qquad \text{Eq. (4.1) (Fatimah et al., 2022)}$$

Where,

- D is the crystallite size,
- K is the shape factor (typically 0.89),
- λ is the X-ray wavelength,
- β is the Full width half maximum (FWHM) of the peak, and
- Θ is the Bragg angle.

Table 4.1 XRD results and crystallite size analysis of sample 1

S.N	2Θ	λ(nm)	FWHM (β) (rad)	Phase	$D = \frac{K\lambda}{\beta COS\Theta}$ (nm)	Average Crystallite size (nm)
1	67.5	0.138683	0.0133	Θ	11.2	20.6
2	66.8	0.1400	0.0119	δ	12.5	
3	31.5	0.30328	0.0073	Θ	38.2	

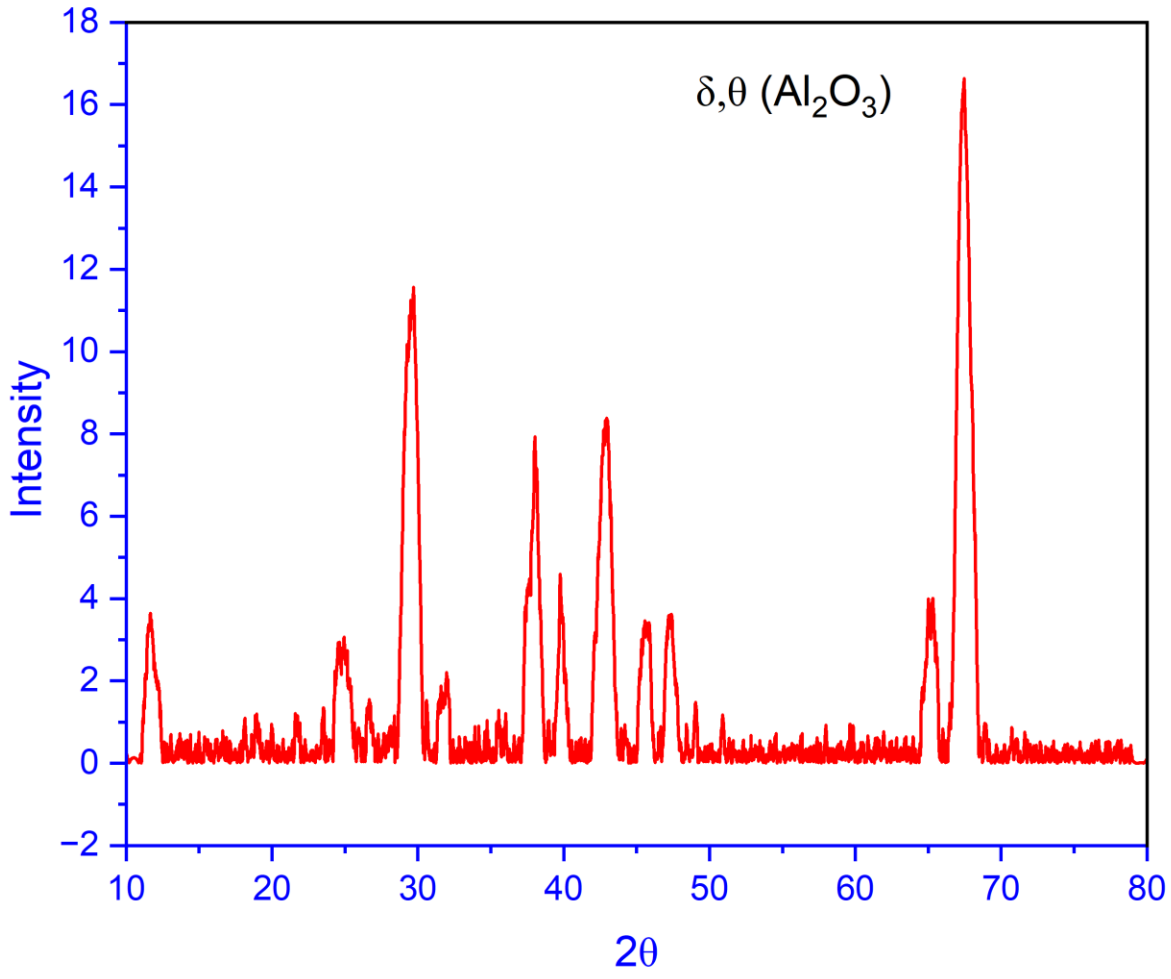

Figure 4.2 XRD graph for sample 1

4.1.1.2 XRD result and analysis for sample 2

As per figure 4.3 the XRD pattern of sample 2 shows that it's crystalline structure and the main three peaks appeared at 67º, 45.9 º, and 37.6º which indicated that the presence a mixture of γ/δ and formation of α and the crystallite sizes are, 5nm, 5.65nm, and 8.9nm respectively which is calculated using Scherrer equation. With this the average crystallite size is 6.5nm as shown in table 5 Sample 2 was synthesized using Aluminum nitrate nonahydrate as a precursor material and calcinate at temperature of 1000ºC for about 4hours. Kept other parameters (i.e. Concentration, solvent, stirring temperature, stirring time, stirring speed, pH level, pH level, drying temperature, and drying time) process parameters constant. In this XRD pattern, the phase obtained as a consequence of calcinating the powder at 1000ºC for about 4hours are the mixture of γ/δ and the early formation of α alumina.

A mixture of gamma (γ) and delta (δ) alumina, particularly from the transition alumina phases, is applied for their unique properties like high surface area, catalytic efficiency, and ability to support catalysts. These phases are especially important in catalysis, adsorption, and as precursors for ceramics as per the study done by (El-Sawaf et al., 2024). The basic application area for alpha alumina; abrasive, cutting tools and different machine parts, and refractory materials

Table 4.2 XRD results and crystallite size analysis of sample *2*

S.N	2Θ (deg)	λ(nm)	FWHM β (rad)	Phase	$D = \frac{K\lambda}{\beta COS\Theta}$ (nm)	Average Particle Size (nm)
1	67.0	0.139522	0.02975	γ/δ	5	6.5
2	45.9	0.1974	0.0343	γ/δ	5.65	
3	37.6	0.239	0.0252	α	8.9	

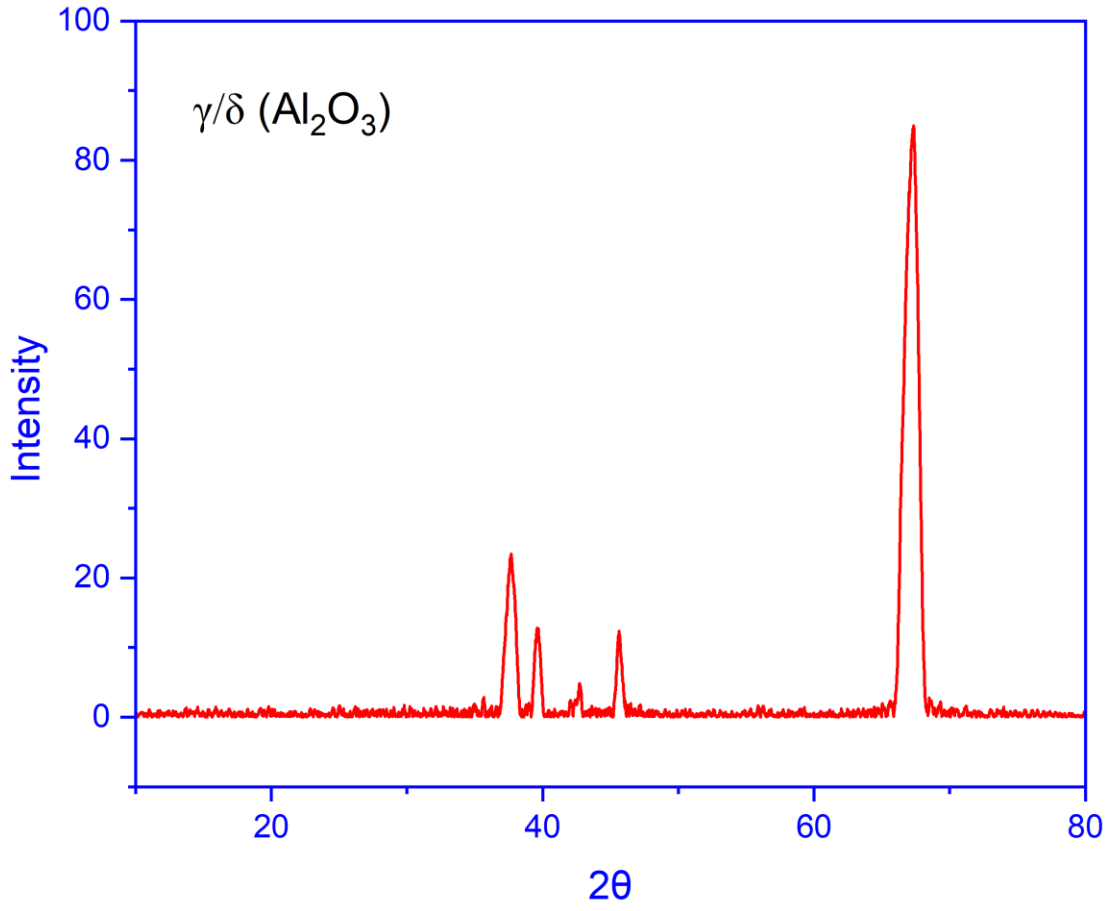

Figure 4.3 XRD graph of sample 2

4.1.1.3 XRD result and analysis for sample 3

In Figure 4.4 the XRD pattern of sample 3 confirms its crystalline nature and the prominent peaks observed at 43.5, 35.2°, and 57.6° showed the presence α phase taking the reference of the study done by (Kaur et al., 2020). The corresponding crystallite sizes, determined using the Scherrer equation, are 5 nm, 6 nm, and 6.4nm. The average crystallite size is approximately 5.8 nm, as listed in the table. Sample 3 was synthesized using aluminum nitrate nonahydrate and was calcinated at 1200°C for 4 hours.

All other process parameters, including concentration, solvent, stirring conditions, pH, drying temperature, and drying duration, were kept constant. As observed from the table 6 below, the crystallite size of the nanoparticle appeared to be uniform approximately and this is one of the privileges using the sol-gel method of synthesis. However, in this result impurities observed that are formed during the process. These impurities expected to be formed due to the inefficacy of the synthesis process during the initial stage of the process at solution formation.

As Kumar et al., (2014) and Mgal & Growth, (2017) studied that Corundum, a mineral composed of crystalline aluminum oxide (α -Al_2O_3), is extremely hard second only to diamond on the Mohs scale at level 9. It's the most stable phase of alumina and combination of toughness and thermal resilience makes it valuable in abrasives and other industrial settings. The basic application where alpha alumina is abrasive, cutting tools, bearing and other machine parts, refractory materials, and space application, hardening concert floors.

Table 4.3 XRD results and crystallite size analysis of sample 3

S.N	2Θ	λ(nm)	FWHM (β) (rad)	Phase	$D = \frac{K\lambda}{\beta COS\theta}$ (nm)	Average Crystallite Size (nm)
1	43.5	0.208	0.0396	α	5	5.8
2	35.2	0.254	0.039	α	6	
3	57.6	0.1589	0.0442	α	6.4	

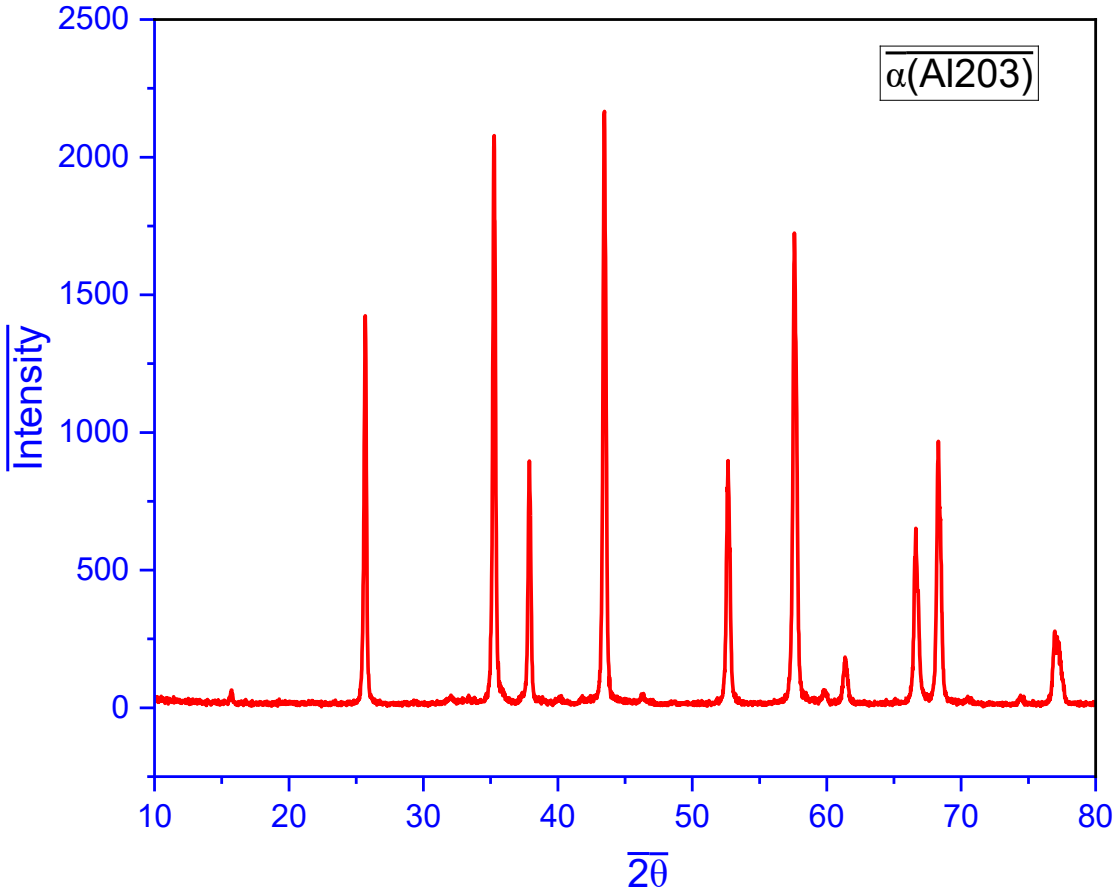

Figure 4.4 XRD graph of sample 3

4.1.1.4 XRD result and analysis for sample 4

The XRD pattern shown for sample 4 illustrates in the Figure 4.5 below as it is crystalline structure, with major diffraction peaks located at 67.4°, 66.6°, and 65.3°as shown in Table 4.4, indicating a mixture of γ/δ phases and early formation of Θ. Crystallite sizes calculated using the Scherrer formula are 5 nm, 5.65 nm, and 8.9 nm, with an average of 6.5 nm as recorded in the table. This sample was prepared using aluminum sulfate and subjected to calcination at 800°C for four 4 hours. All other synthesis parameters such as pH, concentration, solvent type, stirring details, and drying conditions remained unchanged.

A mixture of gamma (γ) and delta (δ) alumina, particularly from the transition alumina phases, is applied for their unique properties like high surface area, catalytic efficiency, and ability to support catalysts. These phases are especially important in catalysis, adsorption, and as precursors for ceramics. (Northwest et al., n.d.) and (El-Sawaf et al., 2024) theta alumina (θ-Al_2O_3) is a metastable form of alumina with many applications, particularly in catalysis and as a support for catalysts. Its high surface area and specific physical and chemical features make it effective for both adsorption and catalytic processes. It is also used as a substrate in metal-catalyzed hydrogenation reactions.

Table 4.4 XRD results and crystallite size analysis of sample 4

S.N.	2Θ	λ(nm)	FWHM(β)	Phase	$D = \frac{\kappa\lambda}{\beta cos\theta}$ (nm)	Average Crystallite Size (nm)
1	67.4	0.1388	0.0154	Θ	9.6	8
2	66.6	0.1403	0.0203	γ/δ	7.4	
3	65.3	0.1428	0.1428	Θ	7.2	

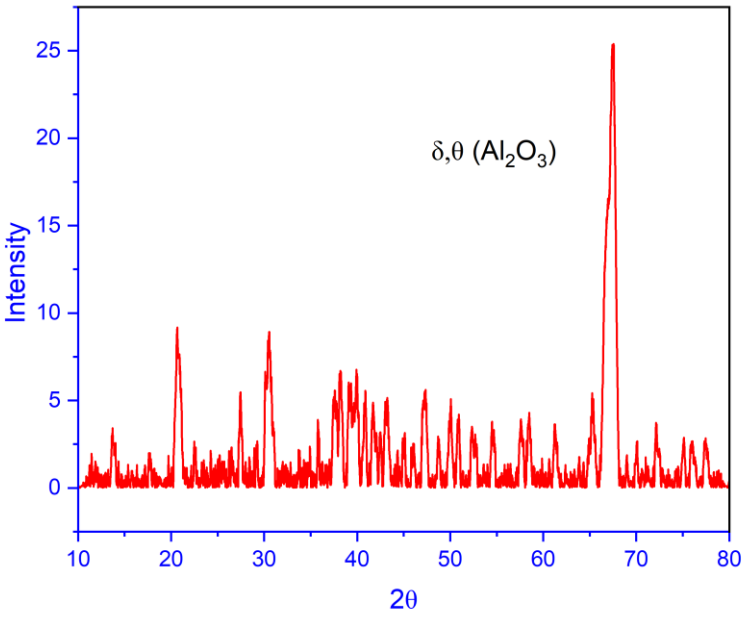

Figure 4.5 XRD graph of sample 4

4.1.1.5 XRD result and analysis for sample 5

According to the Figure 4.6 below, the XRD pattern of sample 5 displays a crystalline structure with three main peaks at 57.6°, 25.7°, and 67.4°. These peaks point to both phase Θ and α mixture and the formation of α phase. Using the Scherrer equation, the crystallite sizes are found to be 4.8 nm, 5.2 nm, and 10.6 nm, averaging around 6.6 nm, as detailed in table 8 below. Aluminum sulfate was used as the precursor, and the sample was calcinated at 1000°C for 6 hours. All other process conditions, such as concentration, solvent, pH, and drying/stirring parameters, were kept constant.

Howecer, an alpha phase also appeared in this sample and this could be due to the calcination time of 6 hours. Because, alpha alumina is expected when the Θ phase get transformed up on calcination by the temperature above 1150^{o}C. Despite the fact that the crystallite size was expected to be approximately uniform, it showed that the alpha phase is half of the theta phase.

As per the study done by the Northwest et al., n.d.(2021) and El-Sawaf et al., (2024) theta alumina (θ-Al_2O_3) is a metastable variant of alumina with numerous applications, particularly in the areas of catalysis and catalyst support.

Its elevated surface area and distinctive physical and chemical traits make it well-suited for adsorption and catalytic processes. Additionally, it can be used as a substrate for metal catalysts in hydrogenation reactions.

Kumar et al., (2014) and Mgal & Growth, (2017) studied that the crystalline aluminum oxide (α-Al_2O_3), is extremely hard, with a Mohs hardness rating of 9, placing it just below diamond. Being the most stable form of alumina, its toughness and ability to withstand high temperatures make it valuable in abrasive materials and numerous industrial applications. Common uses for alpha alumina include abrasives, cutting tools, bearings, machine parts, refractory materials, space applications, and in strengthening concrete floors.

Table 4.5 XRD results and crystallite size analysis of sample 5

S.N	2Θ	λ(nm)	FWHM (β) (nm)	Phase	$D = \frac{K\lambda}{\beta COS\Theta}$ (nm)	Average Crystallite Size (nm)
1	57.6	0.1395	0.0295	α	4.8	6.9
2	25.7	0.1964	0.0343	α	5.2	
3	67.4	0.249	0.0252	Θ	10.6	

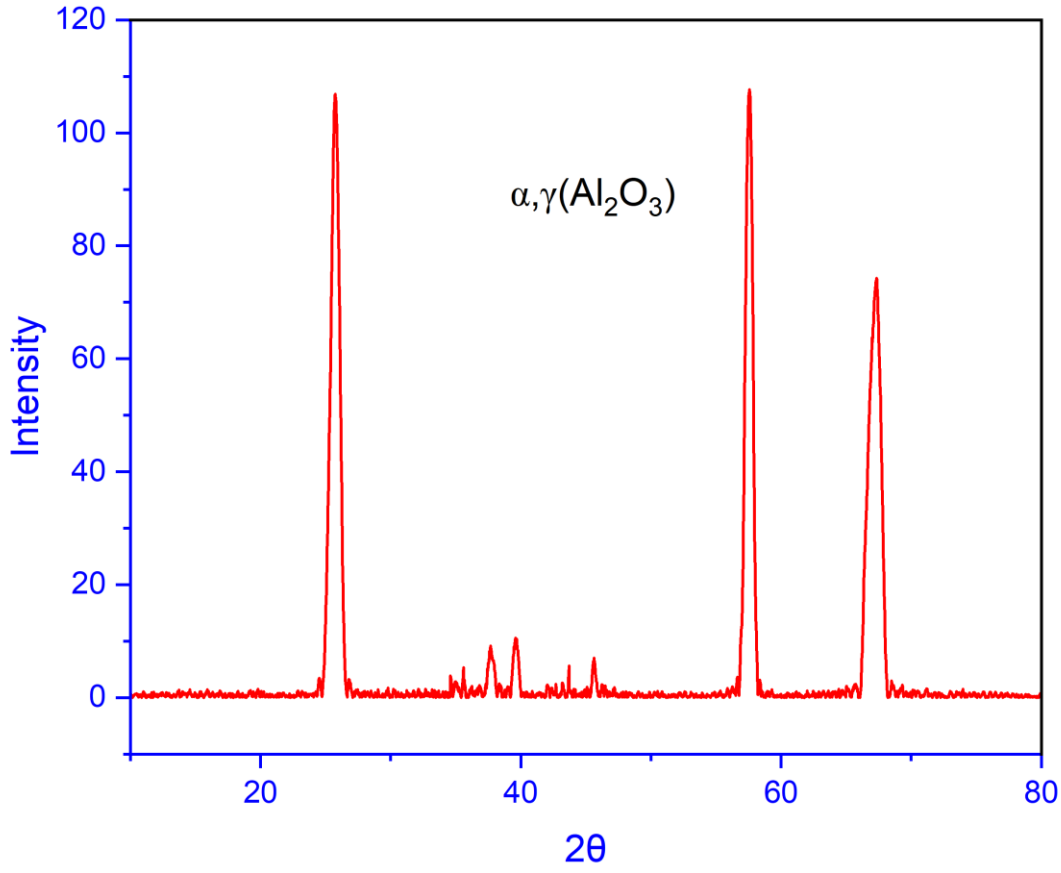

Figure 4.6 XRD graph of sample 5

4.1.1.6 XRD result and analysis for sample 6

The XRD results in Figure 4.7 below show for sample 6 indicate a crystalline phase, with significant peaks appearing at 43.5°, 35.2°, and 57.6°, formation of α phases. The crystallite sizes calculated through the Scherrer equation are 6.7 nm, 5.3 nm, and 3.6 nm, averaging to 5.2 nm as presented in the table. This sample was prepared using aluminum sulfate and underwent calcination at 1200°C for a period of 3 hours.

Corundum, a mineral made up of crystalline aluminum oxide (α-Al_2O_3), is incredibly hard, ranking second only to diamond on the Mohs hardness scale with a rating of 9. Typical uses of alpha alumina include abrasives, cutting tools, bearings, machine components, refractory materials, and space-related applications, as well as in hardening concrete floors based on the study of Kumar et al., (2014) and Mgal & Growth, (2017).

Table 4.6 XRD results and crystallite size analysis of sample 6

S.N	2Θ	λ(nm)	FWHM (β) (rad)	Phase	$D = \frac{K\lambda}{\beta COS\theta}$	Average Crystallite size Size (nm)
1	43.5	0.290	0.040	α	6.7	5.2
2	35.2	0.255	0.044	α	5.3	
3	57.6	0.16	0.048	α	3.6	

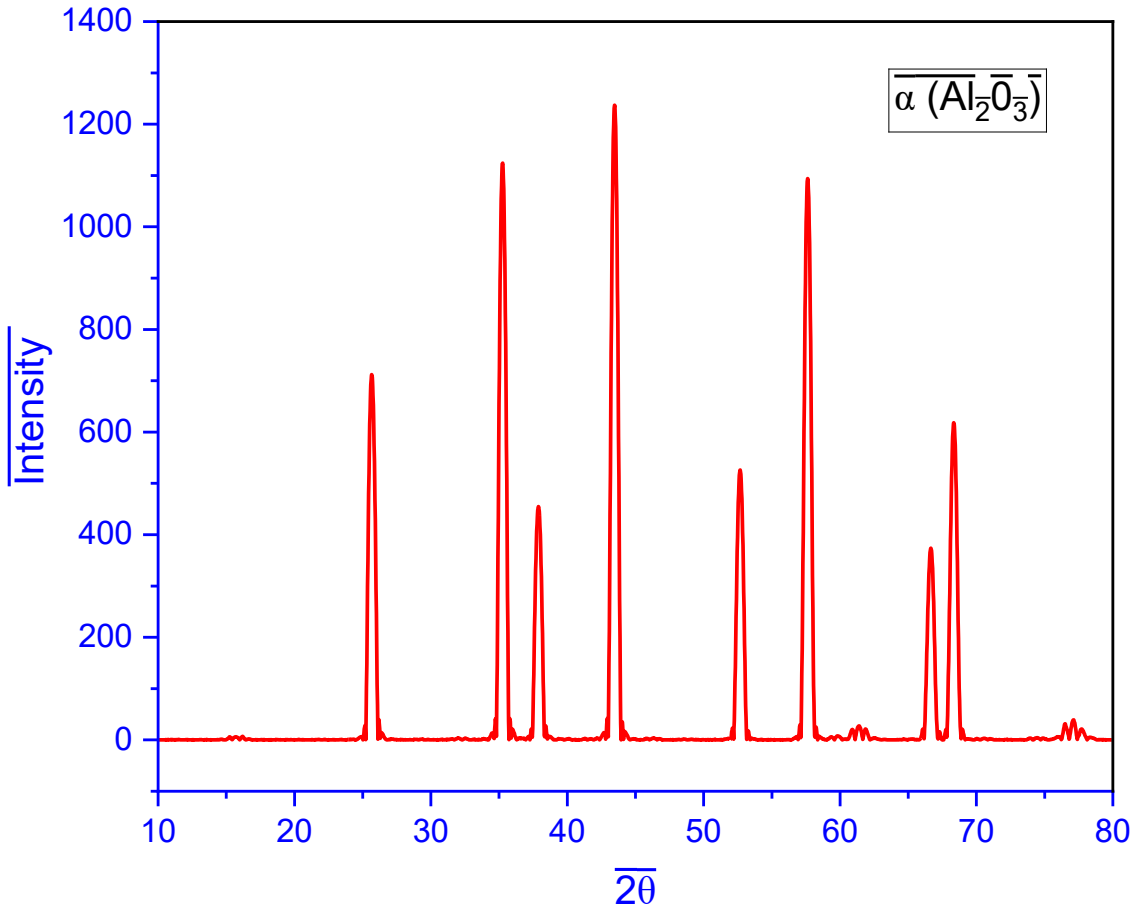

Figure 4.7 XRD graph of sample 6

4.1.1.7 XRD result and analysis for sample 7

As depicted in the Figure 4.8 XRD pattern for sample 7 revealed a crystalline form with dominant peaks at 29.4°, 45.9°, and 37.6°. These suggest the presence of γ/δ phases and α phase development. Crystallite sizes, determined by the Scherrer equation, are 21nm, 11.2nm, and 47.7 nm, giving an average of 26.5nm, as shown in the corresponding table. The sample was synthesized using aluminum chloride and calcinated at 800°C for four 6hours. The rest of the synthesis parameters were kept consistent, including pH, concentration, stirring conditions, and drying parameters.

As per Kaunisto et al. (2023), the transformation of alumina is highly affected by the process setup, particularly the choice of starting materials and how quickly the temperature rises. The γ phase of alumina forms between 300 and 500 °C, remaining intact under 700–800 °C. At higher temperatures, it transitions into δ and θ phases around 800–900 °C and 900–1100 °C, respectively, with final conversion into α-alumina happening close to 1150 °C. so, in this study the phase of the alumina nanoparticle existed in sample 7 is theta (Θ) which was calcinate at temperature of 800ºC despite it was expected to be δ phase. This could be due to the effect of other process parameter like the precursor material which is significant factor as it's showed in the optimization section. Besides,

Theta alumina (θ-Al_2O_3) is a metastable form of alumina with a variety of uses, especially in catalysis and as a catalyst support. Its high surface area and distinct physical and chemical properties make it ideal for adsorption and catalytic processes. It is also employed as a support for metal catalysts in hydrogenation reactions, biomedical (as corrosion resistance and biocompatibility),high temperature application, abrasive refractory ,materials based on the study of both (Northwest et al., n.d.) and (El-Sawaf et al., 2024).

Table 4.7 XRD results and crystallite size analysis of sample 7

S.N	2Θ	λ(nm)	FWHM (β) (nm)	Phase	$D = \frac{K\lambda}{\beta COS\Theta}$ (nm)	Average Crystallite Size (nm)
1	29.4	0.3028	0.0133	Θ	21	26.5
2	67.6	0.1387	0.0119	Θ	11.2	
3	20.2	0.382	0.0073	Θ	47.5	

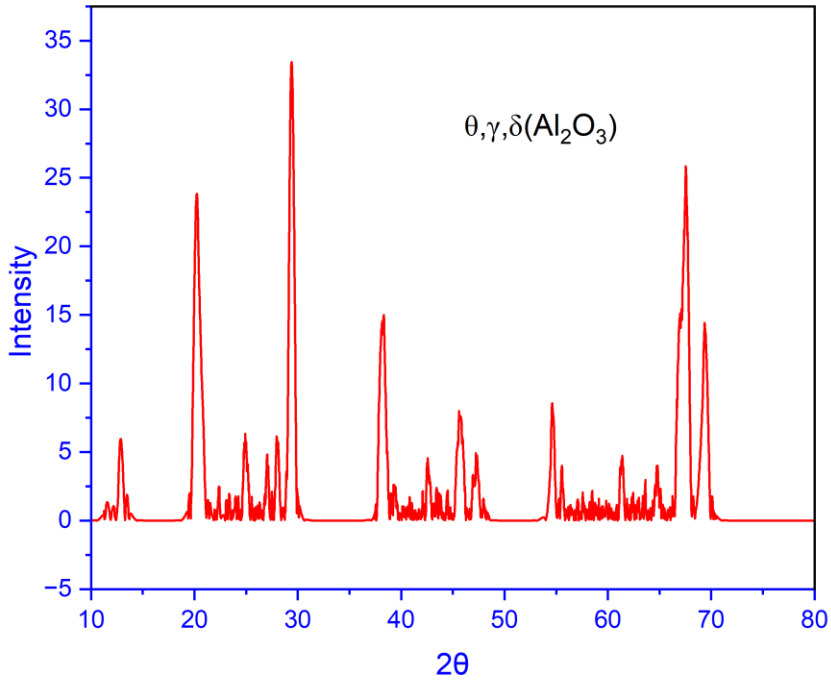

Figure 4.8 XRD graph of sample 7

4.1.1.8 XRD result and analysis for sample 8

Figure 4.9 shows that the XRD pattern for sample 8 demonstrated its crystalline character marked by key peaks at 67°, 45.9°, and 37.6°, which denote the coexistence of γ/δ and the appearance of α phase. Based on the Scherrer equation, the respective crystallite sizes are 9.6 nm, 6.2 nm, and 10 nm, with an overall average of 8.6nm, as illustrated in the Table 4.8. This sample was derived from aluminum chloride and underwent a calcination process at 1000°C for around 3 hours. All other parameters, including concentration, pH, solvent, and drying/stirring conditions, were held constant.

The phase observed in the XRD result of sample 8 are, a mixture of δ /Θ, Θ, and formation of α-phase at a calcination temperature of 1000°C. At this particular temperature Θ-phase is expected and the mixture of δ /Θ is also expected due to some of the delta phase can be left untransformed to theta due to the efficiency of the furnace, the precursor material and so on.

As Northwest et al., n.d.)and El-Sawaf et al., (2024) studied that the theta alumina (θ-Al_2O_3) is a metastable form of alumina with various applications, particularly in catalysis and as a catalyst support. Its high surface area and specific physical and chemical properties make it suitable for adsorbing and catalytic processes. Additionally, it can be used as a substrate for metal catalysts in hydrogenation reactions.

Delta alumina, a metastable transition phase of aluminum oxide (Al_2O_3), finds applications in various fields including catalysis, adsorption, and as a catalyst support due to its unique properties like high surface area and specific surface energy. It's also used in the preparation of materials for biomedical applications and as a component in high-energy-density sodium-sulfur batteries. A mixture of theta and delta alumina is commonly used as a catalyst or catalyst support due to their high surface area and specific properties based on the study done by Kaunisto et al., (2023) and Northwest et al., n.d.) .

As per the research by Kumar et al., (2014) and Mgal & Growth, (2017). crystalline aluminum oxide (α-Al_2O_3) and is known for its exceptional hardness, second only to diamond on the Mohs scale with a rating of 9. As the most stable phase of alumina, its strength and thermal durability make it ideal for abrasive products and a variety of industrial uses. Alpha alumina is typically used in abrasives, cutting tools, bearings, machinery components, refractory materials, space-related technologies, and for hardening concrete floors.

Table 4.8 XRD results and crystallite size analysis of sample 8

S.N	2Θ	λ(nm)	FWHM (β)	Phase	$D = \frac{K\lambda}{\beta COS\theta}$ (nm)	Average Crystallite Size (nm)
1	67.2	0.1389	0.0154	δ /Θ	9.6	8.6
2	70.8	0.124	0.00243	α	6.2	
3	20.6	0.246	0.022	Θ	10	

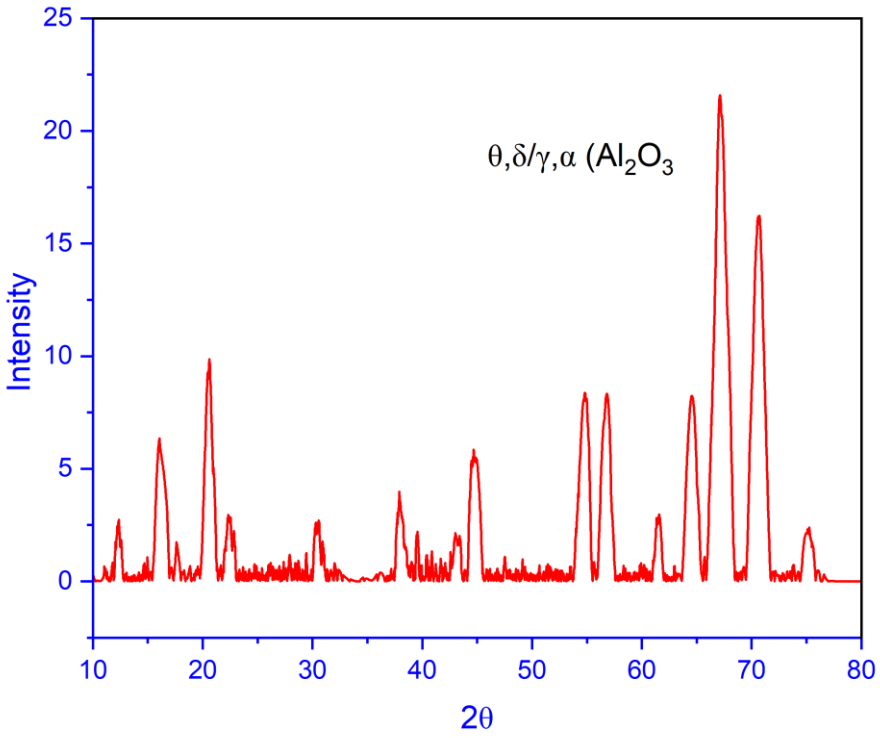

Figure 4.9 XRD graph of sample 8

4.1.1.9 XRD result and analysis for sample 9

In the Figure 4.10 the XRD pattern of sample 9 indicated a crystalline structure with three significant peaks at 43.4°, 35.2°, and 57.6°, suggesting a mix of γ/δ phases and the emergence of α phase. Scherrer equation calculations show crystallite sizes of 8.8nm, 6.7nm, and 4nm, with an average size of 6.5nm listed in the table. Aluminum chloride was used as the precursor, and calcination was carried out at 1200°C for 4 hours. All other processing factors like pH level, solvent, stirring, concentration, and drying settings remained unchanged.

As the per the study done by Kumar et al., (2014) and Mgal & Growth, (2017) Corundum is a crystal structure of aluminum oxide (Al_2O_3). It's the most stable form of alumina and ranks just below diamond on the Mohs hardness scale with a score of 9. Thanks to its exceptional hardness and heat resistance, it's widely used in industrial and abrasive tools. The application area is abrasive, cutting tool, bearing and other machined parts, refractory materials, optics and space application, optical components, artificial bones and hardening concert floors.

Table 4.9 XRD results and crystallite size analysis of sample 9

S.N	2Θ	λ(nm)	FWHM (β) (rad)	Phase	$D = \frac{K\lambda}{\beta COS\Theta}$ (nm)	Average Crystallite Size (nm)
1	43.4	0.288	0.040	α	8.8	6.5
2	35.2	0.266	0.044	α	6.7	
3	57.6	0.188	0.048	α	4	

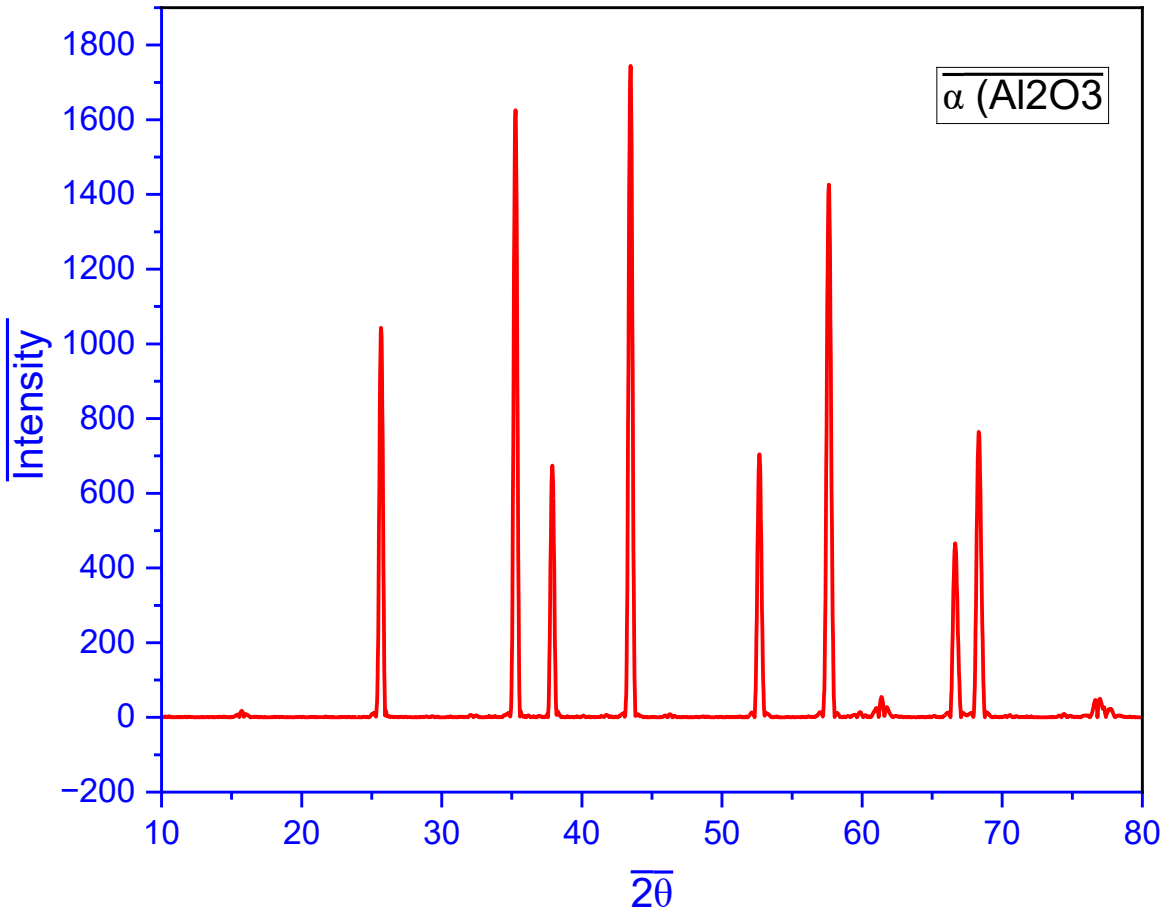

Figure 4.10 XRD graph of sample 9

4.1.2 Thermogravimetric result and analysis

The sol-gel synthesis method often results in alumina nanoparticles with residual organic components and adsorbed water. To determine the purity and thermal stability characterization was conducted. Thermogravimetric analysis (TGA) was performed to assess the thermal stability of the synthesized alumina nanoparticles. However, the focus of the study is to analyze the weight loss of each sample and optimized at which parameter combination would give the minimum weight loss. This thermal analysis required due to the fact that alumina is a ceramic material that has a very good at its thermal stability. The result of this TGA analysis presented and discussed below which provided insights into the thermal behavior of the synthesized nanoparticles.

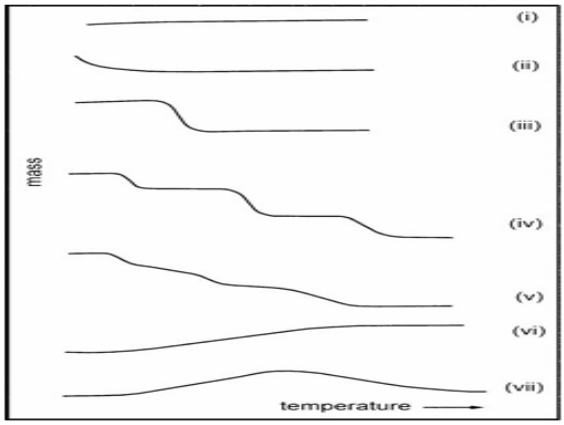

Figure 4.11 classification of thermogravimetric curve Leng and Wiley (n.d., 2008)

Interpretation of thermogravimetric curve curves

According to Leng and Wiley (n.d., 2008), the curves can be categorized into seven types, as illustrated in Figure 4.11 above. Type (i) shows a nearly flat line, suggesting no decomposition or loss of volatile substances across the temperature range. Type (ii) displays a sharp initial mass loss, often due to drying or desorption processes. Type (iii) features a single-stage decomposition, which is common and helps identify the material's thermal stability limit. Type (iv) represents a multi-stage decomposition with stable intermediate compounds. Type (v) also involves multi-stage decomposition but without stable intermediates and may result from higher heating rates compared to type (iv). Type (vi) indicates a chemical reaction involving mass gain. Lastly, type (vii), which is uncommon, shows an initial mass gain followed by a mass loss at higher temperatures.

4.1.2.1 Thermogravimetric analysis (TGA) of sample 1

Interpretation of thermogravimetric analysis (TGA) graph is vital for understanding the thermal stability and behavior of material as it heated. A TGA measures the change in mass of a sample as a function of temperature under controlled atmosphere.

Understanding the TGA graph components: X-axis represents the temperature as it is more informative for understanding materials properties. Y- axis represents the mass of the sample which indicated that the actual mass being lost. TGA curve is the primary curve on the on the graph and displayed the mass loss (or gain) as the temperature changes. It generally slopped downwards because materials usually lose mass as they decompose or release volatile components.

Steps for interpreting a TGA graph.

Identification number of decomposition stage: The distinct steps or drops in the TGA curve shown in Figure 4.12 typically represents the loss of a specific component of particular decomposition process. As shown in the graph below, the it showed a sharp initial mass loss after a short constant beginning due to drying and/or desorption process. The TGA graph of sample 1 most likely related to the single step decomposition process. It began with horizontal and drop down then flattened again.

Determination of temperature range of each stage: For each stage the onset temperature (the temperature at which the mass loss begins) and the offset temperature (the temperature at which the mass loss ends) was identified. From the temperature range of 0-50^{o}C (zero slop) the graph was constant then from 50^{o}C- 465^{o}C it dropped down (negative slop), finally it flattened again (zero slop) starting from 465^{o}C -800^{o}C and becoming stable with certain fluctuation.

Calculation of the percentage mass loss: The total percentage of mass loss was calculated using the mass/weight loss and the initial sample mass used. This provided useful information how much of the sample by weight or mass lost in that particular decomposition step. The percentage of mass loss can be calculated in every stages though as per the interest of this study only the total mass lose percentage was calculated. The total mass loses found to be 5.70% at which the temperature was limited up to 800^{o}C. The smaller the mass lose shows the ability the ceramic material to resist the particular temperature due to their good response to heat.

Above 800ºC oxidation decomposition expected to happened where the metal oxide started to decompose.

$$\%\ mass\ loss = \frac{actual\ mass\ loss}{initial\ mass} \qquad \text{Eq.4.2}$$

$$\%\ mass\ lose = \frac{0.92}{16.2} = 5.70\%$$

Possible decomposition events and temperature ranges identification: As per the study done by Yang et al., (2021) and Bawa et al., (2017) aluminum salt precursors undergoes decomposition at different temperature up to 1200ºC. The possible decomposition events and their temperature range are mentioned. Below 200ºC water loss happened. Different hydrates lost water at distinct temperatures. At the temperature range of 200ºC-600ºC organic decomposition happened. Residual solvents that were used in synthesis process. Above 400ºC inorganic decomposition happened like sulfate, chlorite, and nitrate decomposition. At the temperature above 800ºC oxidation decomposition happened and some metal oxides decomposed at a very high temperature.

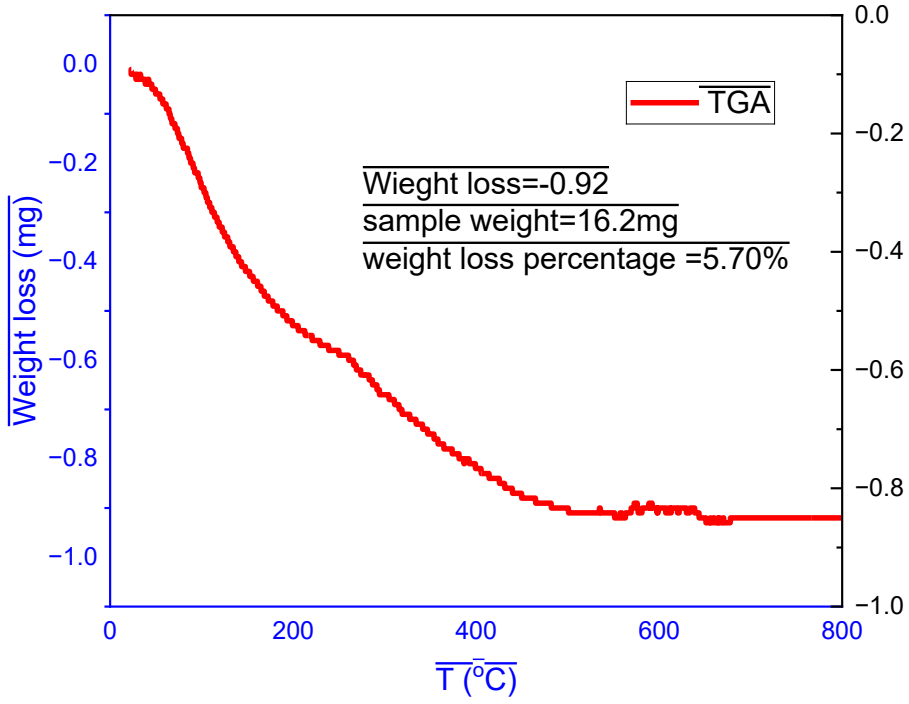

Figure 4.12 TGA graph for sample 1

4.1.2.2 Thermogravimetric analysis (TGA) for Sample 2

Identifying decomposition stages: The individual drops or steps in the TGA curve shown in Figure 4.13 below signified the loss of a particular component during a specific decomposition phase. Aa shown in Figure 4.13, the graph indicated that exhibited the first stage decomposition. First it has got a short constant move up to a temperature of 37ºC and then experienced a very rapid mass loss as it showed in the graph with negative slope up to a temperature of 482ºC. Later, from temperature 482ºC-679ºC started to get flatten with some fluctuation. Finally, after the temperature 679ºC the graph became smoothly horizontal and showed very stable.

Identification of temperature ranges for each stage: For each phase, the onset temperature (where mass loss starts) and the offset temperature (where mass loss ends) were determined. These are the temperatures at which the curve begins to deviate from a plateau and then flattens again. The temperature range for each stage has been discussed above. The first stage with zero slope stayed up to only temperature level of 37ºC. The second stage characterized by its negative slope and possessed in the temperature range of 37ºC-482ºC. And, the final stage has got a temperature range of 482ºC-800ºC

Calculation of the mass lose at each stage: The percentage of weight reduction at each decomposition step was found by dividing the mass lost by the initial sample mass, indicating the proportion lost during that specific stage. The mass loss percentage can be determined at each stage; however, for the purpose of this study, only the total mass loss percentage was considered. The total mass loss was calculated to be 5.70% when the temperature reached a maximum of 800°C. A smaller mass loss indicates the ceramic material's capacity to withstand the given temperature due to its strong heat resistance. Beyond 800°C, oxidation decomposition is anticipated, where metal oxides begin to break down.

$$\%\ mass\ loss = \frac{actual\ mass\ loss}{initial\ mass} \quad \text{Eq.4.2}$$

$$\%\ mass\ lose = \frac{0.86}{14.33} = 6\%$$

Identification of decomposition event: The study by Yang et al. (2021) and Bawa et al. (2017) identifies various decomposition events of aluminum salt precursors at temperatures up to

1200°C. These events are categorized within specific temperature ranges. Below 200°C, water loss occurs. Between 200°C and 600°C, organic decomposition takes place, including the removal of residual solvents used during synthesis. Above 400°C, inorganic decomposition such as sulfate, chloride, and nitrate breakdown occurs. Finally, at temperatures above 800°C, oxidation decomposition happens, causing certain metal oxides to decompose at very high temperatures.

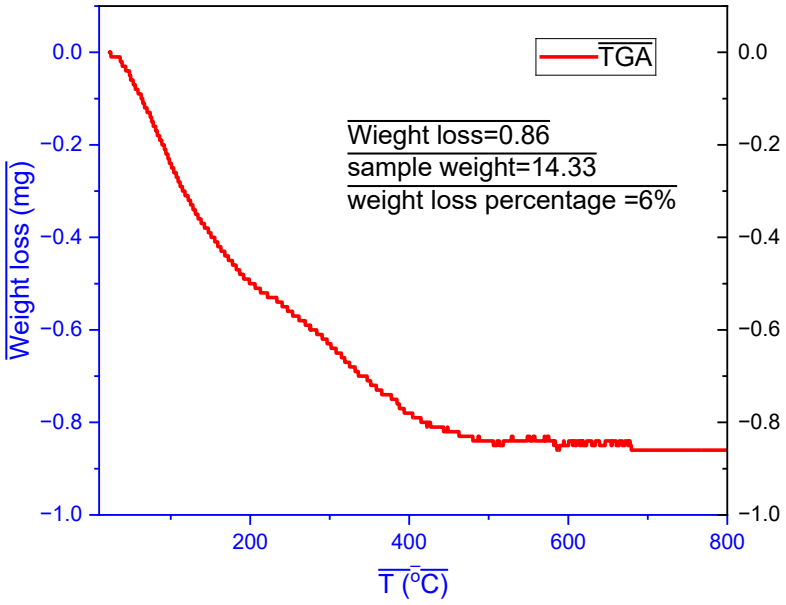

Figure 4.13 TGA graph for sample 2

4.1.2.3 Thermogravimetric analysis (TGA) for Sample 3

Identification of decomposition phases: The clear drops or stages on the TGA curve typically indicate the removal of a specific component during a distinct decomposition process. The TGA graph shown in Figure 4.14 provided an information that the material experienced the single stage decomposition process. First, it started with a zero slope and then rapidly dropped the mass for a wide range of temperature. Finally, it started to be flattened for the rest of the temperature.

Determining the temperature range for each phase: For each stage, the temperature at which mass loss begins (onset) and ends (offset) was identified. These points correspond to when the curve deviates from a flat region and returns to it.

The first phase with zero slope happened up to a temperature of 36ºC and then started to drop (negative slope) from 36ºC -518ºC. Finally, the temperature range at which the graph came to stability is beyond 518ºC up to 800ºC.

Calculation of the mass lose at each stage: To determine how much material was lost by weight during each decomposition phase, the total percentage mass loss was calculated using the measured weight reduction and the starting sample mass. Although mass loss can be calculated at each stage, this study focused only on the total percentage of mass loss. The total mass loss was found to be 5.70% when the temperature was capped at 800°C. A lower mass loss suggests the ceramic material's ability to resist high temperatures due to its excellent thermal stability. Above 800°C, oxidation decomposition is expected, leading to the breakdown of metal oxides.

$$\%\ mass\ loss = \frac{actual\ mass\ loss}{initial\ mass} \quad \text{Eq.4.2}$$

$$\%\ mass\ lose = \frac{0.84}{15.60} = 5.40\%$$

According to research by Yang et al. (2021) and Bawa et al. (2017), aluminum salt precursors undergo decomposition at various temperatures, with a range extending up to 1200°C. The decomposition events are associated with specific temperature ranges. Below 200°C, water is lost from both loosely bound surface water and chemically bound water within hydrates. Different hydrates lose water at distinct temperatures. Between 200°C and 600°C, organic materials decompose, including the evaporation of residual solvents from the synthesis process. Above 400°C, inorganic components such as sulfates, chlorides, and nitrates decompose. At temperatures exceeding 800°C, oxidation decomposition occurs, and certain metal oxides break down at very high temperatures.

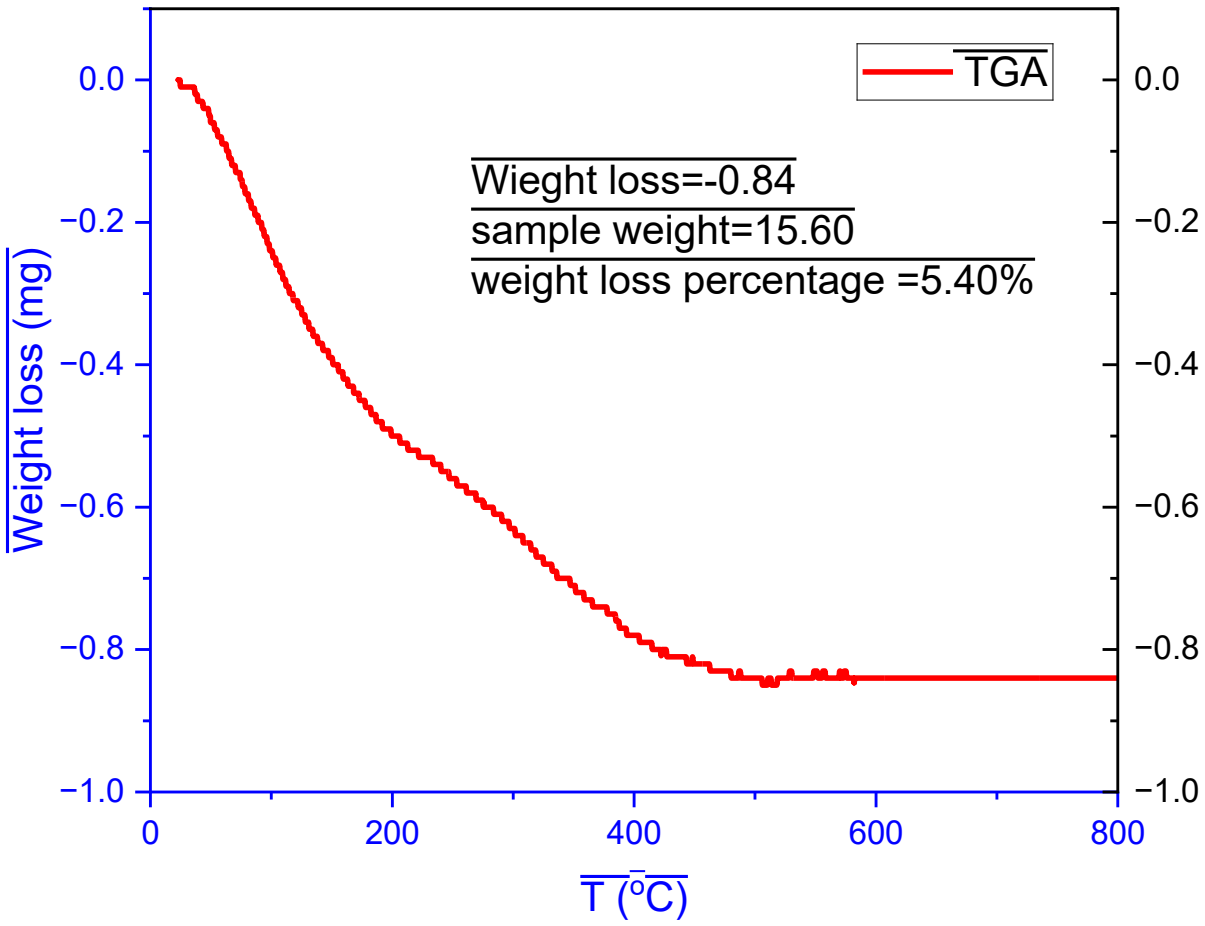

Figure 4.14 TGA graph for sample 3

4.1.2.4Thermogravimetric analysis (TGA) for Sample 4

Identification of decomposition stages: The various steps or declines observed in the TGA curve generally correspond to the loss of a particular component during each decomposition step. As shown in the TGA graph of Figure 4.15, it resembled most likely to multi stage decomposition stage based on the reference of Figure 4.15 above. In its first phase, it was horizontal and then rapidly drop down with negative slope. Later, it dropped suddenly vertically down then flattened for some range of temperature. Finally, it then started to gain a mass till it became flattened.

Temperature range identification for each stage: The temperature at which mass loss begins (onset) and ends (offset) was specified for each stage. These are the temperatures at which the curve moves away from a plateau and later returns to it. The temperature ranges the multi stage decomposition happened is, the first flattened stage happened up to 45^{o}C then started to drop rapidly from 45^{o}C-480^{o}C. For the range between 480^{o}C-679^{o}C, it became horizontal again with some instability. At 680^{o}C, the graph dropped down vertically then from 720^{o}C it started gaining mass till it became to flatten around 770^{o}C.

Calculation of the mass lose at each stage: The percentage mass loss for each stage can be calculated from the weight lost relative to the initial sample mass, showing the fraction decomposed in that step. While the mass loss percentage can be evaluated at each stage, this study only calculated the total mass loss. The total mass loss was determined to be 5.70% at a temperature limit of 800°C. A lower mass loss indicates the ceramic material's ability to resist temperature changes, reflecting its good heat resistance. Exceeding 800°C, oxidation decomposition is likely to occur, where metal oxides begin to decompose.

$$\%\ mass\ loss = \frac{actual\ mass\ loss}{initial\ mass} \quad \text{Eq.4.2}$$

$$\%\ mass\ lose = \frac{0.836}{17.72} = 4.90\%$$

As outlined in studies by Yang et al. (2021) and Bawa et al. (2017), aluminum salt precursors experience decomposition at various temperature points, reaching up to 1200°C. The decomposition events occur within specific temperature ranges. Below 200°C, water loss takes place, including both loosely bound water on the surface and the hydration water chemically integrated within the crystal structure. Different hydrates release water at different temperatures. From 200°C to 600°C, organic decomposition happens, involving the release of solvents from the synthesis process. Inorganic decomposition, including the breakdown of sulfates, chlorides, and nitrates, occurs above 400°C. Finally, above 800°C, oxidation leads to the decomposition of certain metal oxides at extremely high temperatures.

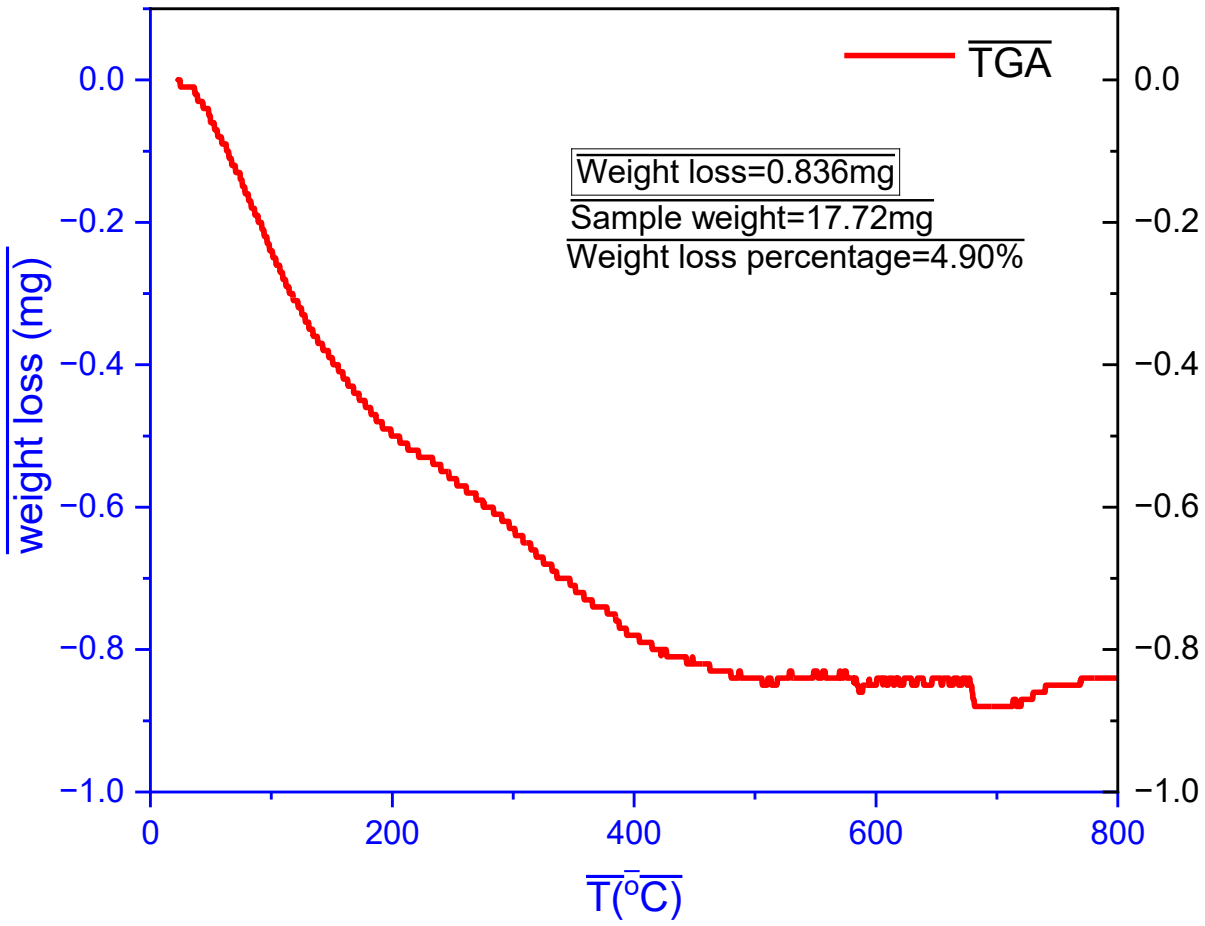

Figure 4.15 TGA graph for sample 4

4.1.2.5 Thermogravimetric analysis (TGA) for Sample 5

Identification of stages of decomposition: The noticeable drops or steps in the TGA curve usually represent the loss of a specific component in a particular decomposition event. The TGA graph displayed that a very sharp initial mass loses with some instability, often due to drying and/or decomposition process and then tried to be flattened by gaining some mass for some temperature ranges.

Identifying the temperature range for each stage: The onset temperature (the point where mass loss begins) and the offset temperature (the point where mass loss ends) were recognized for each stage.

These temperatures mark the points where the curve shifts away from and then returns to a plateau. The material experienced an initial rapid mass loss as shown in the TGA graph below up to the temperature of 249ºC. Then later, the graph stared to be horizontal with some fluctuation till it became horizontal. During this temperature interval of 250ºC-800, it gained a mass then got stable before the temperature reached 800ºC. The mass gained after a certain loss is due to the impurities and reaction happened in different stage of the process.

Calculation of the mass lose ate each stage. We determined the proportion of mass lost at every decomposition stage by calculating the percentage change based on the initial sample weight and the measured weight decrease. In this study, only the total mass loss percentage was calculated, though it can be determined at each stage. The total mass loss was recorded as 5.70% when the temperature reached 800°C. A smaller mass loss indicates that the ceramic material has a high resistance to heat. When the temperature exceeds 800°C, oxidation decomposition is expected, causing the metal oxides to break down.

$$\%\ mass\ loss = \frac{actual\ mass\ loss}{initial\ mass} \qquad \text{Eq.4.2}$$

$$\%\ mass\ lose = \frac{0.43}{7.2} = 5.97\%$$

The research by Yang et al. (2021) and Bawa et al. (2017) reveals that aluminum salt precursors decompose at varying temperatures, with the process extending to temperatures as high as 1200°C. These decomposition events occur within different temperature ranges. Below 200°C, water is lost, which includes both loosely bound surface water and chemically bound water in the form of hydrates. Various hydrates lose water at different temperatures. Between 200°C and 600°C, organic decomposition occurs, releasing residual solvents from the synthesis. At temperatures above 400°C, inorganic decomposition happens, such as the breakdown of sulfates, chlorides, and nitrates. Lastly, oxidation decomposition happens above 800°C, leading to the decomposition of some metal oxides at very high temperatures.

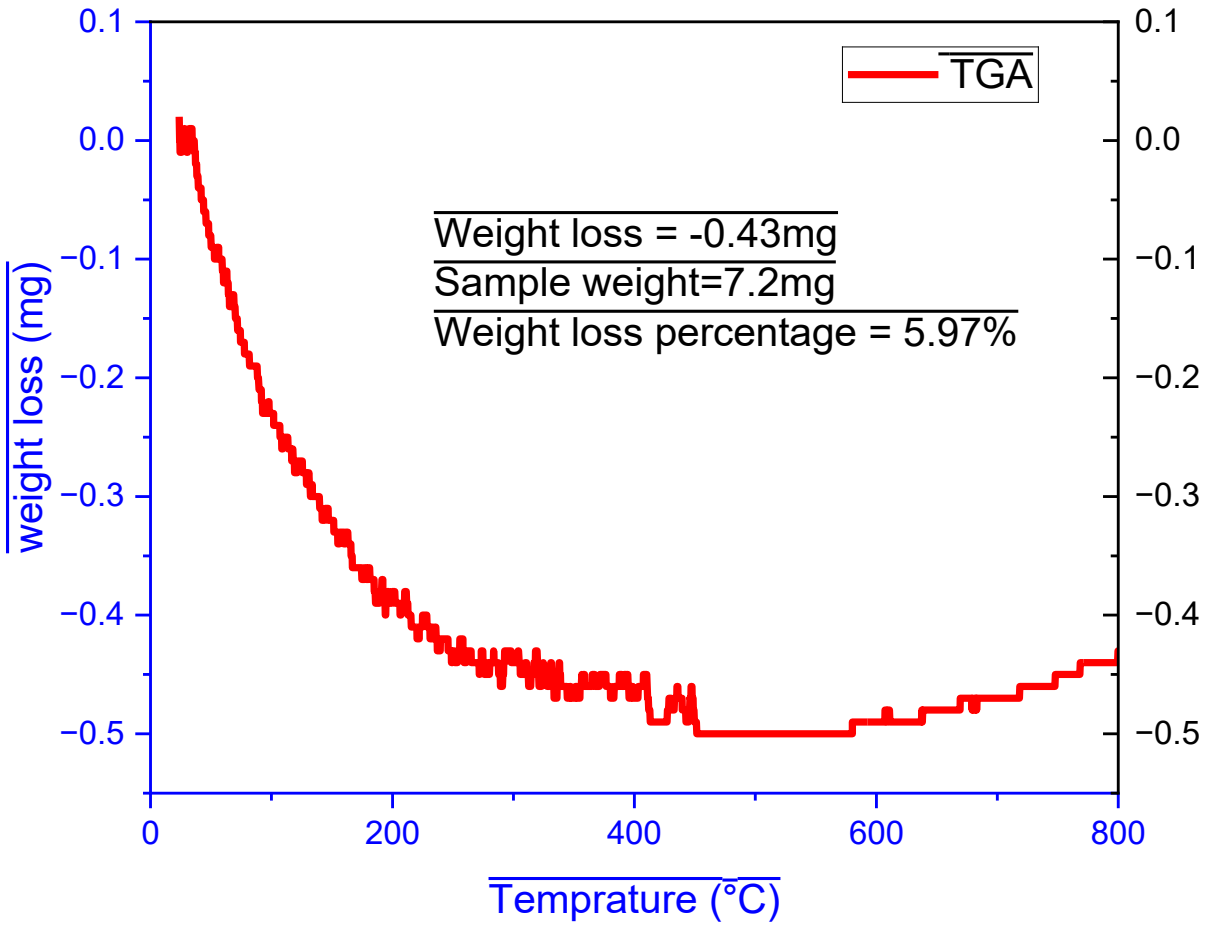

Figure 4.16 TAG graph for sample 5

4.1.2.6 Thermogravimetric analysis (TGA) for Sample 6

Decomposition stage identification: The distinct reductions or changes in the TGA curve in Figure 4.17 typically correspond to the loss of specific components during each stage of the decomposition process. The TGA graph in Figure 4.17 indicated that the material underwent a single-step decomposition. Initially, the mass remained stable with no change, followed by a sharp decline across a broad temperature range. Eventually, the curve leveled off, showing little to no further mass loss.

Defining the temperature range for each stage: The temperature at which mass loss begins (onset) and concludes (offset) was identified for every stage. These temperatures represent the points where the curve departs from and later returns to a plateau.

These points represented when the curve moved away from a flat region and later returns to it, as it's a first stage decomposition process. The first phase with no slope lasted until 54°C, after which the mass began to decrease (negative slope) from 54°C to 500°C. Finally, the graph stabilized at temperatures beyond 500°C, reaching up to 800°C.

Calculation of the mass lose at each stage: Understanding the sample fraction lost per decomposition step involved calculating the percentage mass loss, which relied on the weight change data and the original sample mass. The percentage of mass loss can be calculated at each stage; however, this study only focused on the overall mass loss. The total mass loss was found to be 5.70% at a temperature limit of 800°C. A smaller mass loss indicates the ceramic material's ability to endure high temperatures, thanks to its strong thermal properties. Beyond 800°C, oxidation decomposition is expected, where metal oxides decompose.

$$\%\ mass\ loss = \frac{actual\ mass\ loss}{initial\ mass} \quad \text{Eq.4.2}$$

$$\%\ mass\ lose = \frac{0.91}{18.2} = 5.0\%$$

According to Yang et al. (2021) and Bawa et al. (2017), aluminum salt precursors undergo decomposition at various temperatures up to 1200°C. The decomposition events are categorized based on specific temperature ranges. Water loss occurs below 200°C, involving both loosely bound water on the surface and chemically bound water within hydrates. Different hydrates release water at specific temperatures. Between 200°C and 600°C, organic decomposition occurs, including the loss of solvents used in the synthesis. Above 400°C, inorganic decomposition takes place, such as the breakdown of sulfates, chlorites, and nitrates. At temperatures over 800°C, oxidation decomposition occurs, resulting in the breakdown of certain metal oxides at high temperatures.

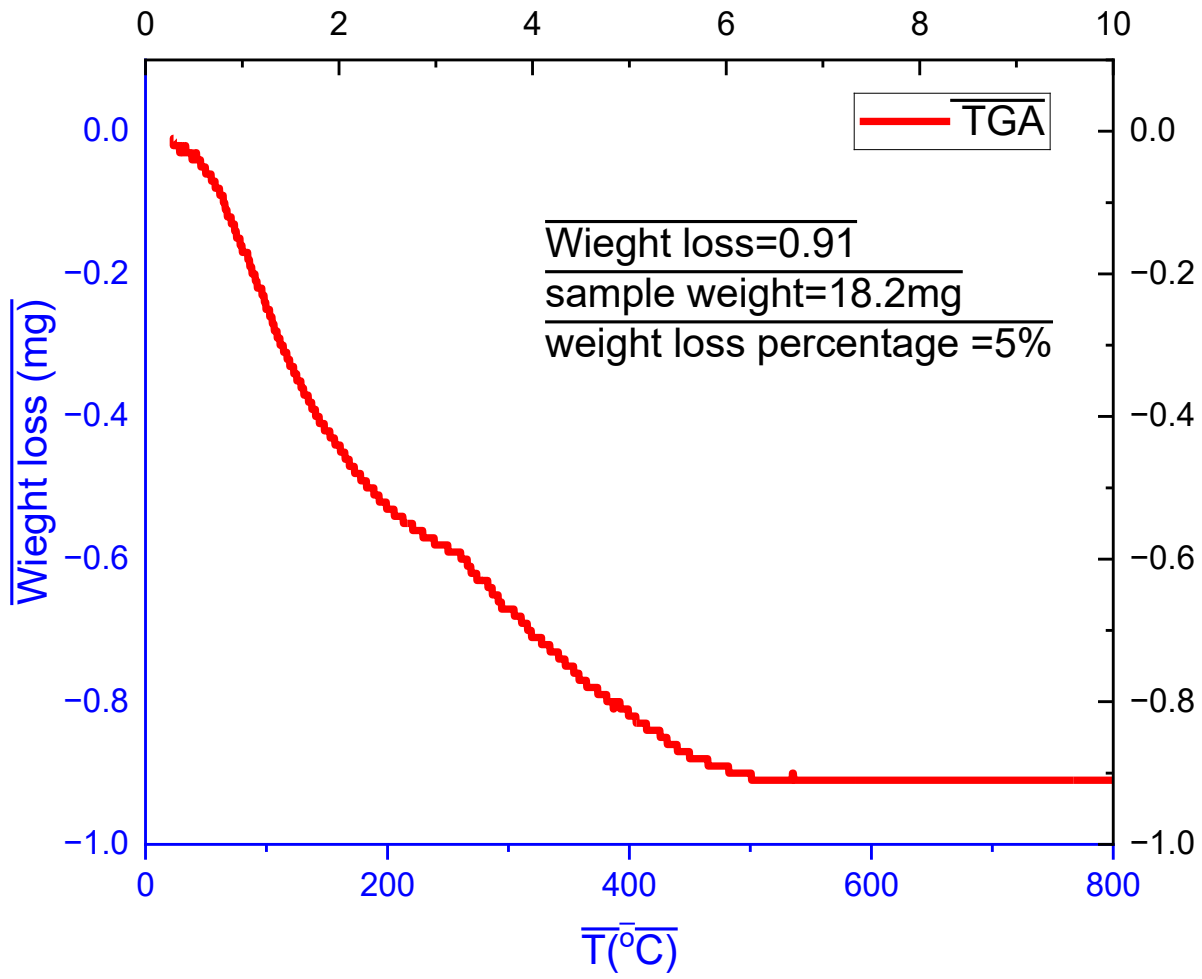

Figure 4.17 TGA graph for sample 6

4.1.2.7 Thermogravimetric analysis (TGA) for Sample 7

Identification the TGA graph components: The X-axis shows temperature, offering valuable insights into material properties. The Y-axis represents the sample's mass, indicating how much mass is being lost. The TGA curve, the main curve on the graph, illustrates how the mass changes with temperature. It usually slopes downward because materials typically lose mass when they decompose or release volatile components.

Recognizing the decomposition phases: The distinct steps or declines in the TGA curve shown in Figure 4.18 often indicate the loss of individual components during different stages of decomposition.

The TGA graph showed a rapid initial mass loss with some fluctuations, likely caused by drying and/or decomposition, followed by a period where the mass began to stabilize and even increase over certain temperature ranges.

The temperature intervals for each stage: For each phase, the temperature at which the mass loss starts (onset) and ends (offset) was noted. These temperatures indicate where the curve deviates from a plateau and eventually flattens again. As the TGA graph indicated that the graph rapidly dropped down and then started to be stable with all its all instability. The material rapidly lost its mass up to 300ºC and then from the temperature range of 300ºC-800ºC the material struggled to be stable and during this moment its graph showed that it gained a mass.

Calculation of mass lose at each stage: For every distinct decomposition step, the mass loss was expressed as a percentage, computed by comparing the weight reduction to the starting mass of the sample. Although the mass loss percentage can be determined at each stage, this study only calculated the total percentage of mass loss. The total mass loss was 5.70% when the temperature was limited to 800°C. A lower mass loss indicates the ceramic material's ability to withstand heat due to its excellent heat tolerance. Above 800°C, oxidation decomposition is anticipated, leading to the decomposition of metal oxides.

$$\%\ mass\ loss = \frac{actual\ mass\ loss}{initial\ mass} \quad \text{Eq.4.2}$$

$$\%\ mass\ lose = \frac{0.43}{7.2} = 6.53\%$$

In their studies, Yang et al. (2021) and Bawa et al. (2017) found that aluminum salt precursors decompose at different temperatures, with a range extending up to 1200°C. The decomposition events occur within various temperature ranges. Below 200°C, water loss takes place, including both loosely bound water on the surface and chemically bound hydration water in hydrates. Various hydrates lose water at distinct temperatures. Between 200°C and 600°C, organic materials decompose, including the evaporation of residual solvents. Inorganic decomposition, such as the breakdown of sulfates, chlorites, and nitrates, occurs above 400°C. At temperatures over 800°C, oxidation leads to the decomposition of some metal oxides.

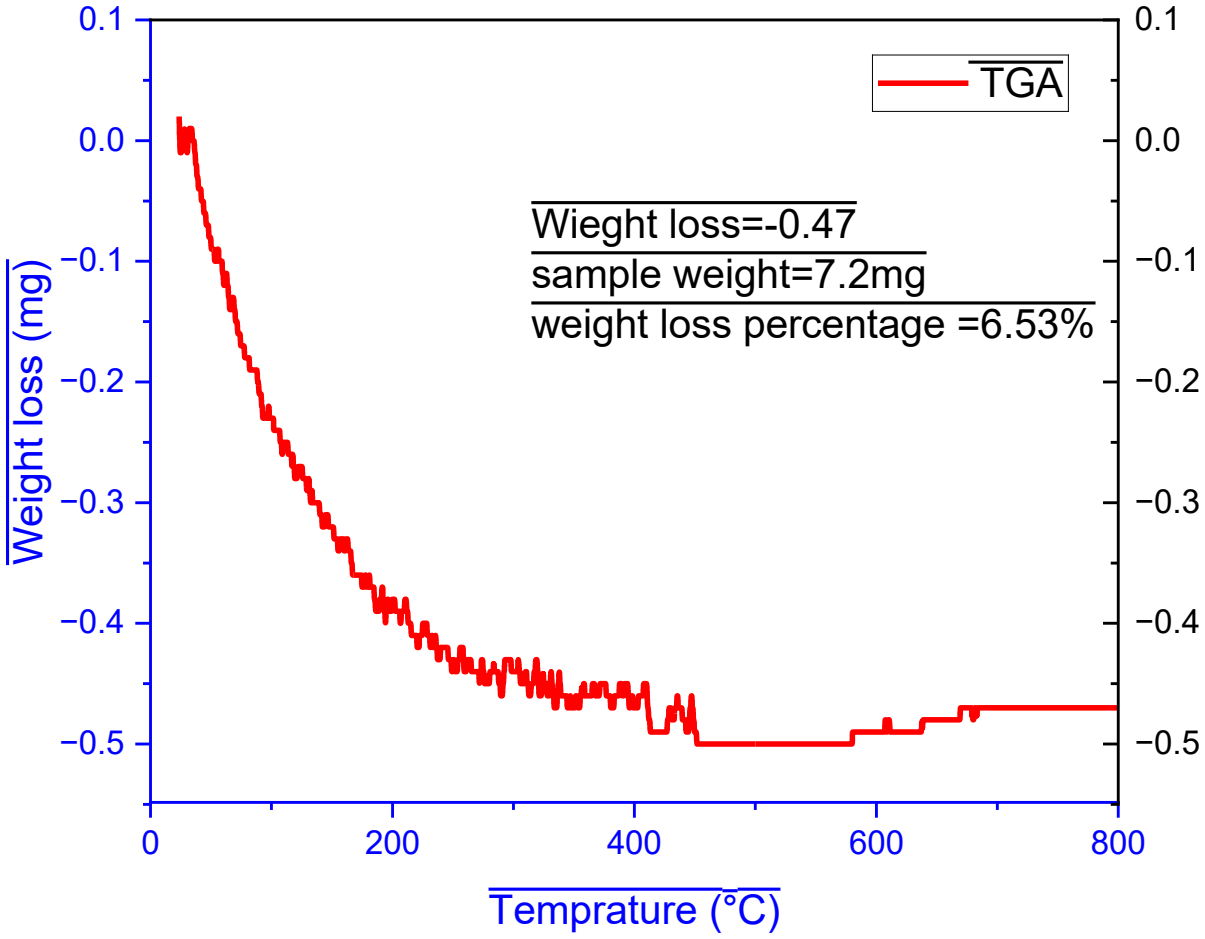

Figure 4.18 TGA graph for sample 7

4.1.2.8 Thermogravimetric analysis (TGA) for Sample 8

Decomposition stage identification: The clear steps or drops in the TGA curve of Figure 4.19 typically reflect the loss of a specific substance during a particular decomposition phase. The TGA graph revealed a steep initial mass reduction, accompanied by some instability, which is typically attributed to drying and/or decomposition, before the curve flattened out as the material gained mass in certain temperature intervals based on the reference taken in Figure 4.19 above.

Temperature range determination for each stage: The onset temperature (where mass loss initiates) and the offset temperature (where mass loss concludes) were determined for each stage. These temperatures represent when the curve moves away from and then returns to a plateau. The TGA graph showed a steep initial drop, followed by an attempt at stability, though with some fluctuations. The material experienced a rapid mass loss up to 400°C, and between 400°C and 800°C, it struggled to stabilize, during which the graph indicated a mass gain.

Calculation of the weight loss at each stage: the calculation for percentage mass loss per stage utilized the measured mass decrease and the initial sample mass, yielding data on the extent of degradation in each specific step. Mass loss percentage can be determined at every stage; however, in this study, the focus was on calculating only the total mass loss percentage. The total mass loss was 5.70% when the temperature was kept at 800°C. A smaller mass loss shows that the ceramic material can resist higher temperatures due to its efficient heat resistance. Above 800°C, oxidation decomposition is expected, causing metal oxides to break down.

$$\%\ mass\ loss = \frac{actual\ mass\ loss}{initial\ mass} \quad \text{Eq.4.2}$$

$$\%\ mass\ lose = \frac{0.43}{7.3} = 5.89\%$$

As demonstrated in the research of Yang et al. (2021) and Bawa et al. (2017), aluminum salt precursors undergo a series of decomposition events at temperatures up to 1200°C. These events occur within defined temperature ranges. Water loss is observed below 200°C, including both loosely bound water on the surface and hydration water within the crystal structure of hydrates. Different hydrates release water at different temperatures. Between 200°C and 600°C, organic decomposition occurs, involving the removal of residual solvents. Inorganic decomposition of substances like sulfates, chlorites, and nitrates takes place above 400°C. Finally, oxidation decomposition occurs above 800°C, causing metal oxides to break down at extremely high temperatures.

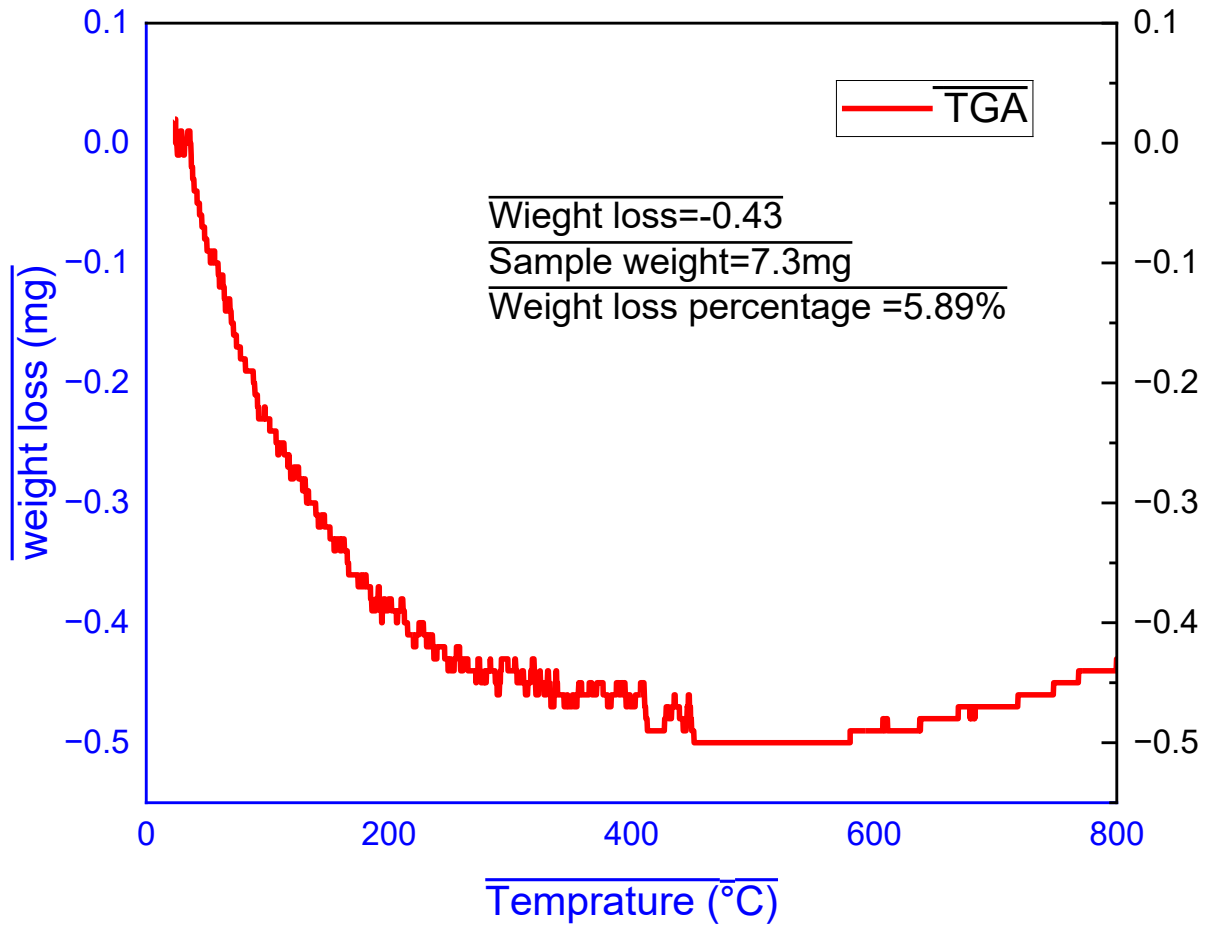

Figure 4.19 TGA graph for sample 8

4.1.2.9 Thermogravimetric analysis (TGA) for Sample 9

Identification of distinct decomposition stages: The changes or drops in the TGA curve of Figure 4.20 generally correspond to the loss of a specific component during the respective decomposition process. According to the TGA graph, the material showed a one-stage decomposition behavior. At first, there was no change in mass, but then a significant drop occurred over a wide temperature span. After this, the mass loss stabilized and the graph became nearly flat.

Determining the onset and offset temperatures for each phase: For every stage, the onset temperature (where mass loss begins) and offset temperature (where mass loss stops) were identified. These points correspond to where the curve deviates from and flattens out from a plateau. The initial phase with no slope occurred until 51°C, after which the mass began to decrease (negative slope) between 51°C and 506°C. The graph then stabilized at temperatures above 506°C, continuing up to 800°C.

Calculation of the mass lose at each stage: The amount of mass lost in each step was calculated as a percentage of the starting sample weight, based on how much weight was actually lost. While mass loss can be measured at each stage, only the total mass loss percentage was calculated for this study. The total mass loss was 5.70% when the temperature was capped at 800°C. A lower mass loss indicates that the ceramic material is better able to resist heat, thanks to its good thermal properties. Exceeding 800°C, oxidation decomposition is expected, where metal oxides begin to decompose.

$$\%\ mass\ loss = \frac{actual\ mass\ loss}{initial\ mass} \quad \text{Eq.4.2}$$

$$\%\ mass\ lose = \frac{0.89}{16.8} = 5.30\%$$

Research by Yang et al. (2021) and Bawa et al. (2017) shows that aluminum salt precursors decompose at varying temperatures, with a range reaching up to 1200°C. The decomposition events are associated with different temperature ranges. Below 200°C, water is lost, including both loosely bound surface water and chemically bound water in the hydrate structure. Various hydrates lose water at different temperatures. Between 200°C and 600°C, organic decomposition happens, releasing residual solvents from the synthesis. Above 400°C, inorganic decomposition occurs, breaking down sulfates, chlorites, and nitrates. Lastly, above 800°C, oxidation decomposition happens, with some metal oxides decomposing at very high temperatures.

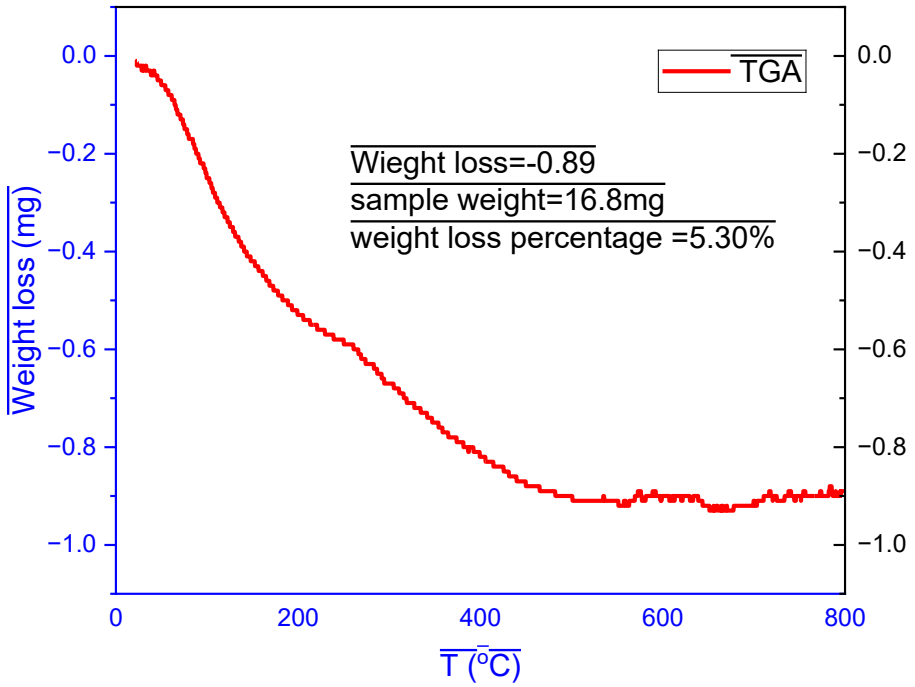

Figure 4.20 TGA graph for sample 9

In conclusion, the x-ray diffraction analysis revealed distinct structural characteristics among the nine alumina nanoparticle samples as shown in the summary Table 4.10 below. While all samples exhibited diffraction patterns indicative of different phase of alumina (i.e. alpha, theta, delta, gamma, and others), significant variation was observed in their crystallite size, peak intensity, presence of secondary phase specifically in sample 1,2,4, 5, and 8. However, sample 3,6, and 9 happened to be only alpha phase and sample 7 occurred as only theta phase only.

The selected calcination temperature highly affected presence of mixture of phases and combination of different phase together as showed in sample 1,2,4, 5, and 8. These different structural properties suggested that as they can be suitable for different application as it is discussed in each sample analysis above. The crystallite size obtained in this study are less than the previous studies which are conducted using sol-gel process reviewed so far. As per the study of Krishnan et al., (2018) the average crystallite size obtained was 45nm which is greater than an average crystallite size obtained in this particular research of all nine samples.

This study also investigated the thermal behavior of nine samples synthesized under different or varying process parameters as revealed by the thermogravimetric analysis (TGA). The results demonstrated that a significant impact of these parameters on the samples' thermal stability and mass loss profile and this provided valuable insights into their decomposition mechanism and suitability of different application accordingly. The observed differences in mass loss profiles indicated that the importance of precise parameter control during synthesis for achieving desired thermal characteristics and the analysis enabled recommendation for optimal process parameter to obtain superior thermal performance depending up on the required application

Table 4.10 Summary of the XRD and TGA results

Samples	Phases	Crystallite size	Mass Loss	Application
Sample 1	Θ, δ	20.6nm	5.70	**Θ**-(Adsorption, catalyst, abrasive, biomedical, high temperature application) **δ**-(Water purification, medical delivery, and medical device)
Sample 2	γ/δ, α	6.5nm	5.40	Catalyst, adsorption and precursor for ceramics.
Sample 3	α	5.8nm	4.90	Abrasive, cutting tools, bearing and other machine parts, refractory materials, and space application.
Sample 4	γ/δ, Θ	8nm	6.00	**γ/δ** -Catalyst, adsorption and precursor for ceramics. **Θ**-(Adsorption, catalyst, abrasive, biomedical, high temperature application)
Sample 5	Θ, α	6.9nm	5.50	**Θ**-(Adsorption, catalyst, abrasive, biomedical, high temperature application)
Sample 6	α	5.2nm	5.00	Abrasive, cutting tools, bearing and other machine parts, refractory materials, and space application.
Sample 7	Θ	26.5nm	6.53	**Θ**-(Adsorption, catalyst, abrasive, biomedical, high temperature application)
Sample 8	δ/Θ, α	8.6nm	5.60	Catalyst, abrasive, high temperature application
Sample 9	α	6.5nm	5.30	Abrasive, cutting tools, bearing and other machine parts, refractory materials, and space application.

4.1.3 Scanning Electron Microscopy (SEM) results and analysis

The Scanning Electron Microscopy (SEM) is a powerful tool for characterizing the surface morphology, microstructure, and particle distribution of materials at high magnification possible. In this study, SEM was employed to investigate and compare the morphology of nine distinct samples that were synthesized under different process parameters. These samples were prepared by varying combination of precursor materials, calcination temperature, and calcination time while maintaining all other parameters constant. By altering these parameters, the objective was to gain insight in to how each factor influences the material's microstructure and particle size distribution.

The precursor materials used in the synthesis play a crucial role in determining the chemical composition and overall morphology of the final product. The calcination temperature and time was particularly significant as they can affect the crystallization and phase formation, thereby influencing the material's performance and application. By varying these synthesis conditions, it helped to understood how the interplay between these factors affects the surface features and structural properties of the final product.

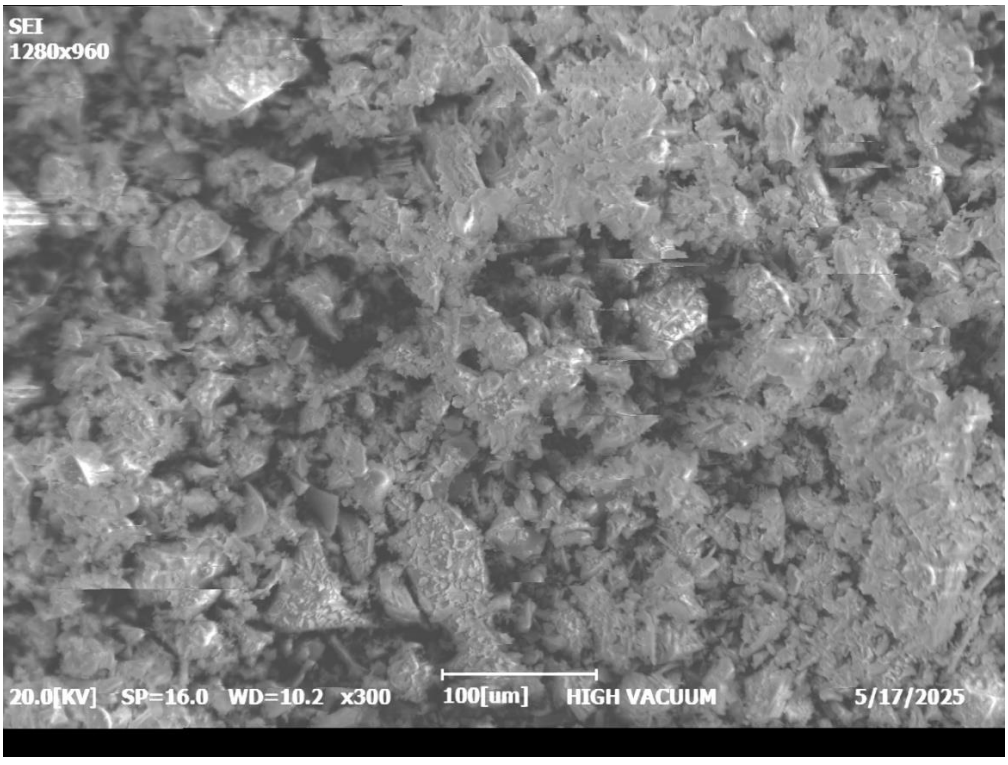

Figure 1.21 SEM result of Sample 1

The SEM image of sample 1 as shown in Figure 4.21 above revealed a relatively varying particle size distribution as it was indicated in the XRD analysis too with well-defined morphology. The particles appeared to have a spherical shape and this determined by the precursor material along with the calcination temperature and time. However, the result shown in the Figure 4.22 below for sample two indicated that relatively uniform particle size and distribution. The image showed a noticeable change in particle size compared to sample 1. The change in calcination temperature and time possibly caused for this change.

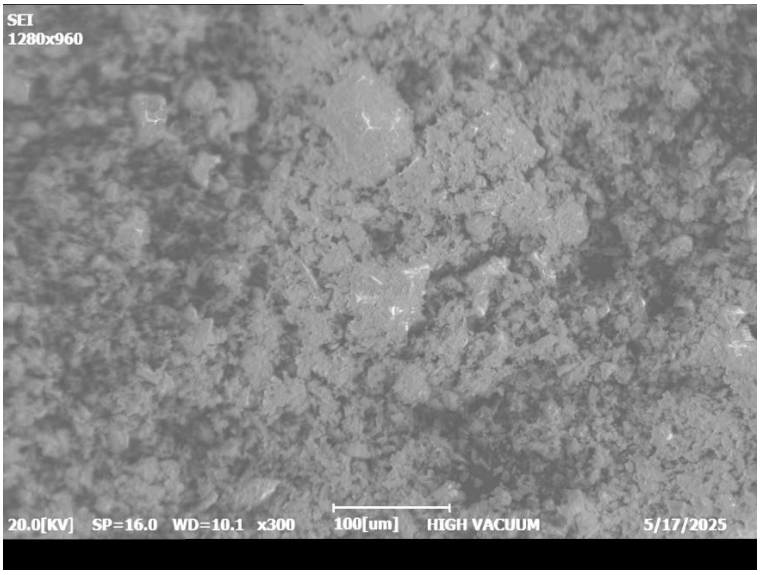

Figure 4.22 SEM result for sample 2

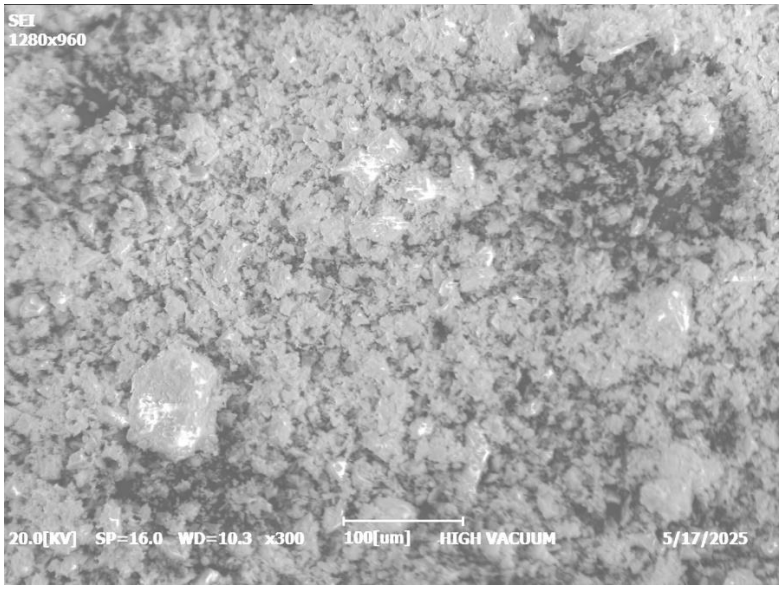

Figure 4.23 SEM results of sample 3

The image shown in Figure 4.23 for sample 3 indicated that a very smaller particle size compared to sample 1 and 2. The combination of the precursor materials and the calcination parameters appeared to result in smaller particle size with seemingly agglomeration. This suggested that the parameter combination used for sample 3 promoted a more controlled growth and resulted materials for application required uniform particle size and high surface area. Sample 4 in Figure 4.24 below also illustrated a smaller particle size with different size as it's shown in the XRD results too. The lower the calcination time influenced to have different phase and size.

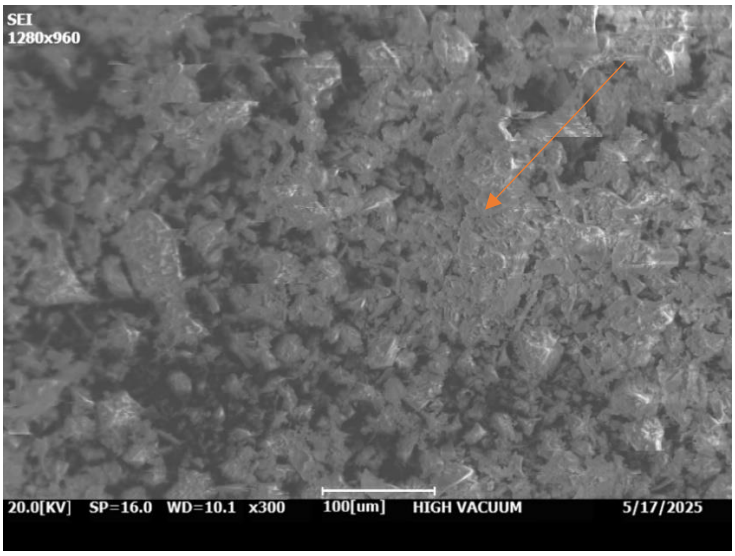

Figure 4.24 SEM result for sample 4

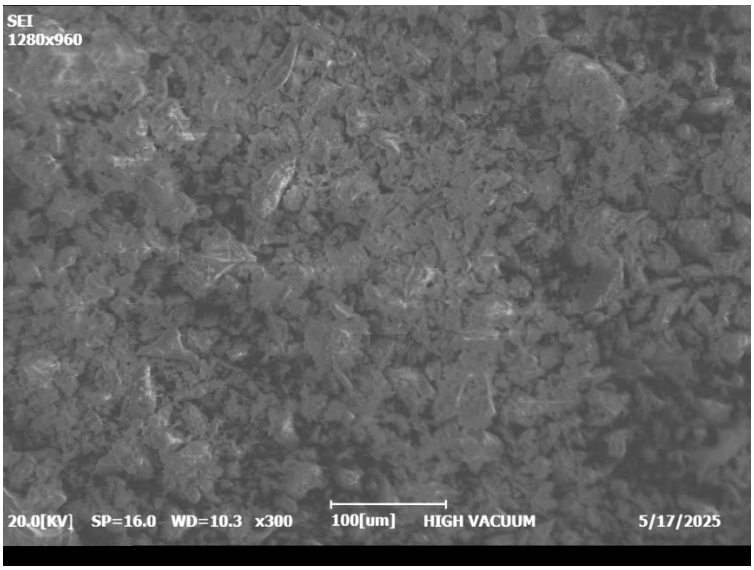

Figure 4.25 SEM result for sample 5

The SEM analysis of sample 5 as shown in Figure 4.25 indicated a significant difference in the morphology compared to sample 4. The higher calcination temperature and extended time results nearly uniform particle size and the image of sample 6 in Figure 4.26 below indicated that the particle size are smaller than in sample 4 despite the precursor material used is the same. The calcination parameter brought this effect in combination with the precursor and this makes suitable for catalyst activity and adsorption. The particle distribution seemed to be similar with sample 5.

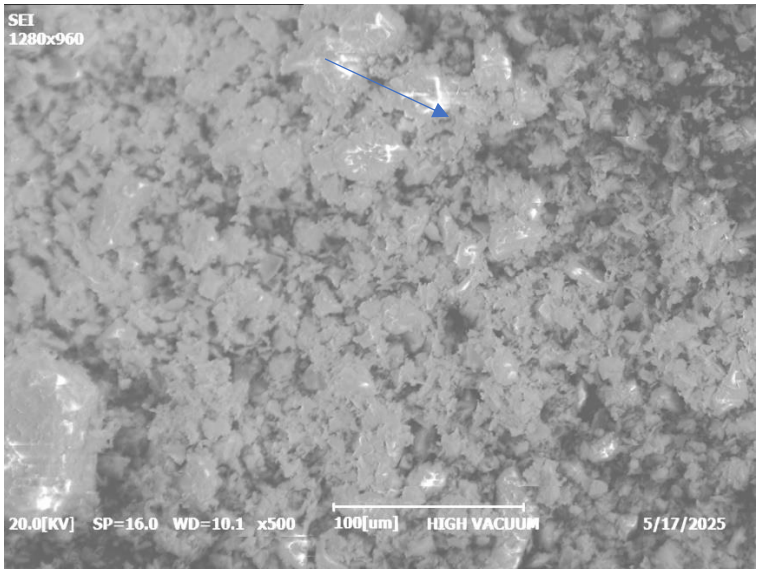

Figure 4.26 SEM result for sample 6

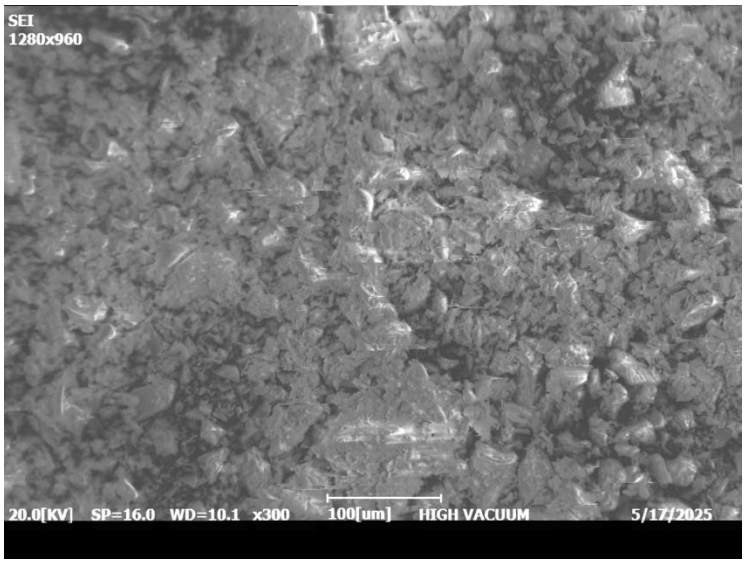

Figure 4.27 SEM result for sample 7

The SEM results for sample 7 in Figure 4.27 provided that particles with a more irregular shape composed to those of other samples and larger particle size. The surface is rougher, and some degree of agglomeration is shown. The variation in precursor material appeared to have influenced the particle morphology, suggesting that the chemical nature of the precursor can strongly affect the final material's surface characteristics in addition to the effects of calcination parameters. Sample 8 below however, brought a smaller particle size despite the fact that the precursor material is similar. The difference in the particle size happened by the calcination parameters in combination with precursor material.

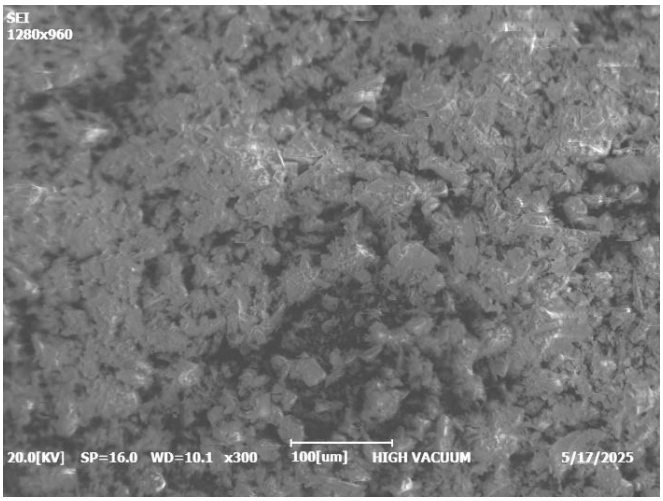

Figure 4.28 SEM result for sample 8

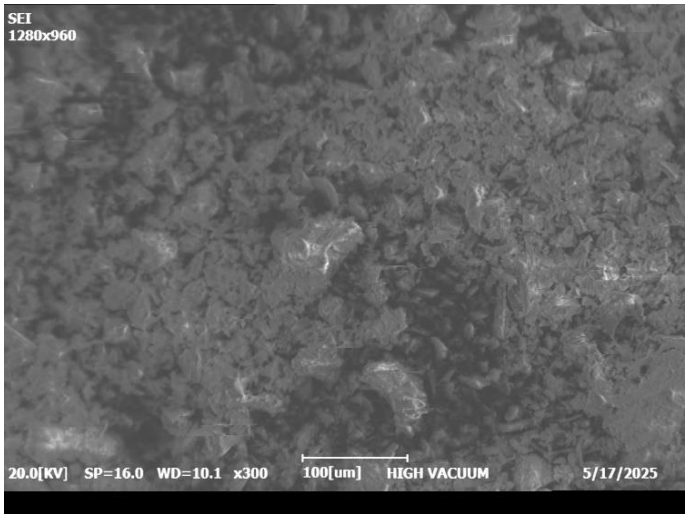

Figure 4.29 SEM result for sample 9

Finally, Sample 9 as shown in Figure 4.29, synthesized with the third precursor material in combination with the calcination parameters, displayed a particle that are relatively smaller. The SEM image suggested that the higher the calcination conditions in combination with the precursor material favor for the formation of smaller particle size well crystallized particles.

In Summary, the SEM characterization results show clear difference in particle size, morphology, and surface feature across the nine samples. The precursor materials significantly influenced the structure of the final product, while calcination temperature and time played crucial role in determining particle size and surface roughness. By adjusting these parameters, it's possible to tailor the morphology and surface characteristics of the materials for specific application, including catalysis, adsorption, and other fields that depend on material surface properties.

Energy Dispersive X-ray Spectroscopy (EDX) Characterization Results

Energy Dispersive X-ray spectroscopy (EDX) is a vital analytical technique used in conjunction with Scanning Electron Microscopy (SEM) to determine the elemental composition of synthesized materials. In this particular study, EDX analysis was performed on three samples and each prepared under varying synthesis conditions. The EDX results offer insight into how the choice of precursor material and thermal treatment (calcination time and temperature) influences the incorporation, retention, and distribution of key elements within the synthesized samples. This information is essential for understanding the formation mechanism, purity, potential presence of impurities or secondary phase, all of which have a direct impact on the physical, chemical, and functional properties of the materials.

The EDX image shown in Figure 4.30 below indicated the elemental composition founded in sample 3 which was synthesized using the aluminum nitrate precursor material along 1200^{o}C calcination temperature for six hours. The EDX result showed that aluminum and oxygen are the available elements mainly with their first and second ranked abundances or concentration (504cps and 56cps) respectively as shown in the figure below. However, impurities that was produced from different sources as it discussed in the XRD analysis above was also indicated despite their concentration is very low.

o

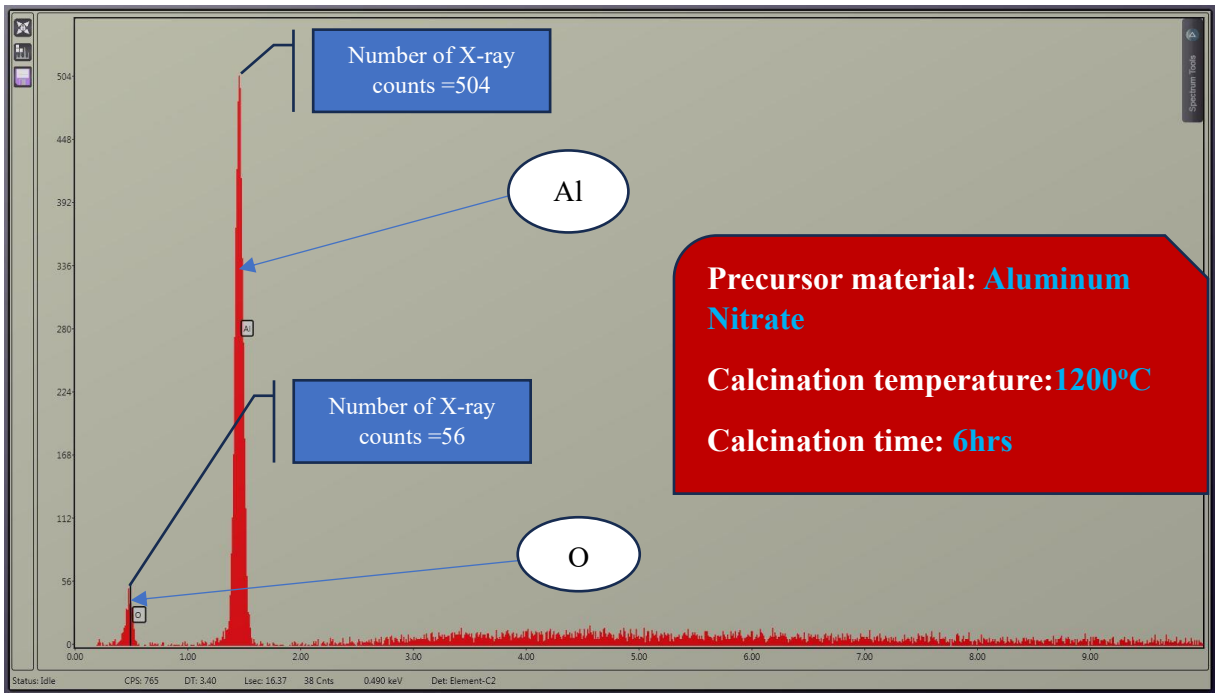

Figure 4.30 EDX result for sample 3

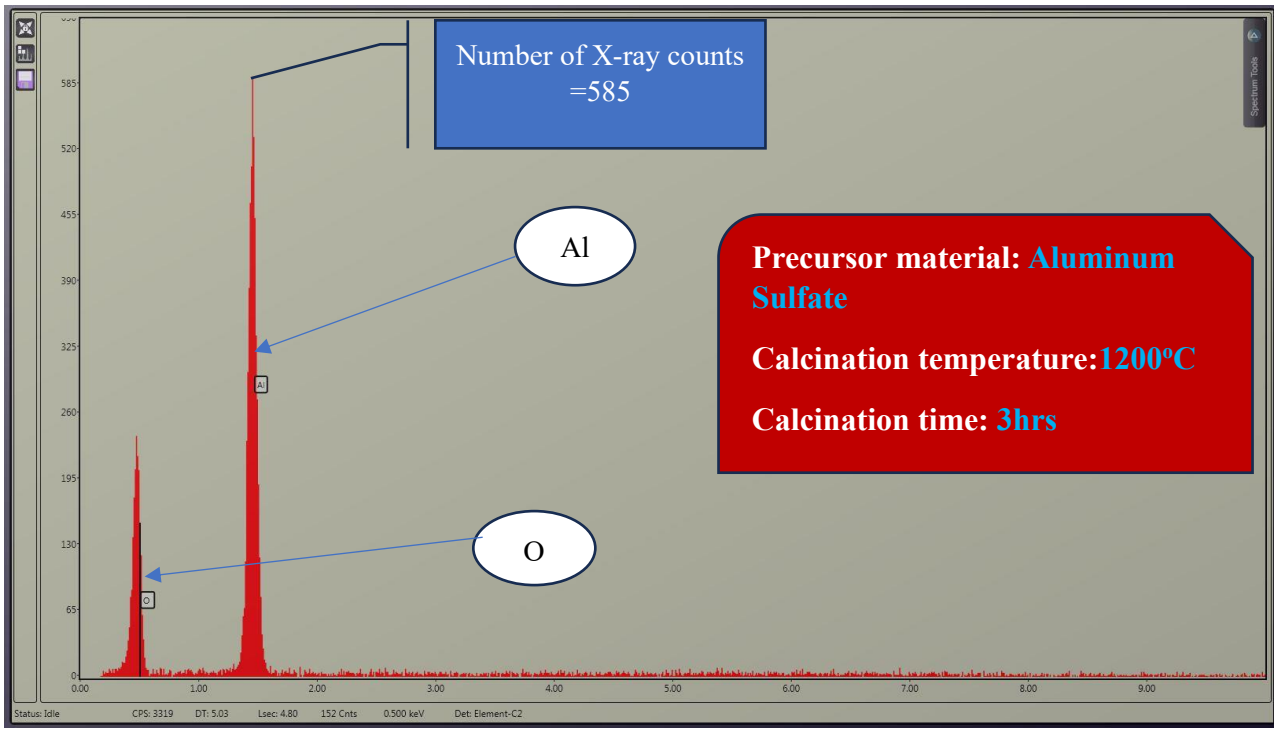

Figure 4.31 EDX result for sample 6

As per the EDX image of sample 6 which shown in Figure 4.31 was synthesized with aluminum sulfate precursor material and calcinate at temperature of 1200ºC for three hours, the elemental composition found to be aluminum and oxygen. Aluminum with greater abundance with an intensity of the X-ray 585 counts per second which is higher than found in sample 3 and 9. The combined interplay of the parameter caused to vary from sample 3. Similarly, the EDX result as shown below in Figure 4.32 for sample 9 synthesized with aluminum chloride which was calcinated a temperature of 1200 for four hours. The elemental composition turned out to be both aluminum with higher concentration and oxygen lower concentration relatively.

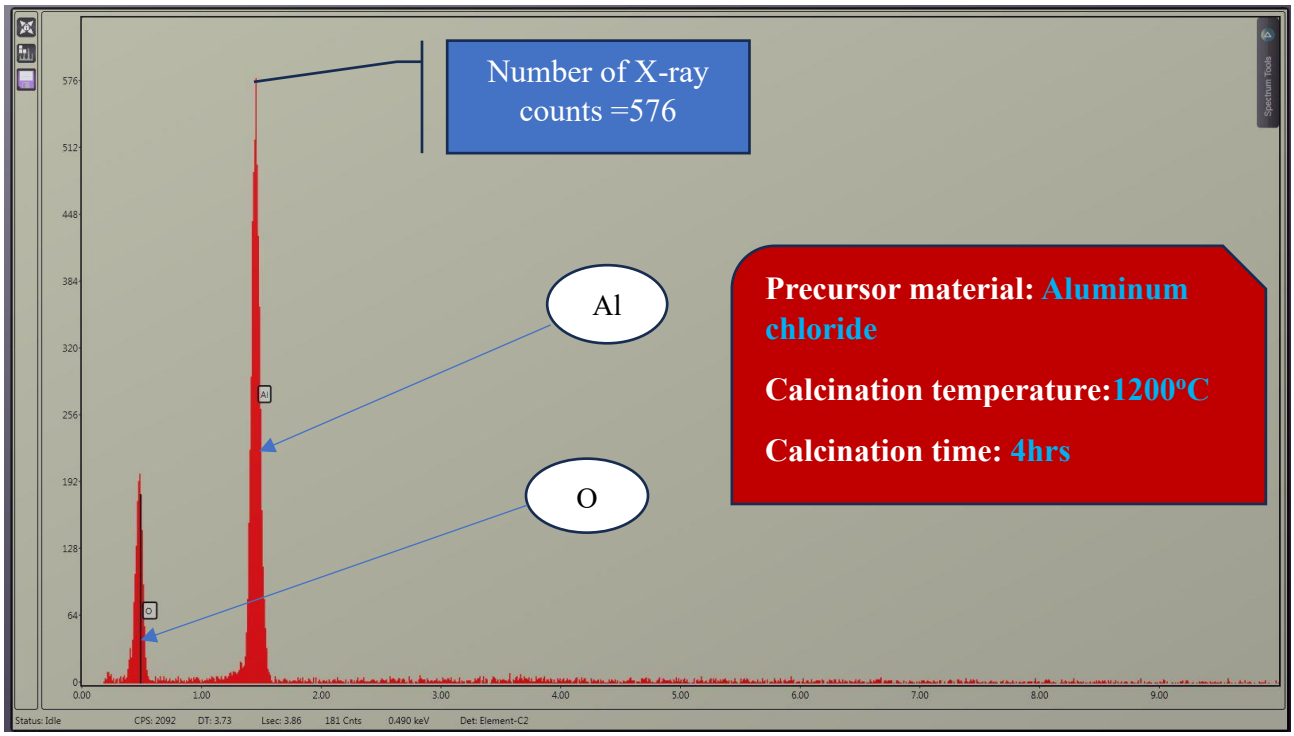

Figure 4.32 EDX result for sample 9

The EDX characterization provided essential insights into the chemical composition of the synthesized materials and the impact of varying synthesis parameters. Precursor material influenced the elemental baseline and impurity profile, calcination temperature affected phase purity and elemental retention, while calcination time influenced the degree of reaction completion and homogenization. Together, these parameters define the quality and functional potential of the final product, and the EDX results serve as a crucial validation tool for synthesis optimization. In addition, the EDX result shows the samples happened to have similar purity level.

4.2 Optimization of the process parameters

4.2.1Single and multi-response optimization

The synthesis of nanoparticles with controlled properties required carful optimization of the process parameters. In this study, the Taquchi method was employed to optimize the synthesis the synthesized alumina nanoparticle by considering precursor material, calcination temperature, and calcination time as a key process parameter. The goal was to simultaneously minimize crystallite size and the weight loss. This is because, controlling both the crystallite size and weight loss during nanoparticle synthesis is often critical for achieving desired performance characteristics. However, this response may be influenced differently or even antagonistically by process parameters. The aim was to determine the optimal combination of these parameters to simultaneously achieve a small crystallite size and minimal weight loss. The Taguchi experimental design followed by a detailed presentation and analysis of the results, ultimately identifying the optimal process conditions for synthesizing nanoparticles with the desired properties. The alumina ceramic's performance is highly dependent on their crystallite size and purity, which are directly related to weight loss during processing.

Single response optimization (crystallite size): Crystallite size versus Precursor material, Calcination Temperature, Calcination time

The need to optimize crystallite size is due to the fact that it highly influenced the properties of alumina ceramic materials. As Okada et al., (2003) studied the crystallite size influenced the sinterabilty of the material. A smaller crystallite size of the nanoparticle lead to high thermal stability as Series, (2024) investigated in their paper.

Crystallite size influences material properties, especially in nanomaterials. Smaller crystallites have higher surface area, increased reactivity, and distinct physical and chemical behaviors. They enable lower temperature sintering and denser materials but may have fewer structural defects. Larger crystallites show better bulk properties, reduced surface effects, and increased structural integrity but lower reactivity. For magnetic nanoparticles, smaller crystallites may display super para magnetism, while larger ones exhibit multi-domain behavior as per the study of Albedwawi et al., (2021).

Linear Model Analysis: SN ratios versus Precursor material, Calcination Temperature, Calcination time

Estimated Model Coefficients for SN ratios

Table 4.11 Estimated Model Coefficients for SN ratios

Term	Coef	SE Coef	T	P
Constant	-14.8474	0.08196	-181.151	0.000
Precursor A1	0.7578	0.11591	6.538	0.023
Precursor A2	0.0411	0.11591	0.355	0.757
Calcination T 800	0.3243	0.11591	2.798	0.108
Calcination T 1000	0.0642	0.11591	0.554	0.635
Calcination t3	0.0705	0.11591	0.608	0.605
Calcination t4	-0.1145	0.11591	-0.987	0.428

Interpretation of estimated model coefficients for SN ratios

Interpreting the estimated model coefficients for S/N (Signal-to-Noise) ratios in a Taguchi experiment involved understanding how each factor level affects the S/N ratio and, consequently, the robustness of the process. The interpretation differs slightly from interpreting coefficient in a typical regression model because the goal is to maximize the S/N ratio, which represents the overall robustness, not necessarily to directly predict a mean response.

The basic concept in the estimated model coefficient

S/N ratio types: The different S/N ratio like, Larger-is better, smaller-is-better, and nominal-is-best) have different aim and in this study the smaller-is-better is selected, since the objective is to minimize the values of the particle size and weight loss. **Baseline level**: Minitab typically uses one level of each factor as a baseline or reference level. The coefficient for this baseline level is implicitly zero (or incorporated into the constant term). The coefficients for the other levels are interested relative to this baseline. **Main effects**: The coefficients represent the main effects of each factor level on the S/N ratio, relative to the base line level to that specific level.

Steps for interpretation

Identify the baseline level: The level of factor which is used as the baseline was identified from the Minitab result or output. This is often the first level listed for each factor. As it is shown in Table 4.11.

Interpret the sign and the magnitude of the coefficients: Positive coefficient for a factor level indicates that switching from the baseline level to that specific level is expected to increase the S/N ratio. This always indicates an improvement in robustness, regardless of the S/N ratio type. A negative coefficient for factor level indicates that switching from the baseline level to that specific level is expected to decrease the S/N ratio like that of calcination time. This always indicates a decrease in robustness. Magnitude is the absolute value of the coefficient. A larger absolute value indicates a stronger effect on the S/N ratio. A factor level with a larger absolute coefficient has a greater impact on the process's robustness compared to a factor level with a smaller coefficient. So, in this case the precursor material 1 had a greater impact on the responses.

Identify the optimal level for each factor: For each factor, the level with the largest positive coefficient (or the smallest negative coefficient which is still better than a larger negative one) supposed to affect more. This is because of higher S/N ratio are always preferred for robustness, regardless of the S/N ratio type. If all coefficients are negative then the smallest absolute value is selected to minimize the reduction in the S/N ratio compared to other levels. Therefore, the optimal level of all factor happened to be the first level.

Model Summary

Table 4.12 Model Summary

S	R-Sq	R-Sq(adj)
0.2459	97.37%	89.49%

Interpreting the model summary

Interpreting a model summary in statistical software like Minitab involves understanding the key statistical that describe the overall fit and performance of statistical model. These statistical helped to assess how well the model explains the variation in the dependent variable (or the outcome the is in need of predict or understand). The specific statistics included in the model summary could vary depending on the model. However, the model used in this study is ANOVA.

Common statistics in a Model Summary and how to interpret them.

R-squared (R^2): Coefficient of determination; R-squared represents the proportion of variance in the dependent variable that is explained by the independent variables in the model. It's a measure of how well the model fits the data. This value ranges from 0 to 1. When $R^2 = 0$; implies that the model explains none of the variance in the dependent variable and the independent variables have no predictive power. When $R^2 = 1$; provide an information that all the variance in the dependent variable and shows the independent variables perfectly predict the dependent variable. Values between 0 and 1 indicates the percentage of variance explained by the independent variable in the model. With this interpretation $R^2 = 0.9737 = 97.37\%$ which implied that 97.37% variance explained by the independent variable.

Adjusted R-squared (Adjusted R^2): R-squared always increases as independent variables added to the model even if those variables are not that related to the dependent variables. This is why looking for adjusted R-squared is vital. Adjusted R-squared is the modified version of R-squared that adjusts for the number of independent variables in the model. It avoids the addition of unnecessary variables that do not significantly improve the model fit. It ranges from 1 to 0, but can also be negative if the model is very poor. The adjusted R-squared is always less than the r-squared value and the difference between the two value shows how much the R-squared is being inflated by the inclusion of unnecessary variables. The Adjusted R^2 in this optimization happened to be 89.49% and the difference between R-squared and Adjusted R-squared is 7.88% which indicated that was being inflated by the inclusion of unnecessary variables.

Standard Error of the estimate (S or SEE): This value measures the average distance that the observed values fall from the regression line. It represents the typica size of the prediction errors made by the model. A smaller standard error of the estimate indicates a more accurate model. This standard error of estimate can be used to create prediction intervals for future observation. The value or magnitude of this error indicates the model prediction is off by that value from the dependent variable. So, in this optimization result the Standard error of the estimate is 0.2459 and provided that the model is deviated by this value from the dependent variables.

Analysis of Variance for SN ratios

Table 4.13 Analysis of Variance for SN ratios

Source	DF	Seq SS	Adj SS	Adj MS	F	P
Precursor material	2	3.64234	3.64234	1.82117	30.12	0.032
Calcination Temperature	2	0.78055	0.78055	0.39027	6.46	0.134
Calcination time	2	0.06001	0.06001	0.03000	0.50	0.668
Residual Error	2	0.12092	0.12092	0.06046		
Total	8	4.60381				

Interpretation of analysis of variance (ANOVA)

Interpreting the analysis of variance (ANOVA) table for S/N ratio in a Taguchi experiment is essential for determining which factors have a statistically significant effect on the robustness of the process or product. The ANOVA table provided the statistical evidence to support the conclusions drawn from the main effect plot for S/N ratio. Basically, the p-value on the ANOVA table is used to identify the significant factor. As provided in the table p=0.03 which is less than α=0.05 and implied that precursor material is a significant factor. The factors are considered to have a statistically significant effect on the S/N ratio, meaning that their levels influenced the robustness of the process or the final product. Considering the magnitude of the F-statistic to evaluate the strength of the effect. While the P- value provides whether an effect is statistically significant, the F-statistic showed a measure of the strength of the effect. A larger

F-statistic indicate a stronger effect, even if the p-value is only marginally significant. In this case the F value for the corresponding p value is 30.12.

Response Table for Signal to Noise Ratios

Table 4.14 Response Table for Signal to Noise Ratios

Smaller is better

Level	Precursor material	Calcination Temperature	Calcination time
1	-14.09	-14.52	-14.78
2	-14.81	-14.78	-14.96
3	-15.65	-15.24	-14.80
Delta	1.56	0.71	0.18
Rank	1	2	3

Interpreting the response table for S/N ratio

A response table for a S/N ratio in Taguchi experiment is a concise way to summarize the effect of different factor levels on the S/N ratio. It provided a clear overview of which factor level contribute to a more robust process, allowed to identify the optimal settings. Unlike ANOVA the response table provides the average S/N ratio for each level of each factor directly.

Understanding the structure of the response table: Each row represents a factor and the column represent a level of factor. In addition, each cell contains the average S/N ratio for that specific factor level and the rank (or delta) is included to show the relative importance of each factor.

Steps for interpretation

Identify the optimal level for each factor: For each factor, the level with the highest average S/N ratio is the level that contributes the most to robust process, regardless of the S/N ratio type. As it's observed from the table the minimum negative value for factor one found to be level one, for factor two also level one, and for factor three also level one.

Determine the relative importance of the factors: Examining the rank column and/or the delta values provided an information on the relative importance of the factors. Delta statistic (calculated as the difference between the highest and lowest average S/N ratio for a factor) indicated that the magnitude of the effect of that factor on the S/N ratio.

A larger Delta indicates a stronger effect. As a result, the factors are ranked based on their delta values, with the factor having the largest delta assigned a rank of 1 which is the most important. From this explanation it can be conclude as per the rank and delta value from the table, the relative importance of the factor ranked precursor material as first and calcination time as least with second rank the calcination temperature.

Consider the magnitude of the S/N ratios: While the response table helps identified the best levels, it's important to consider the actual S/N ratio values. If the difference in S/N ratio between different levels is high, then the choice of that level is critical.so, considering the delta value from the table above, the maximum difference between the highest and lowest value found to be 1.56 which on the precursor material and this showed that it had a great influence than others. However, the delta value of the calcination time happened to be 0.18 which lowest and this implied that its effect was almost insignificant.

Compare and contrast effect: The effect of different level should be compared for each factor in order to assess the factor's level have similar effect size or have significant effects. Unlike the other factors, the calcination time has got almost similar value for different levels and this implied that it had no a significant effect.

Response Table for Means

Table 4.14 Response Table for Means

Level	Precursor material	Calcination Temperature	Calcination time
1	5.067	5.333	5.500
2	5.500	5.500	5.633
3	6.067	5.800	5.500
Delta	1.000	0.467	0.133
Rank	1	2	3

Interpreting the response table for mean

A response table for means is a tool used to summarize the effect of different factor level on the average value of a response variable. It's particularly useful in the context of experimental design for quick identification of the factor levels that result in the desired outcome. Understanding the structure of response table: Each row in the table represents a factor (independent variable) and each column represents a level of that factor. The other element found in the table is the cell which contains the average (mean) value of the response variable for all observations that have the specific factor level. The basic concepts are; Factor level: this is the specific value or categories that the factor take on. Mean response: this value is the average of the response variable for all observation with a specific factor level. Delta statistic: the difference between the highest and lowest average response for a factor this indicates the magnitude of the effect of that factor on the response. Rnak: the factors are ranked based on their Delta values. **Interpretation of the response table for mean**

Determine the optimization goal: the goal of this optimization is to minimize the response variable crystallite size. **Identify the optimal level for each factor:** As the aim of this study is to minimize the response variables, the factor level with the lowest average response in the table is selected. With this deduction, the first level for factor one, the first level for factor two and the first and the third level for factor three are the optimal levels.

Determine the relative importance of the factor: As shown in table 4.14 above the delta value or the rank provided an information about the relative importance of the factors. From this analysis, factors with larger Delta values have a greater effect on the response than factors with smaller delta values. As provided in the table the delta value with a larger value (precursor=1) showed that the factor with higher importance influence to the response variable. Whereas the factor with a very least delta value (calcination time =0.133) indicated that its influence in the property found to be less or insignificant. **Consider the magnitude of the effect**: The actual average response values in the table is the difference between the highest and the lowest values for a factor and this difference could be small or greater. The factor (precursor material) showed greater value on its difference from the highest and lowest value of its level and this indicated that the factor had a very significant effect.

Main effects plot for means

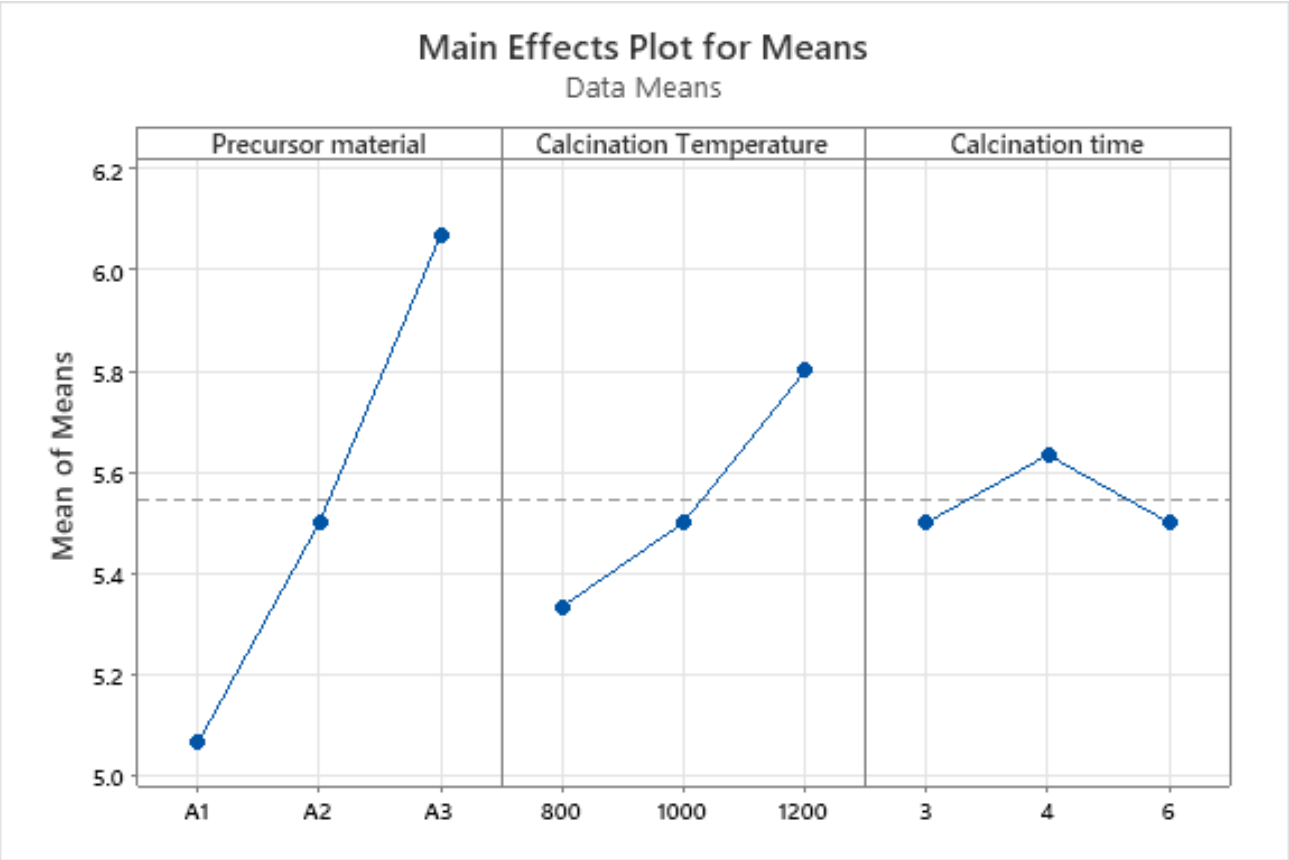

Figure 4.32 main effect plot for mean

Interpretation of main effects plot for means

Interpreting a main effects plot for means in Minitab involves understanding how each factor (input variable) affects the average (mean) response variable. The plot visually shows the relationship between each factor level and mean response. To analyze better understanding the component of the plot plays an important role.

Understanding the component of the plot: X- axis represents the different levels of each factor and each factor has its own x-axis. Y- axis represents the mean response variable (the average value of the output measured). Points on the plot represents the average (mean) value of the response variable for a specific level of factor and the lines connect the points for each factor indicated the direction and the magnitude of the effect of the factor on the response.

Steps for interpretation:

Identifying the Factors with Largest Effect: The factors with the steepest line have a greater effect in the response. The steep line indicates that changing the level of that factor significantly changed the mean response. As shown in Figure 4.32 above the factor with steepest almost to be vertical line is factor 1 (precursor materials) which indicated that it had a very greater effect on the response variable. Whereas, the result of factor three (calcination time) showed that the graph almost to be horizontal and the difference between the maximum and minimum is very low and this indicate that its effect was insignificant.

Determine the direction of the effect (positive or Negative): If the line slops upward as moved from left to right (or from lower to higher levels), it indicates a positive effect. This means that increasing the level of the factor tends to increase the mean response. If the line slops download as moved from left to right (or from lower to right level), it indicates a negative effect. This means that increasing the level of the factor to decrease the mean response. When we look at the first factor, the graph increases as increased the level and this provided an information as it had a positive effect and so does with the second factor. However, with the third factor, it showed both increasing and decreasing.

Determine the optimal level for Each Factor: To optimize the response, the factor levels that correspond to the desired outcome identified. If the response needs to maximize the response, the factor level with the highest mean response value on the y-axis. If the response needs to minimize the response, the factor level with the lowest mean response value on the y-axis. As this optimization aimed to minimize the response, the for factor it became minimum at level 1, for factor two at level 1 again, but for factor three both level one and there turned the same.

Consider the Magnitude of the Effect: While the slope of the line indicates the direction of the effect, the vertical distance between the highest and lowest points on the line indicates the magnitude of the effect. A larger vertical distance means that the factor has a more substantial influence on the response than a factor with a smaller vertical distance. Both factor one and two has positive slope and has a positive effect despite the fact that the magnitude of the effect provided in the graph as it's calculated in the response table. This showed that the response table and the main effect plot provided the same information.

Watch Out for Flat Line: A nearly horizontal (flat) line indicates that the factor has a little to no effect on the mean response variable over the range of level tested. The factor three has nearly a straight line and this made it to be considered as less significant.

Main effects plot for S/N (Signal to Noise) Ratios

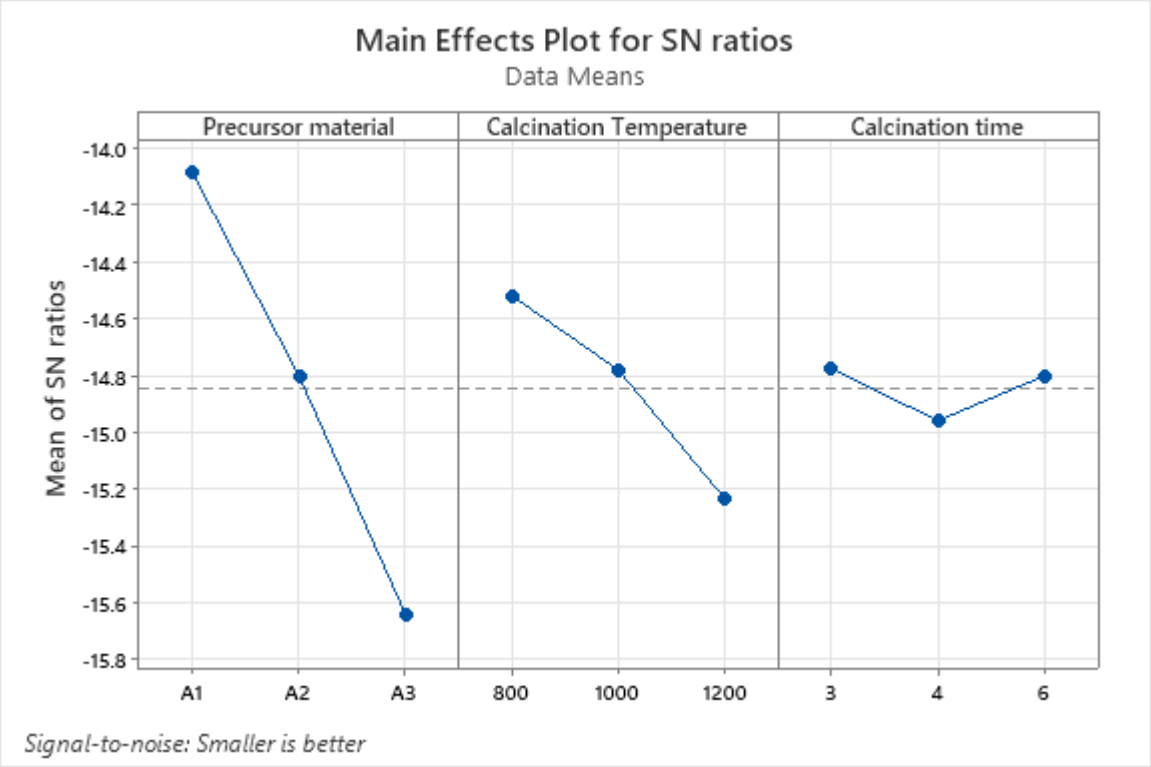

Figure 4.33 main effect plot for S/N ratio

Interpretating a main effects plot for S/N (Signal to Noise) Ratios

Interpretating a main effects plot for S/N (Signal to Noise) Ratios in Minitab involves understanding how each factor (input variable) influences the robustness of the process or product. S/N ratios are used in Taguchi methods to identify factor setting that minimize the effect of noise (uncontrollable variation) on the desired response.

Understanding the components of the plot: X- axis represents the different levels of each factor and each factor has its own x-axis. The Y-axis represents the S/N ratio. In this particular study smaller-is-better is the S/N ratio required which used when the response need to minimize.

A higher S/N ratio indicates a more robust process that consistently produces smaller value, even in the presence of noise. Each point on the plot represents the average S/N ratio for a specific level of the factor and the line which connect the points for each factor. The slope of the line indicates the direction of and the magnitude of the effect of the factor on the S/N ratio.

Steps for interpretation:

Identify the Factors with the largest Effects on Robustness: Focusing and looking for the factor with the steepest line and the steeper the line based on Figure 4.33, the greater the effect that factor has on the S/N ratio. This means the setting of that factor significantly affect the process's ability to resist noise and produce consistent results. Among the selected factors the precursor material showed a steepest line and this indicated that factor had a significant effect than others.

Determine the optimal level for Each Factor (Based on the S/N Ratio): For all S/N ratio type (Larger-is-better, smaller-is-better, Nominal-is-best) the factor levels with highest S/N ratio values on the y-axis. Higher S/N ratio always indicate more robust performance, regardless of the objective. Unlike for main effect plots for mean, in this scenario the greater S/N ratio turned the minimal value of the response. For this reason, for factor one level one, for factor level one and for factor three both level one and three are the optimal levels and this analysis squarely fits with the previous analysis. **Understanding the impact on Variation (Robustness):** The S/N ratio plot told the process need to be more resistant to noise factors (uncontrollable variable). The goal is to maximize the S/N ratio, which minimizes the impact of variation on your process output.

Therefore, the factor with steepest line (the precursor material) had a great impact on the minimizing the noise factor. **Consider the magnitude of the Effect:** The vertical distance between the highest and lowest points on the line indicates the magnitude of the effects on the S/N ratio. A larger vertical distance means the factor has a more substantial influence on the process's robustness. From the plot, the precursor material found to be the top ranked impactful effect to the response variable because it has got a larger vertical distance between the highest and the lowest value.

Watch out for Flat lines: A nearly horizontal (flat) line indicates that the factors have a little to no effect on the S/N ratio. Changing the level of this factor will not significantly improve the process's robustness. In general, the S/N ratio plots tell on how to minimize the impact of noise, not necessarily how to achieve the absolute best mean response. Unlike for factor one, the line for factor three showed that approximately to be flat or horizontal and this shows its impact on the response variable is less or no significant as it has been discussed in all pervious topics.

Residual plots for S/N ratio

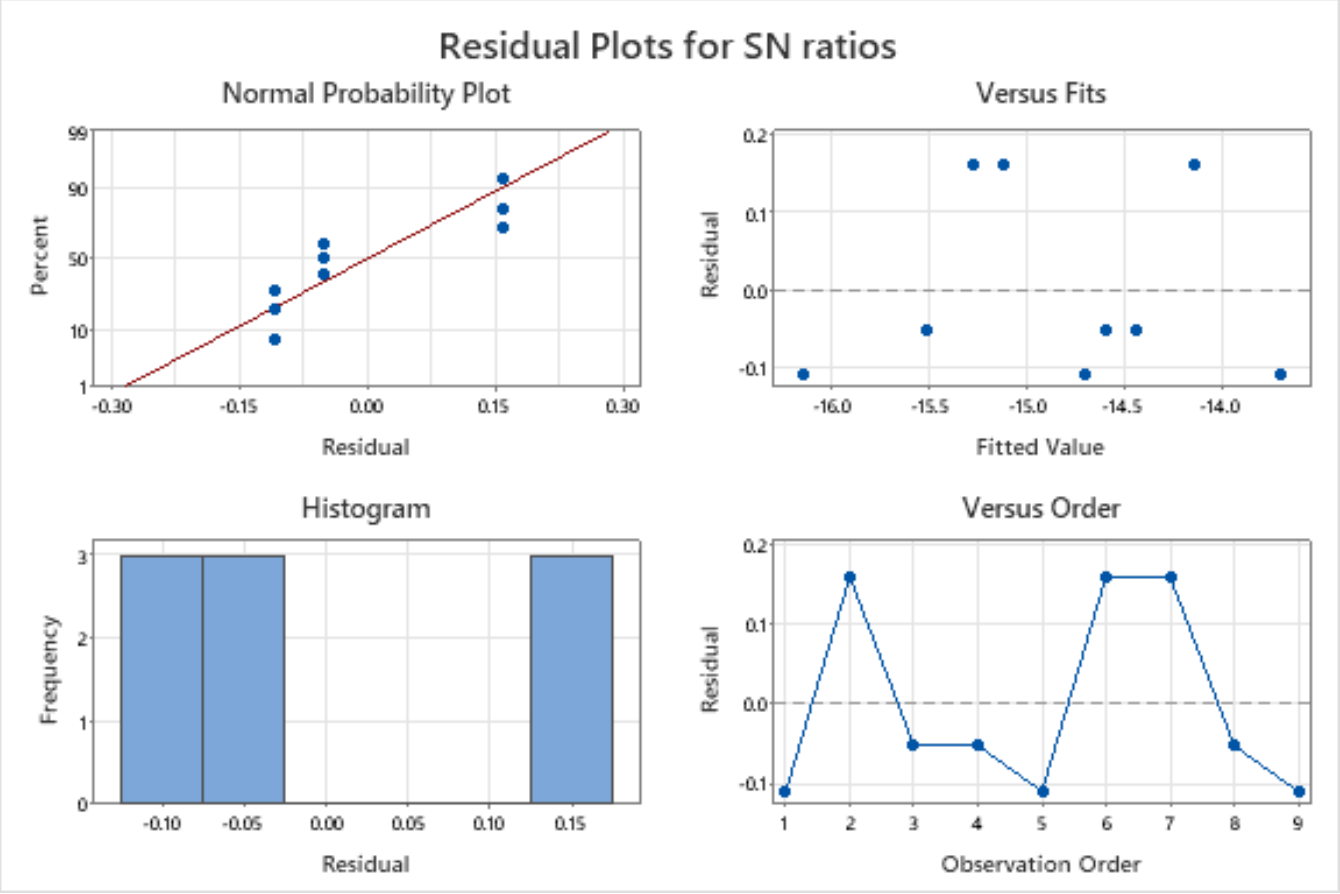

Figure 4.35 Residual plots for S/N ratio

Interpreting residual plots for S/N ratio

Interpreting residual plots for S/N ratio analysis in Minitab is essential for validating the assumptions of the statistical model used to analyze the Taguchi experiment. Residual plots help assess whether the model is a good fit for the data and whether the conclusions drawn from the S/N ratio analysis are reliable.

Key assumption of the statistical model used for S/N analysis

Normality of residuals: The residuals (the differences between the observed S/N ratios and the predicted S/N ratios from the model) should be approximately normally distributed. As shown in the plot of Figure 4.35, the data approximately distributed in the normal line and there no outliers observed. **Constant Variance:** The variance of the residuals should be constant across all levels of the factors. The versus fit graph in the plot shows that the residuals are scattered randomly. **Independence of Residuals:** The residual should be independent of each other as the graph of versus order in the plot indicated that the graph do not show any pattern and this implies the assumption is kept.

Common residual plots and their interpretation

Normal probability plot of residuals: The purpose assessed the normality of the residuals and the residuals failed approximately along a straight line. As shown in the plot residuals failed along the line with no outlier observed.

Residual vs. Fitted value (Residual vs. predicted values) plot: This plot assessed the constant variance assumption and detects non linearity and the residuals randomly scattered around zero, with no discernible patterns. The plot showed that the residuals appeared as randomly scattered.

Residual vs order of data (or Residual vs time) plot: This plot assessed the independence of residuals and detects any time related effects. The residual randomly scattered around zero, with no discernible patterns over time or data order. Therefore, the residuals are scattered or drown with no specific pattern and this indicated that their independence.

Histogram of residuals: This plot also provided another visual assessment of the normality of residuals. The histogram should be approximately bell-shaped and centered around zero. Despite the fact that the histogram in this plot showed a uniform histogram and this indicated that the residuals are uniformly distributed among the class.

Residual plot for mean

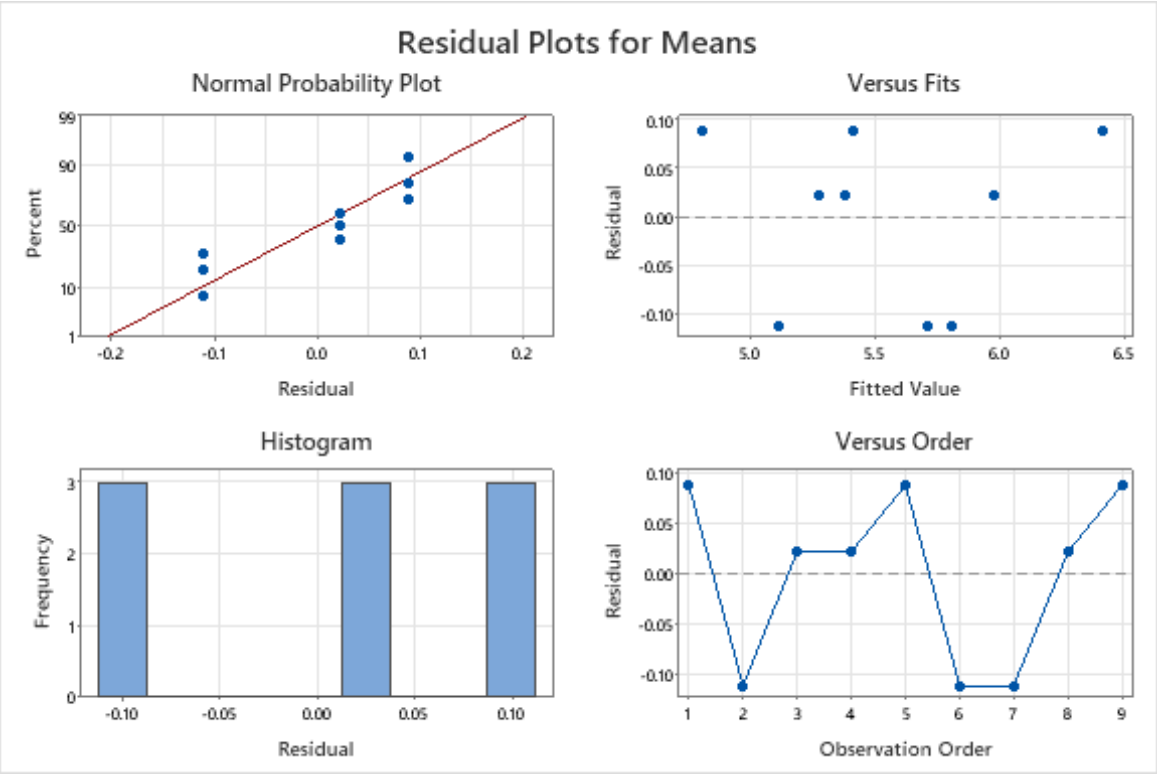

Figure 4.36 Residual plot for mean

Interpretation of residual plot for mean

Interpreting residual plots is a crucial step in regression analysis and other statistical modeling techniques. The key assumption are the errors (or residual) are random, have mean of zero, have constant variance, and are independent of each other.

Common residual plots and how to interpret them

Residuals vs Fitted value (or residuals vs predicted) plot: The residuals are randomly scattered around zero and this indicated that there was a constant variance Normal probability plot of residuals: As shown in the graph the residuals failed along the normal line even no outliers was observed. Residual vs order of data (or Residuals vs Time) plot: This graph shows in Figure 4.36 showed that the residuals have no pattern and it validated the assumption. Histogram of residuals: the uniform histogram showed that the residuals are uniformly distributed.

4.2.2 Single response analysis for (Weight/mass loss)

Taguchi Analysis: Weight loss versus Precursor material, Calcination temperature, Calcination time

Linear Model Analysis: SN ratios versus Precursor material, Calcination temperature, Calcination time

Estimated Model Coefficients for SN ratios

Table 4.16 Estimated Model Coefficients for SN ratios

Term	Coef	SE Coef	T	P
Constant	-14.8518	0.06215	-238.984	0.000
Precursor A1	0.3287	0.08789	3.740	0.065
Precursor A2	0.0686	0.08789	0.781	0.517
Calcination T 800	-0.8078	0.08789	-9.191	0.012
Calcination T 1000	0.0455	0.08789	0.518	0.656
Calcination t 3	0.1649	0.08789	1.877	0.201
Calcination t 4	-0.0470	0.08789	-0.534	0.646

Interpreting the estimated model coefficients for S/N ratio

Interpreting the estimated model coefficients for S/N (Signal-to-Noise) ratios in a Taguchi experiment involves analyzing how each factor level influences the S/N ratio and the overall robustness of the process. This interpretation differs from that of a typical regression model because the focus is on maximizing the S/N ratio, which reflects process robustness, rather than predicting a mean response. In this study, the "smaller-is-better" S/N ratio type was selected, as the goal is to reduce weight loss.

Steps for interpretation:

Identify the baseline level: The baseline level is determined from Minitab's output, usually the first factor level listed or the constant. **Interpret the sign and magnitude of the coefficients:** A positive coefficient indicates that moving from the baseline level to a given level improves the S/N ratio, enhancing robustness. A negative coefficient indicates a decrease in robustness.

The magnitude of the coefficient represents the strength of the effect on the S/N ratio. Based on Table 4.16 level of factor 1 have positive and higher coefficient. **Identification of the optimal level for each factor:** The level with the largest positive coefficient (or the least negative) is preferred because it leads to the highest S/N ratio. If all coefficients are negative, the level with the smallest absolute value should be selected to minimize S/N ratio reduction. Therefore, the optimal value of factor one found to be level one, for factor two is level two, and for factor three is level one.

Model Summary

Table 4.17 Model Summary

S	R-Sq	R-Sq(adj)
0.1864	98.53%	94.11%

Understanding the Model Summary

When reviewing a model summary in statistical software like Minitab, it's important to understand the key statistics that reflect how well the model performs. These figures help assess how effectively the model accounts for variations in the dependent variable the outcome you're trying to predict or explain. In this study, the analysis was conducted using ANOVA, so the statistics discussed apply to that method.

Key Statistics in a Model Summary and Their Interpretation:

R-squared (R^2): This value shows how much of the variation in the dependent variable is explained by the independent variables in your model. R^2 ranges from 0 to 1. **$R^2 = 0$** means the model explains none of the variation there's no predictive power. **$R^2 = 1$** indicates a perfect fit the model explains all variability in the outcome. Values between 0 and 1 represent the proportion of explained variance, with higher values indicating a better fit. As per Table 4.17 the R^2 = 98.53% indicated the model explained all variability in the outcome with 98.53% percent accuracy.

Adjusted R-squared: Unlike R^2, which can increase even when irrelevant variables are added, the adjusted R^2 accounts for the number of predictors in the model. It provides a more reliable measure by penalizing the inclusion of unnecessary variables.

It can be lower than R^2, and sometimes even negative if the model performs poorly. A big gap between R^2 and adjusted R^2 suggests overfitting or inclusion of insignificant predictors. The adjusted R^2 obtained from the optimization is 94.11% which is less than the R^2 value. The difference between the two values is, 4.42% and this result indicated that the inclusion of unnecessary variables is happened.

Standard Error of the Estimate (SEE or S): This metric measures the average deviation of observed values from the model's predicted line. In essence, it reflects the typical error in the model's predictions. Smaller values indicate more accurate predictions. It's also useful for creating prediction intervals, helping understand the expected range for future observations. The Standard error of the estimate obtained is 0.1864 and this implies that the model deviated from the dependent variable by the value of 0.1864.

Analysis of Variance for SN ratios

Table 4.18 Analysis of Variance for SN ratios

Source	DF	Seq SS	Adj SS	Adj MS	F	P
Precursor material	2	0.81198	0.81198	0.40599	11.68	0.079
Calcination temperature	2	3.70660	3.70660	1.85330	53.32	0.018
Calcination time	2	0.13000	0.13000	0.06500	1.87	0.348
Residual Error	2	0.06952	0.06952	0.03476		
Total	8	4.71809				

Analyzing the ANOVA table for S/N ratio

Analyzing the ANOVA table for the signal-to-noise (S/N) ratio in a Taguchi experiment is crucial for identifying which factors significantly impact the process or product robustness. This table offers statistical backing for the findings observed in the main effects plot for the S/N ratio. The p-value helps determine which factors are statistically significant.

When a factor is statistically significant, it suggests that its levels affect the robustness of the process or product. Additionally, the F-statistic is used to assess how strong the impact is.

While the p-value tells us whether an effect exists, the F-statistic indicates the intensity of that effect higher F-values suggest a stronger influence, even when the p-value is only somewhat significant. The significate factor which influenced the thermal stability of the final product found to be the calcination temperature as the p value (0.018) as per the result in Table 4.18 which is much less than the significant level (α=0.05). Whereas, the other factors found to be less significant as their value is registered greater than the significance level.

Response Table for Signal to Noise Ratios

Table 4.19 Response Table for Signal to Noise Ratios

Level	**Precursor material**	**Calcination temperature**	**Calcination time**
1	-14.52	-15.66	-14.69
2	-14.78	-14.81	-14.90
3	-15.25	-14.09	-14.97
Delta	0.73	1.57	0.28
Rank	2	1	3

Interpreting the Response Table for S/N Ratio

Interpreting the Response Table for S/N Ratio in a Taguchi Experiment The response table for the signal-to-noise (S/N) ratio in a Taguchi experiment efficiently summarizes how various factor levels impact the S/N ratio. It offers a straightforward look at which levels enhance process robustness and helps pinpoint the best settings. Unlike ANOVA, which focuses on statistical significance, this table shows the average S/N ratio for each level of every factor directly.

Interpretation of response table for S/N ratio

Find Optimal Levels: The level with the highest average S/N ratio for each factor, as this level contributes most to a robust process strict consideration need to be taken. As per table 4.19, the optimal level for factor one is level one, for factor two is level three, and for factor three is level one which can provide the minimum mass loss of the alumina ceramic. **Assess Importance of Factors:** Use the delta value (the difference between the highest and lowest average S/N ratios for a factor) to gauge the impact of each factor. A higher delta means a greater influence, and factors are ranked accordingly. Based on the delta value provided in Table 4.19, factor two has the top ranked in its influence on the thermal stability of the material and factor three impacts the least.

Analyze S/N Ratio Values: Beyond ranking, it's important to look at the actual S/N ratio differences. If the range is large, selecting the right level becomes crucial. The difference between the highest level and lowest level describes the factors impact level. So, with this the highest difference (with delta value of 1.57) observed in factor two which means it's the dominant factors. The second most important factor ranked to be factor one and then factor three. **Compare Factor Effects:** Comparing and analyzing the different levels within each factor to see if the effects are similar or significantly different. As shown in Table 4.19, the S/N ratio value of the three levels of factor two appeared to have significant difference. Whereas, the values in factor three appeared to be closed to each other.

Response Table for Means

Table 4.20 Response Table for Means

Level	Precursor material	Calcination temperature	Calcination time
1	5.333	6.077	5.433
2	5.500	5.500	5.567
3	5.810	5.067	5.643
Delta	0.477	1.010	0.210
Rank	2	1	3

A response table for means helps summarize how different levels of factors influence the average value of a response variable. It's especially handy in experimental setups for quickly spotting which factor levels lead to the most favorable outcome.

Table Structure: Each row represents a factor (an independent variable), while the columns show the various levels of that factor. Each cell in the table shows the mean value of the response variable for that specific level. Factor level refers to a specific setting or category of a factor. Mean response is the average response for that level. Delta value is the range between the highest and lowest average responses for a factor, indicating the strength of its impact. Rank orders the factors by the size of their delta values.

Steps to Interpret:

Clarify the Optimization Goal: In this case, the objective is to **minimize** the response variables (weight loss). **Find the Best Factor Levels:** The level with the lowest mean response for each factor is more desirable. Based on Table 4.20, the level at which the smallest mean value observed is, for factor one is level one, for factor two is level three and for factor three is level one is found to be the smallest values which contributed highly for the thermal stability of the product.

Assess Factor Significance: The **delta** or **rank** helps to understand which factors have the most influence the larger the delta, the more significant the effect. The delta value in Table 4.20 provided an information about the relative importance of the factors, so factor two has got delta value of 1.010 which is the highest one and indicated that it's most important than others and the other factor become important based on their delta value. Factor two is the second important factor and factor is the least important.

Review Effect Size: The difference between the maximum and minimum mean response values for each factor shows how much that factor can affect the outcome. This range may be small or large, depending on the factor. Based on the evaluation of the difference in mean values factor two appeared with highest value which indicted that selecting this factor is the right decision to minimize the mass lose.

Main effects plot for mean

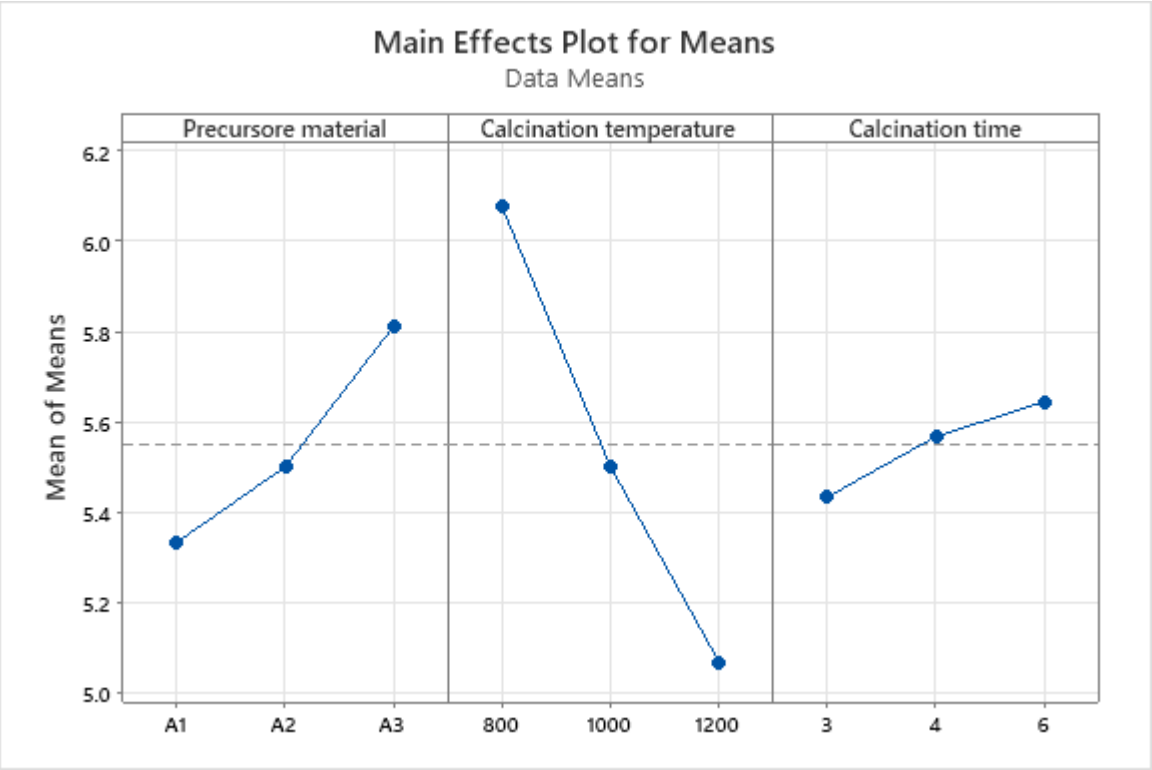

Figure 4.37 main effect plot for means

Interpreting a main effects plot for mean

Interpreting a main effects plot in Minitab involves analyzing how each factor (or input variable) influences the average (mean) response variable. This plot provides a visual representation of the relationship between factor levels and the mean response. To interpret the plot effectively, it is crucial to understand its components.

Understanding the plot components: The x-axis represents the levels of each factor, with each factor having its own x-axis. The y-axis shows the mean response variable, which is the average value of the measured output. Points on the plot indicate the mean response for a specific factor level, and the lines connecting these points illustrate the direction and magnitude of the factor's effect on the response.

Steps for interpretation:

Identify factors with the largest effect: Factors with steepest lines have a greater impact on the response. A steep slope indicates that changing the factor level significantly alters the mean response. Based on the information obtained from Figure 4.37, the steepest graph is observed in factor two which implied that this factor has a greatest impact than the others. The next steeper is factor one and then factor three provided that their effect is moderate and least.

Determine the direction of the effect: If the line slopes upward from left to right, the factor has a positive effect, meaning higher levels of the factor increase the mean response. Conversely, a downward slope indicates a negative effect, where increasing the factor level decreases the mean response. To determine the direction of the effect, the graph is easiest way. As moved from left to right factor one's and three's graph increases, factor two's graph decreases.

Find the optimal factor levels: To optimize the response, identify the factor levels that achieve the desired outcome. For maximizing the response, choose the level with the highest mean response on the y-axis. For minimizing it, select the level with the lowest mean response. As the minimum value are required, level one for factor one, level three for factor two, and level one for factor three are the optimal levels for minimizing the mass loss

Evaluate the magnitude of the effect: The slope of the line shows the direction of the effect, while the vertical distance between the highest and lowest points on the line indicates the magnitude. A larger vertical distance means the factor has a stronger influence on the response. As the plot shows that the maximum vertical distance observed at factor two and this provide an information about the magnitude of the effect.

Watch for flat lines: A nearly horizontal line suggests that the factor has little to no effect on the mean response across the tested levels. From the plot, unlike for factor two factor three have nearly flat line and this is the indication its effect on the final property of the product is most likely insignificant.

Main effects plot for S/N

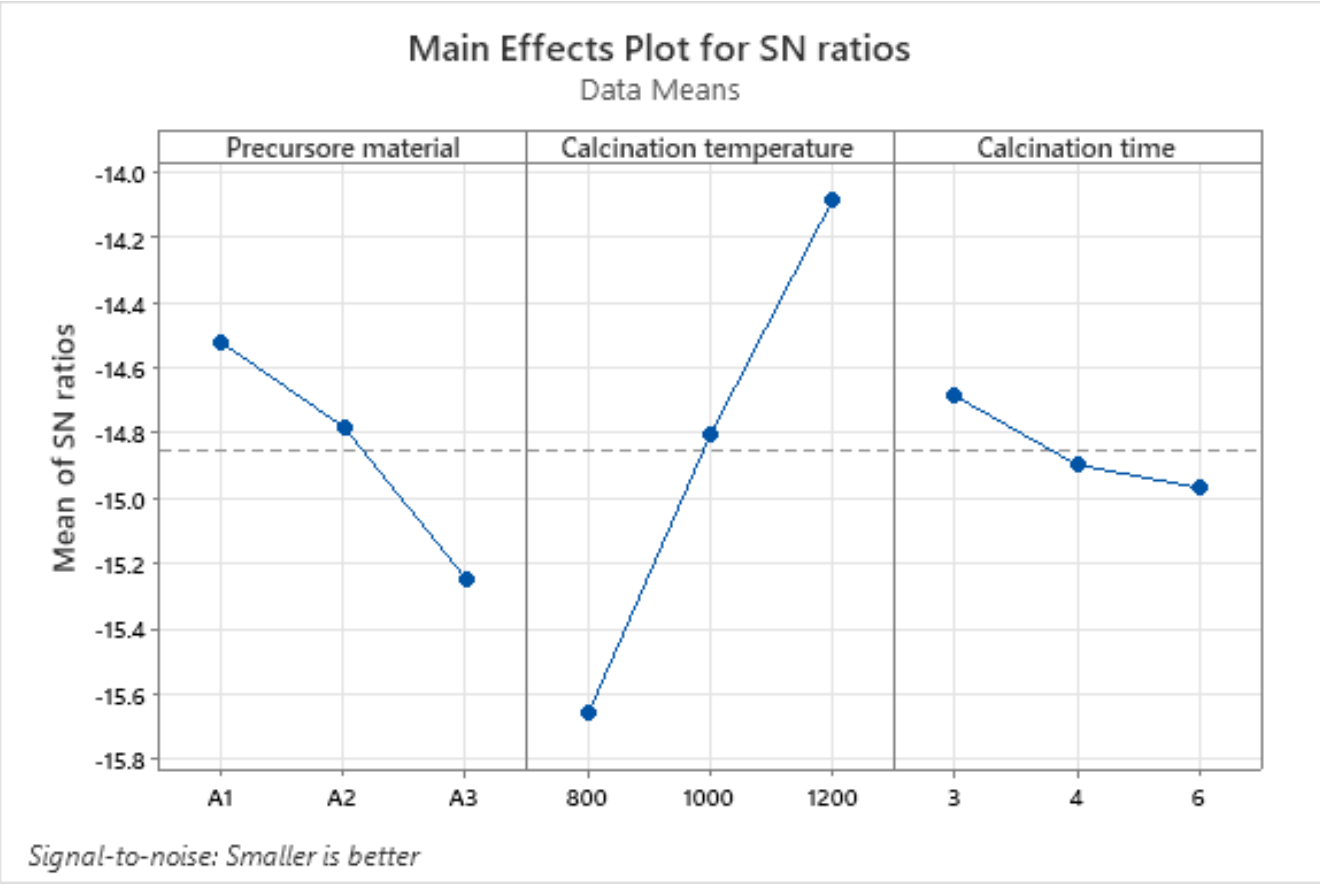

Figure 4.38 main effect plot for S/N ratio

Interpreting a main effects plot for S/N

Interpreting a main effects plot for S/N (Signal-to-Noise) ratios in Minitab involves analyzing how each factor (input variable) impacts the robustness of a process or product. S/N ratios, commonly used in Taguchi methods, help identify factor settings that reduce the influence of noise (uncontrollable variation) on the desired response.

Understanding the plot components: The x-axis represents the levels of each factor, with each factor having its own x-axis. The y-axis shows the S/N ratio, which varies depending on the experiment's objective in this case, the Smaller-is-better S/N ratio is used, which is appropriate when the goal is to minimize the response.

A higher S/N ratio indicates a more robust process that consistently produces smaller values, even in the presence of noise. Each point on the plot represents the average S/N ratio for a specific factor level, and the lines connecting these points show the direction and magnitude of the factor's effect on the S/N ratio.

Steps for interpretation:

Identification of factors with the largest effects: The steeper the line, the greater the factor's impact on the S/N ratio, meaning that factor significantly affects the process's ability to resist noise and produce consistent results. Therefore, factor has got steepest line relative to others as shown in Figure 4.38 and implied that the factor has a significant influence on the thermal stability of the product. Factor one and three impacts second and third respectively.

Determine the optimal level for each factor: Regardless of the S/N ratio type (Larger-is-better, Smaller-is-better, or Nominal-is-best), the factor levels with the highest S/N ratio values on the y-axis indicate more robust performance. Based on the plot on figure 25, the optimal level for factor one is level one, for factor two level three, and for factor three is level one.

Evaluate the magnitude of the effect: The vertical distance between the highest and lowest points on a line reflects the magnitude of the factor's effect on the S/N ratio. A larger vertical distance indicates a stronger influence on the process's robustness. The largest vertical distance observed from the graph at factor two and the least is factor three.

Watch for flat lines: A nearly horizontal line suggests that the factor has little to no effect on the S/N ratio. Changing the level of such a factor will not significantly improve the process's robustness. Overall, S/N ratio plots focus on minimizing the impact of noise rather than achieving the best mean response. The very nearly flatten line is observed at factor three and it implies that factor has low or no significant to the properties in need.

Residual plots for S/N ratio

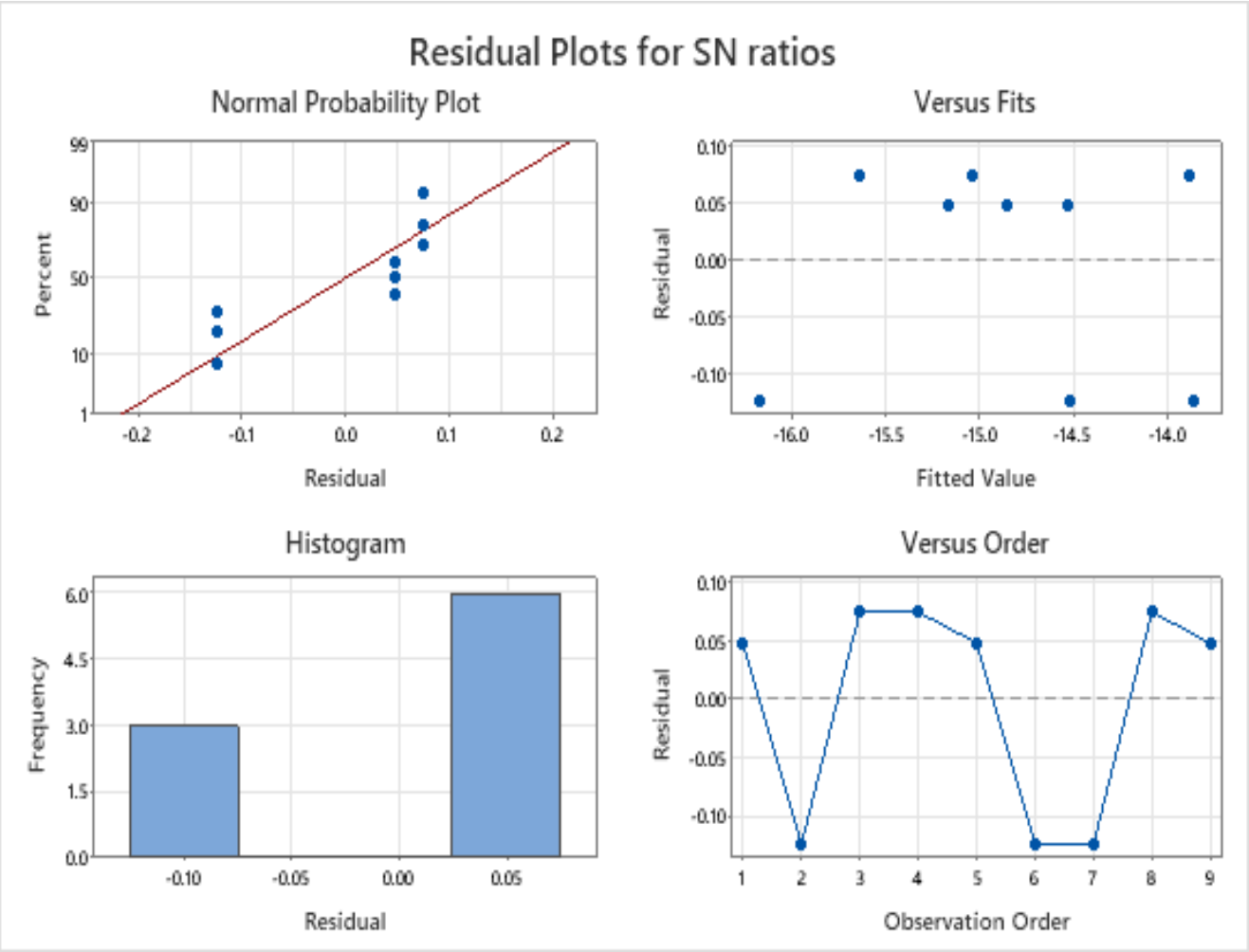

Figure 4.39 residual plot for mean

Interpreting residual plots for S/N ratio

Interpreting residual plots for S/N ratio analysis in Minitab is a critical step in validating the assumptions of the statistical model used in a Taguchi experiment. These plots help determine whether the model fits the data well and whether the conclusions drawn from the S/N ratio analysis are reliable. Unlike residual plots for mean responses, the focus here is on the validity of the model predicting S/N ratios rather than the raw data itself.

Key assumptions of the statistical model for S/N analysis:

Normality of residuals: The residuals, which are the differences between observed and predicted S/N ratios, should follow a normal distribution. It's shown that the residuals are normally distributed along the normal line and the assumption is kept. **Constant variance:** The residuals should have consistent variance across all factor levels. As it's shown in the versus fit graph of the residuals are scattered randomly around zero according to the plots in Figure 4.39.

Independence of residuals: Residuals should not show patterns or correlations, meaning they should be independent of one another. The graph of versus order shows that it has not a pattern and indicated that the residuals are independent to each other. Residual plots are essential for ensuring that the statistical model used for S/N ratio analysis is appropriate. If the assumptions are not met, the model may not provide reliable results. However, in this case the assumptions are met as discussed above based on the graph in the plot.

Residual plots for the mean

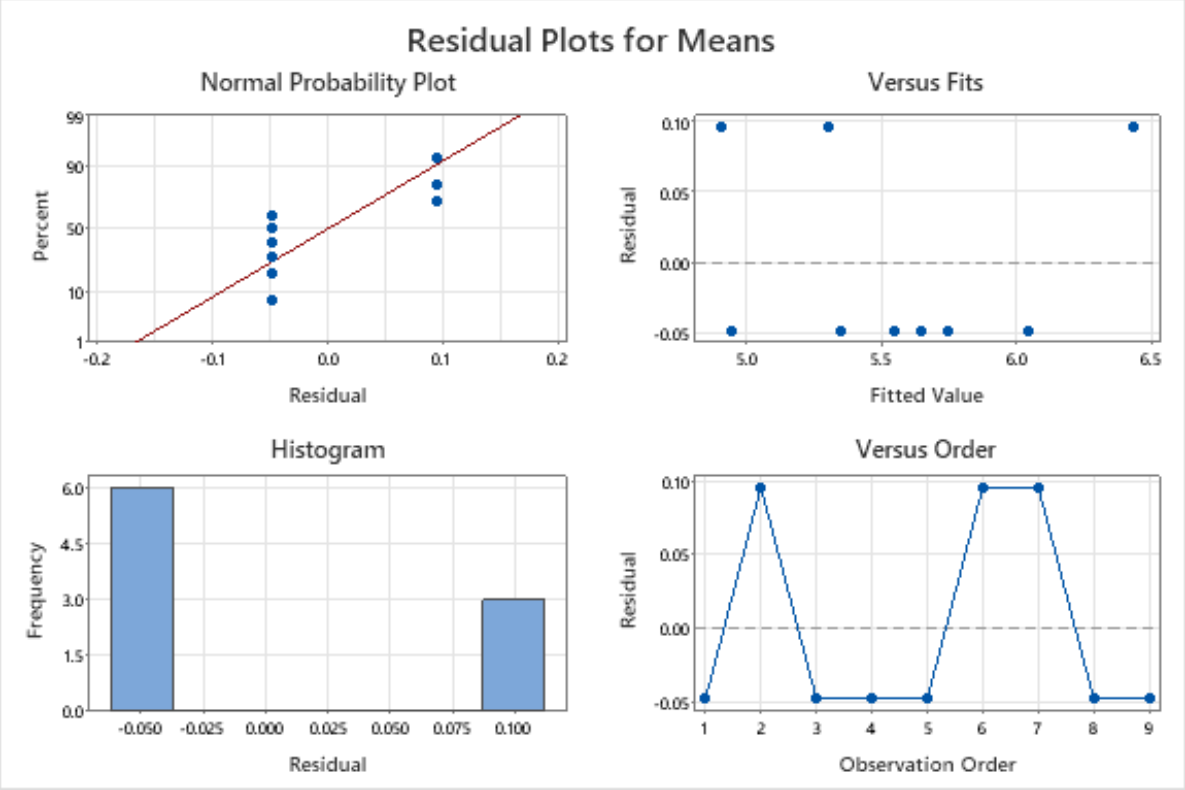

Figure 4.40 residual plot for mean

Analyzing residual plots for the mean

Analyzing residual plots for the mean is an essential part of regression analysis and other statistical modeling methods. These plots help evaluate whether the model's assumptions hold true, which is crucial for ensuring reliable results. Essentially, they indicate whether the model is a good fit for the data. The primary assumptions include that the errors (or residuals) are random, have a mean of zero, display constant variance, and are independent of one another. Common types of residual plots and their interpretations include:

Residuals vs. Fitted values (or predicted values) plot: This plot is useful for checking the constant variance assumption and identifying non-linearity. The residuals should be randomly distributed around zero with no obvious patterns. The graph in figure 4.40, showed that the residuals are scattered randomly around zero which met the constant variance assumption.

Normal probability plot of residuals: This plot helps assess whether the residuals follow a normal distribution, with the residuals roughly aligning along a straight diagonal line. Therefore, the residuals failed around the normal line and no outliers are observed.

Residuals vs. Order of data (or Residuals vs. Time) plot: This plot helps determine if the residuals are independent and if any effects are present. The residuals should be randomly scattered around zero with no apparent patterns. The graph in the plot indicated that the residuals have no known pattern and this implies that the residuals are independent.

Histogram of residuals: This plot offers a visual check of the normality of the residuals. The histogram should resemble a bell curve, centered around zero. However, in this plot the histogram is most likely uniform distribution which means residual is uniformly distributed among the class.

4.2.3 Multi-response optimization (Crystallite size and mass loss)

Taguchi Analysis coupled with Grey Relational Analysis (GRA): Crystalline size, Weight loss versus Precursor material, Calcination Temperature, Calcination as shown in table 4.24.

Grey Relational Analysis (GRA) converts multiple responses into a single, composite score and this has the following steps

Normalization: GRA first normalized the responses based on the "smaller is the better "criteria and each individual response was transformed into comparable scale, typically between 0 and 1. The normalized value show in Table 4.21 was calculated using the equation 4.3 shown below.

$$Z_{ij} = \frac{max(Y_{ij}) - Yij}{max(Y_{ij}) - min(Y_{ij})}$$ Equation (4.3) (Panda et al., 2016)

Table 4.21 response and normalized value

	Response	
	Crystallite size	Weight loss
1	20.60	5.70
2	6.50	5.40
3	5.80	4.90
4	8.00	6.00
5	6.90	5.50
6	5.20	5.00
7	26.50	6.53
8	8.60	5.60
9	6.50	5.30
Min.	5.20	4.90
Max.	26.50	6.53

	Normalized Values	
	C4	C5
	0.277	0.5092
	0.93897	0.69325
	0.97183	1
	0.86854	0.32515
	0.92019	0.6319
	1	0.93865
	0	0
	0.84038	0.57055
	0.93897	0.7546
Min.	0	0
Max.	1	1

Grey Relational Coefficient (GRC): The GRC quantifies the similarity between the actual experimental result and the ideal result. A higher GRC value means the experimental results is closer to the ideal, normalized results. To calculate GRC value shown in Table 4.22 using equation 4.5, the deviation sequence is a crucial step in qualifying the difference between a reference sequence (the ideal or best possible outcome) and the actual experiments the absolute difference between each data point in the reference sequence and the corresponding data point in the comparability sequence using equation 4.4 as indicated in Table 4.22 the value for the two responses.

$$\Delta_o j(k) = |Yo_i(k) - Y_i(k)|$$

Equation (4.4) (Panda et al., 2016)

$$\gamma\left(Yo_i(k), Y_i(k)\right) = \frac{\Delta min + \xi \Delta max}{\Delta_o j(k) + \xi \Delta max}$$

Equation (4.5) (Panda et al., 2016)

Table 4.22 Deviation sequence and GRC values

	Deviation Sequence		GRC	
	Crystallite size	Mass loss	Crystallite size	Mass loss
	0.723	0.4908	0.40883	0.50464
	0.06103	0.30675	0.89121	0.61977
	0.02817	0	0.94667	1
	0.13146	0.67485	0.79182	0.42559
	0.07981	0.3681	0.86235	0.57597
	0	0.06135	1	0.89071
	1	1	0.33333	0.33333
	0.15962	0.42945	0.75801	0.53795
	0.06103	0.2454	0.89121	0.67078
Min.	0	0		
Max.	1	1		

Grey Relational Grade (GRG): the GRG is an average an aggregate score of all the GRCs for multiple responses. The GRG acts as a single performance index that represents the overall performance of the experimental run. Optimization objective: The purpose of Taguchi is to find the parameter settings that yield the best overall performance. Since the GRG combines all response into a single score that reflects overall' 'goodness," Taguchi optimization aims to maximize the GRG calculated using the equation 4.6.

Therefore, a higher GRG score as shown in Table 4.23 indicates that on average, all responses are collectively closer their optimum value.

$$GRG = \frac{1}{k}\sum_{i=1}^{m} \gamma_{ij}$$ Equation 4.6 (Panda et al., 2016)

Table 4.23 GRG values and their grade

GRG	Grade
0.456737	8
0.755493	4
0.973333	1
0.608705	7
0.719160	5
0.945355	2
0.333333	9
0.647980	6
0.780998	3

Table 4.24 process parameters and GRG value of the two responses

Precursor material	Calcination Temperature	Calcination time	Crystallite size and mass loss
A1	800	3	0.456737
A1	1000	4	0.755493
A1	1200	6	0.973333
A2	800	4	0.608705
A2	1000	6	0.719160
A2	1200	3	0.945355
A3	800	6	0.333333
A3	1000	3	0.647980
A3	1200	4	0.780998

Linear Model Analysis: SN ratios versus Precursor material, Calcination Temperature, Calcination

Estimated Model Coefficients for SN ratios

Table 4.25 Estimated Model Coefficients for SN ratios

Term	Coef	SE Coef	T	P
Constant	-3.62206	0.4297	-8.430	0.014
Precursor material A1	0.46311	0.6077	0.762	0.526
Precursor material A2	1.06757	0.6077	1.757	0.221
Calcination temperature 800	-3.26494	0.6077	-5.373	0.033
Calcination temperature 1000	0.59951	0.6077	0.987	0.428
Calcination time 3	-0.06579	0.6077	-0.108	0.924
Calcination time 4	0.65730	0.6077	1.082	0.392

Interpretation of estimated model coefficients for SN ratios

In a Taguchi experiment, interpreting the estimated model coefficients for Signal-to-Noise (S/N) ratios requires understanding how different factor levels influence the S/N ratio and process robustness. This interpretation is distinct from a typical regression analysis because the aim is to maximize the S/N ratio, which indicates robustness, rather than predict a mean response. For this study, the "smaller-is-better" S/N ratio type was chosen, as the objective is to minimize particle size and weight loss.

Steps for interpretation:

Identification of baseline level: The baseline level, typically the first factor level listed in Minitab's results, is identified. So, the constant term indicates to the baseline which is helpful to us as a reference to deal with process parameters whether they do have negative or positive effect and the like.

Interpreting the sign and magnitude of the coefficients: A positive coefficient shows that switching to a particular level improves the S/N ratio, enhancing process robustness. Conversely, a negative coefficient suggests a decline in robustness.

The magnitude of the coefficient tells how strongly a factor level affects the S/N ratio. As per the data in Table 4.25, the sign of the first level of each factor happened to be negative which implied that the change to the other level reduces the S/N ratio and by that the robustness decreases.

Identify the optimal level for each factor: The optimal level corresponds to the factor with the largest positive coefficient (or the smallest negative coefficient). In cases where all coefficients are negative, the level with the smallest absolute value is preferred to minimize S/N ratio reduction. Therefore, the optimal level for factor one is level two, for factor two, and for factor three is level two.

Model Summary

Table 4.26 Model Summary

S	R-Sq	R-Sq(adj)
1.2891	95.33%	81.31%

Interpretation of Model Summary

R-squared (R^2): R^2 is known as the coefficient of determination. It tells you how much of the variability in the dependent variable is accounted for by the independent variables. A value of 0 means the model explains none of the variation and a value of 1 means the model accounts for all of it. Values between 0 and 1 represent the proportion of variance explained, indicating how well your model fits the data. Therefore, R-squared obtained from the optimization of Table 4.26 is R^2=95.33% this implied that the created model fits with 95.33% efficiency.

Adjusted R-squared: It's typically lower than R^2 and can even be negative in cases where the model is not useful. The greater the gap between R^2 and Adjusted R^2, the more likely unnecessary variables have inflated the model. As per the result shown in the table the adjusted R-squared found to be 81.31% which is lower than that of R-squared and the difference between the two value is 14.02%. This result shows how unnecessary variables affects the efficiency of the model.

Standard Error of the Estimate (S): This is the average amount that our predictions differ from the actual data points. A lower standard error means more precise predictions. This metric

helps judge the reliability of the model's forecasts and can be used to build prediction intervals. Therefore, the standard error of the estimate obtained to be 1.2891and this value highlighted that the model deviates from the dependent variable by that it.

Analysis of Variance for SN ratios

Table 4.27 Analysis of Variance for SN ratios

Source	DF	Seq SS	Adj SS	Adj MS	F	P
Precursor material	2	11.091	11.091	5.546	3.34	0.231
Calcination Temperature	2	54.371	54.371	27.186	16.36	0.058
Calcination time	2	2.359	2.359	1.179	0.71	0.585
Residual Error	2	3.323	3.323	1.662		
Total	8	71.145				

Interpretation of ANOVA table for the S/N ratio

Understanding the ANOVA table for the S/N ratio in a Taguchi design is vital to pinpoint which variables meaningfully influence the consistency of a product or process. This table supports the interpretations made from the main effect plot by offering statistical confirmation.

Key insights come from the p-values, which highlight which factors have a statistically significant impact on the S/N ratio, reflecting their effect on process reliability. Moreover, the F-statistic measures the extent of each factor's influence. While the p-value identifies significance, the F-statistic quantifies how strong that influence is larger values suggest a more pronounced effect, even if statistical significance is borderline. As it's shown in Table 4.27 the p-value for all factors is a bit greater than the conventional threshold (α=0.05) and this implied that all the parameters have an impact, not that significant. In this case factor two had a better effect on final property (crystallite size and mass loss) of alumina ceramic and its strength of impact expressed by the F-value (F=16.36) which is greater than the others.

Response Table for Signal to Noise Ratios

Table 4.28 Response Table for Signal to Noise Ratios

Larger is better

Level	Precursor material	Calcination Temperature	Calcination time
1	-3.1589	-6.8870	-3.6878
2	-2.5545	-3.0225	-2.9648
3	-5.1527	-0.9566	-4.2136
Delta	2.5982	5.9304	1.2488
Rank	2	1	3

Interpretation of response table for S/N ratio

A response table for S/N ratio in Taguchi analysis simplifies the process of evaluating how different factor levels influence the robustness of a system. It clearly outlines which levels lead to higher S/N ratios, helping in the selection of optimal parameters. In contrast to the ANOVA table, this one provides direct average S/N values for every level of each factor. Each factor is listed in rows, and its levels are shown in columns.

Steps to Interpret:

Select the Best Levels: For each factor, the level with the highest average S/N ratio represents the setting that boosts process stability the most. With this explanation, the best level for factor one is level two has a minimum negative value, so level two has a significant impact. For factor two level three and for factor three level two has a significant factor respectively.

Evaluate Factor Significance: Look at the delta values, which show the range between the highest and lowest average S/N ratios for each factor. The larger the delta, the more that factor influences the outcome. Factors are ranked accordingly, with rank 1 indicating the most impactful. All factor may or may not have similar impact on the response variable and this can be identified by their rank obtained as shown in Table 4.28. The top ranked process parameter is factor two and then factor one.

Examine Actual S/N Differences: Don’t just rely on rankings pay attention to how much the S/N ratios vary. Large differences mean level selection is more crucial. The other way to figure

out the level of impact of the factor is, to look at the difference between the highest and lowest value. Therefore, based on the result on the table the highest difference lied on factor two and this confirmed that this factor influenced the response much better than others.

Analyze Level Comparisons: Compare how much impact each level has within a factor to determine whether the effects are similar or if one stands out significantly. The level of each factor might have large or narrow gab in their response and this indicates that how impactful the factor is. As it's observed from the table factor one and two has a major difference in response with their different level though factor three did bring almost closest results. This analysis helped to conclude that choosing factor as the process parameter was a wrong decision.

Main effect plot for mean

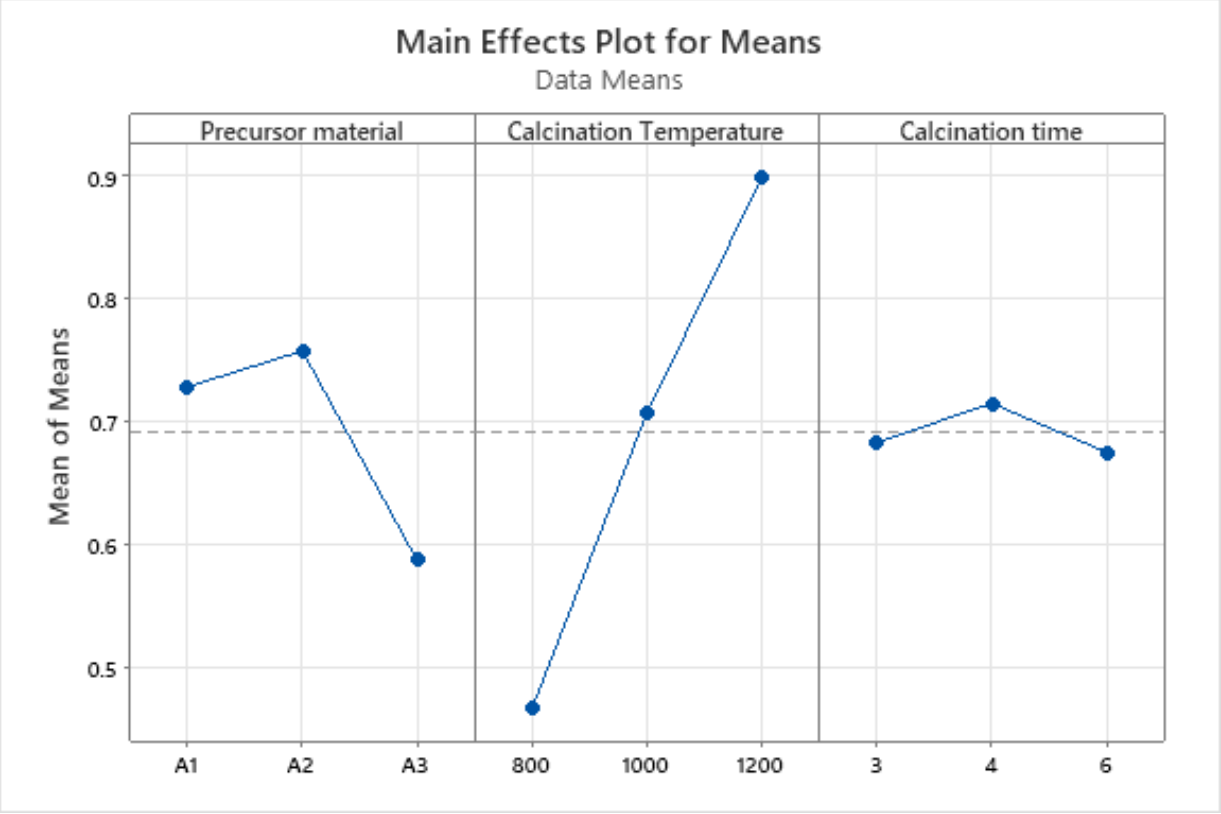

Figure 4.41 main effect plot for mean

Interpretation of main effect plot for mean

To interpret a main effects plot in Minitab, you need to understand how each factor (input variable) impacts the average (mean) response variable. The plot visually demonstrates the relationship between factor levels and the mean response, and understanding its components is key to effective analysis.

Components of the plot: The x-axis represents the levels of each factor, with each factor having its own axis. The y-axis shows the mean response variable, which is the average output value. Each point on the plot corresponds to the mean response for a specific factor level, and the lines connecting these points indicate the direction and strength of the factor's effect on the response.

Steps for interpretation:

Identify the most influential factors: Factors with steeper lines have a stronger effect on the response. A steep slope indicates that changes in the factor level significantly impact the mean response. The graph in the plot showed that factor two has a steeper line relative to other and that demonstrated that the factor has a greatest impact on the others. **Assess the direction of the effect:** According to the plot in Figure 4.41,an upward-sloping line (from left to right) indicates a positive effect, meaning higher factor levels increase the mean response. A downward-sloping line suggests a negative effect, where increasing the factor level reduces the mean response. Based on the graph assessing the direction of the effect; for factor one, as moved from left to right the graph gets downward till level two and then got upward as moved to level three. This demonstrated that this factor has both negative and positive effect and so did for factor three. However, for factor two the graph turned downward through despite there is a slope change.

Determine the best factor levels: To optimize the response, identify the factor levels that produce the desired outcome. For maximizing the response, select the level with the highest mean response on the y-axis. For minimizing it, the level with the lowest mean response.

If aiming for a specific value, find the level closest to the target mean response was chosen. Based on the main plot analyses and its interpretation, the best level for factor one is level two, for factor two is level three, and for factor three is level two.

Analyze the effect size: The slope of the line shows the direction of the effect, while the vertical distance between the highest and lowest points on the line reflects the magnitude of the effect. A larger vertical distance indicates a stronger influence on the response. This is another way to assess the magnitude of the impact on each factor and the factor with greatest vertical distance is factor two. This analysis confirmed or aligned with the other analysis done above.

Look for flat lines: A flat or nearly horizontal line suggests that the factor has little to no impact on the mean response across the tested levels. As per the graphs in the plot both factor one and three has lower vertical distance despite they are not that flat. This indicated that the two factors effect is not that much significant to the combined property of the product.

Residual plots for S/N

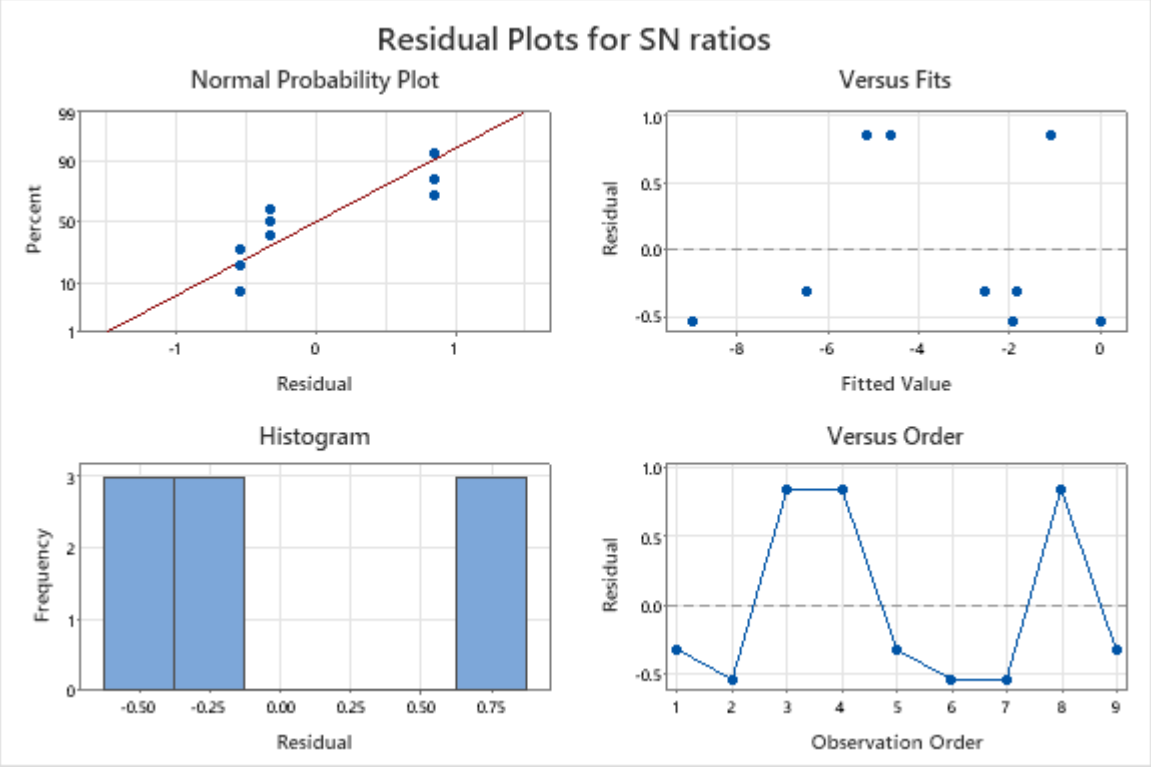

Figure 4.42 Residual plots for S/N ratio

Interpretation of Residual plots for S/N

Key assumptions of the statistical model for S/N analysis:

Normality of residuals: The residuals failed around the normal line and no outliers are observed. This validated that the model met the assumption **Constant variance:** The residuals should exhibit consistent variance across all factor levels. As observed the residual, some of them are stick together instead of scattered randomly. The plot in Figure 4.42 demonstrated that there is constant variance and the model met the assumption of constant variance. **Independence of residuals:** Residuals should not show patterns or correlations, meaning they should be independent of one another. Based on the graph of versus order plot, the residual's graph has no distinct pattern and this indicated as the residuals are independent to each other.

In conclusion, the optimization study successfully identified key factor setting for achieving desirable response in synthesis of nanoparticles. The single response optimization focused individually on the responses (crystallite size) and provided a useful information about the influencing factors and their levels. The crystallite size significantly affected by factor one and level one. The optimal crystallite size is obtained for factor one at level one, for factor two at level two, and for factor three at level one and three. The single response for mass/weight loss optimization gave the optimal value for factor one at level one, factor two at level three, and for factor at level on. Temperature was a dominant factor to influence the mass loss of thermal stability. However, these individually optimized conditions often conflicted the multi-response optimization. Specifically, the optimal conditions for the combined response (crystallite size and mass loss) were determined to be factor one at level two (Aluminum sulfate), factor two at level three(1200^{o}C), and factor three at level two(4hrs). The predicted values represent the significant improvement over the initial conditions and demonstrate the effectiveness of mulit-response optimization approach in simultaneously achieving desired outcomes. While the optimized condition at the process parameter combination of aluminum sulfate precursor material, 1200^{o}C of calcination temperature, and 4hrs calcination time showed a promising result, further validation through and confirmation experiment is done to ensure the robustness and reliability of the optimized solution in practical applications.

4.3 Confirmation experiment

The confirmation experiment is an indispensable step in Taguchi optimization methodology. Following the Taguchi method, optimization of process parameters based on Gray relational Analysis leads to the identification of a set of optimal factor levels. To validate the predicted improvements and ensure the robustness of these optimized conditions, confirmation experiment was crucial to conduct. This experiment was conducted based on the determined optimal parameter settings obtained from the multi response optimization. The confirmation experiment serves as a critical step to verify that the predicted improvement in performance is indeed realized in practice and that the chosen factor level consistently yields desirable results. For this reason, a sample was synthesized based on the optimum parameter settings obtained (Aluminum sulfate, 1200^{o}C, and 4hours) using Sol-Gel method of synthesis as shown in Figure 4.43 below.

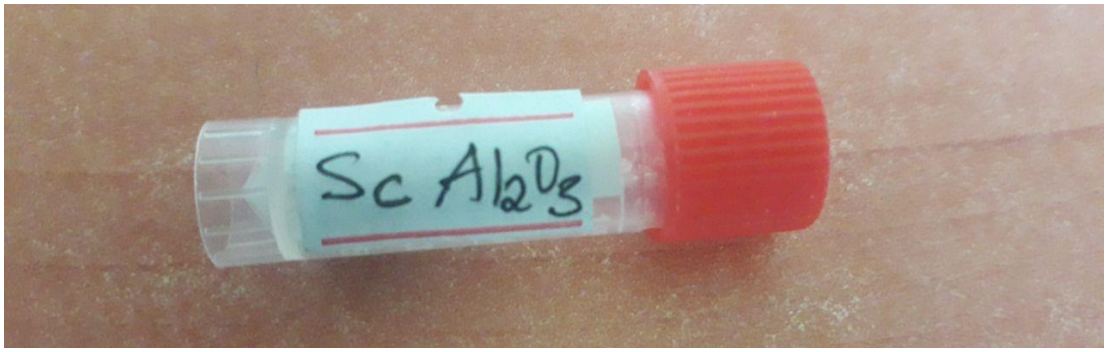

Figure 4.43 confirmation experiment sample

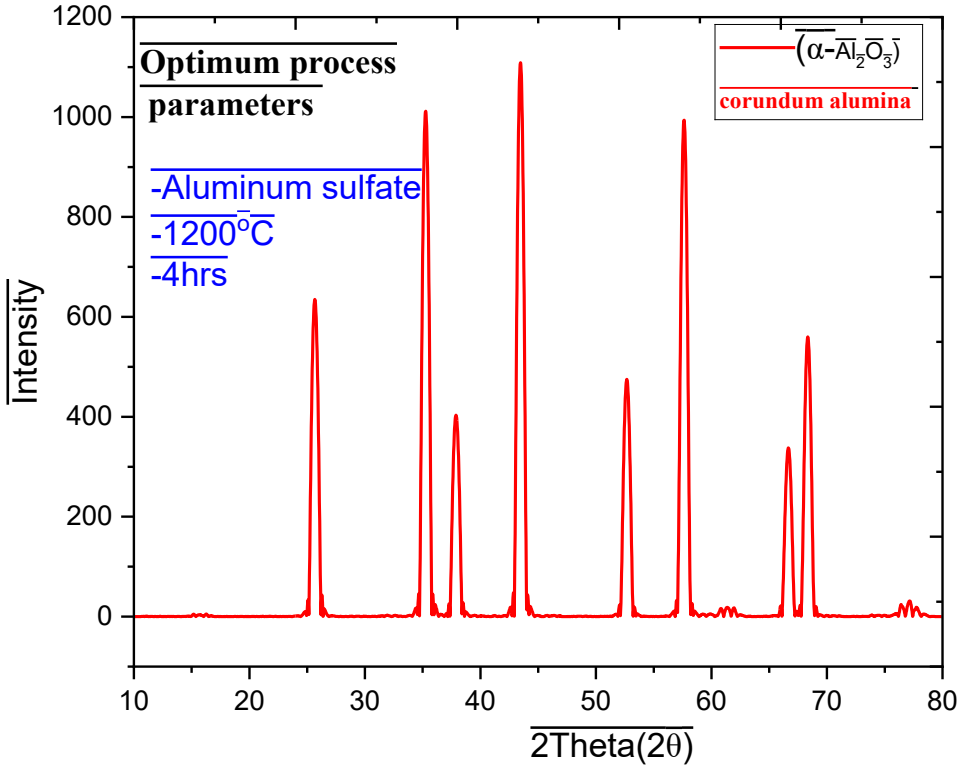

Figure 4.44 the XRD result of confirmation experiment sample.

Table 4.25 XRD result of confirmation experiment sample

S.N	2Θ	λ(nm)	FWHM (β) (rad)	Phase	$D = \frac{K\lambda}{\beta COS\Theta}$	Average Crystallite size Size (nm)
1	43.5	0.290	0.041	α	6.8	5.3
2	35.3	0.240	0.046	α	4.9	
3	57.5	0.20	0.047	α	4.3	

The optimum parameter obtained are similar with the combination of sample six except the calcination time. However, from both single and multi-response optimization the calcination time has no or a little a significant influence on the response. Based on (Kaur et al., 2020) in reference to Joint Committee on Powder Diffraction Standards (JCPDS) stated the angles (2Θ) at which different peaks are formed. XRD patterns which exhibit broad peaks centered at 2Θ

of 43.5,35.3, and 57.5 alpha phase appears as it was discussed in the beginning of the XRD analysis. This deduction was proved using the confirmation experiment that the phase and the average crystallite size is almost similar (5.3nm for the confirmation sample and 5.2nm) except the intensity was observed reduced and a little difference in crystallite size as shown in table 4.25. The could be due to the little effect of the calcination time and the overall control of the synthesis process. Similarly, impurities were observed and these impurities appeared as the consequence of the efficiency of the process and impurities

CHAPTER FIVE

CONCLUSION AND RECOMMENDATION

5.1 Conclusion

Aluminum oxide (alumina) was synthesized using the familiar bottom-up method called Sol-gel method. The synthesis process was based on the application of L_9 orthogonal array design of experiment and provided the suitable combination of the three-process parameter with their three level each. The obtained alumina nanoparticle was characterized using XRD to know the crystalline size (20.6nm,6.5nm,5.8nm,8nm,6.9nm,5.2nm,26.5nm,8.6nm, and6.5nm*)* and the phase (*α, Θ, δ, and γ*) of the synthesized powder, TGA was conducted to know the mass lose in each sample (5.70%,5.40%,4.90%,6.00%, 5.50%, 5.00%, 6.53%, 5.60%,and 5.30% respectively), and SEM to investigate the morphology of the nanoparticles in each sample. The purity of the synthesized nanoparticles was observed from the EDX characterization and determined as the main constituent elements as aluminum and oxygen. Based on the results obtained from the characterization (crystallite size and mass loss), the single response and multi-response optimization was done and the optimum value obtained and the significant factor was identified. This study provided a valuable framework for understanding and controlling the complex interplay of factors influencing the performance of the alumina ceramic and shading a light the way for the future research and development efforts. The different phase of alumina obtained through different combination of the process parameters found to be helpful to synthesis for specific application. In addition, this study shades a light that it's possible to change the levels to change the specific property of the final product.

5.2 Recommendation

The synthesis process that leveraged the design of experiment and the optimized results showed a very promising results to see the optimal synthesis process and study the complex interplay of different process parameters. However, further validation and different and additional consideration is highly recommended. The factor which contributed insignificantly need not to be taken like calcination time and recommended to consider parameters like pH value, different precursor materials (organic and inorganic), stirring conditions and so on. The calcination temperature shouldn't be the transition temperature of phase transformation. The synthesis process should be highly controlled in order to reduce impurity.

Reference

Adeniyi, A. G., Mikaila, M. M., & Ighalo, J. O. (2019). *A Mini-Review on the Application of Alumina Nanoparticles for Water Treatment*. www.fuoye.edu.ng

Ahmad Dar, A., & Anuradha, N. (2018). Use of orthogonal arrays and design of experiment via Taguchi L9 method in probability of default. *Accounting*, 113–122. https://doi.org/10.5267/J.AC.2017.11.001

Albedwawi, S. H., Aljaberi, A., Haidemenopoulos, G. N., & Polychronopoulou, K. (2021). High entropy oxides-exploring a paradigm of promising catalysts : A review. *Materials & Design*, *202*, 109534. https://doi.org/10.1016/j.matdes.2021.109534

Aldbea, F. W., Vazquez, C. V., Abobaker, M. A., Alsteeni, A. Y., Saad, A., Sharma, A., Singh, P. K., Diantoro, M., May, M., Abdullah, T., Edhirej, A., Aldosari, S. M., & Kraini, M. (2025). Structural and optical properties of α aluminum oxide prepared by sol-gel method. *Current Applied Physics*, *71*, 85–90. https://doi.org/10.1016/J.CAP.2024.12.008

Attil, H., AKSAS, A., Sebais, M., & Halimi, O. (2024). Synthesis and Characterization of Alumina Powders Obtained at Various Temperatures Via Sol-Gel Method. *Metallurgical and Materials Engineering*, *30*(3), 67–79. https://doi.org/10.56801/MME1071

Bawa, S. G., Ahmed, A. S., & Okonkwo, P. C. (2017). *ALUMINA PHASE TRANSFORMATION FROM THERMAL DECOMPOSITION OF AMMONIUM ALUM SYNTHESIZED FROM KANKARA KAOLIN*. *36*(3), 822–828.

Bhattacharyya, S., & Behera, P. S. (2017). Synthesis and characterization of nano-sized α-alumina powder from kaolin by acid leaching process. *Applied Clay Science*, *146*, 286–290. https://doi.org/10.1016/j.clay.2017.06.017

Bhoi, N. K., Singh, H., & Pratap, S. (2020). Synthesis and Characterization of Alumina Nanoparticles: A Case Study. *Journal of The Institution of Engineers (India): Series C*, *101*(2), 407–413. https://doi.org/10.1007/s40032-019-00542-w

Bin Mokaizh, A. A., Al Haiqi, O., & Binti Haji Shariffuddin, J. H. (2021). Investigating the effects of calcination time on A-alumina synthesis from aluminum waste can. *Physics and Chemistry of the Earth, Parts A/B/C*, *122*, 102979. https://doi.org/10.1016/J.PCE.2021.102979

Bokov, D., Turki Jalil, A., Chupradit, S., Suksatan, W., Javed Ansari, M., Shewael, I. H., Valiev, G. H., & Kianfar, E. (2021). Nanomaterial by Sol-Gel Method: Synthesis and Application. In *Advances in Materials Science and Engineering* (Vol. 2021). Hindawi Limited. https://doi.org/10.1155/2021/5102014

Čáchová, M., Vejmelková, E., Koňáková, D., Žumár, J., Keppert, M., Reiterman, P., & Černý, R. (2016). *Application of Ceramic Powder as Supplementary Cementitious Material in Lime Plasters*. *22*(3), 440–444.

Callister, W. D., & Wiley, J. (n.d.). *Materials Science*.

Danks, A. E., Hall, S. R., & Schnepp, Z. (2016). *Materials Horizons technique for materials*

synthesis. 91–112. https://doi.org/10.1039/c5mh00260e

Dar, A. A., Ahmad Dar, A., & Anuradha, N. (2018). Use of orthogonal arrays and design of experiment via Taguchi L9 method in probability of default. *Accounting*, *4*, 113–122. https://doi.org/10.5267/j.ac.2017.11.001

de Oliveira, L. A. S., López-Ruiz, R., & Pirota, K. R. (2015). Multiferroic and heterogeneous ferromagnetic nanowires prepared by sol-gel, electrodeposition, and combined techniques. *Magnetic Nano- and Microwires: Design, Synthesis, Properties and Applications*, 105–124. https://doi.org/10.1016/B978-0-08-100164-6.00003-5

Dunn, B., & Lan, E. H. (2020). Sol-gel process. *AccessScience*. https://doi.org/10.1036/1097-8542.757455

El-Sawaf, A. K., El-Dakkony, S. R., Zayed, M. A., Eldesoky, A. M., Nassar, A. A., El Shahawy, A., & Mubarak, M. F. (2024). Green synthesis and characterization of magnetic gamma alumina nanoparticlesfor copper ions adsorption from synthetic wastewater. *Results in Engineering*, *22*, 101971. https://doi.org/10.1016/J.RINENG.2024.101971

Farahmandjou, M., Golabiyan, N., & Branch, V. P. (2016). *Synthesis and characterization of Alumina (Al 2 O 3) nanoparticles prepared by simple sol-gel method*. *5*(1), 73–77.

Fatimah, S., Ragadhita, R., Fitria, D., Husaeni, A., Bayu, A., & Nandiyanto, D. (2022). *ASEAN Journal of Science and Engineering How to Calculate Crystallite Size from X-Ray Diffraction (XRD) using Scherrer Method*. *2*(1), 65–76.

Giesche, H. (2007). *PREPARATION and APPLICATIONS of COATED POWDERS in CERAMICS and RELATED FIELDS*. *2691*. https://doi.org/10.1080/01932699808913174

Kam, O. R., Garikoe, I., Bakouan, C., & Guel, B. (2021). Low-cost synthesis of alumina nanoparticles and their usage for bisphenol-a removal from aqueous solutions. *Processes*, *9*(10). https://doi.org/10.3390/pr9101709

Kaunisto, K., Lagerbom, J., Honkanen, M., Varis, T., Lambai, A., Mohanty, G., Levänen, E., Kivikytö-Reponen, P., & Frankberg, E. (2023). Evolution of alumina phase structure in thermal plasma processing. *Ceramics International*, *49*(13), 21346–21354. https://doi.org/10.1016/J.CERAMINT.2023.03.263

Kaur, P., Khanna, A., Kaur, N., Nayar, P., & Chen, B. (2020). Synthesis and structural characterization of alumina nanoparticles. *Phase Transitions*, *93*(6), 596–605. https://doi.org/10.1080/01411594.2020.1765245

Khazaei, A., Nazari, S., Karimi, G., Ghaderi, E., Moradian, K. M., Bagherpor, Z., & Nazari, S. (2016). Synthesis and Characterization of γ-Alumina Porous Nanoparticles from Sodium Aluminate Liquor with Two Different Surfactants. In *Int. J. Nanosci. Nanotechnol* (Vol. 12, Issue 4).

Krishnaiah, & Shahabudeen. (n.d.). *APPLIED DESIGN OF EXPERIMENTS AND TAGUCHI METHODS*.

Krishnan, S. V., Palanivelu, S., Ambalam, M. M. M., Venkatesan, R., Arivalagan, M., Pearce,

J. M., & Mayandi, J. (2018). Chemical synthesis and characterization of nano alumina, nano composite of carbon-alumina and their comparative studies. *Zeitschrift Fur Physikalische Chemie*, *232*(12), 1827–1842. https://doi.org/10.1515/zpch-2017-1075

Kumar, E., Bhatnagar, A., Hogland, W., Marques, M., & Sillanpää, M. (2014). *Interaction of anionic pollutants with Al-based adsorbents in aqueous media – A review*. *241*, 8947.

Kuo, Y., Yang, T., & Huang, G. (2008). *The use of a grey-based Taguchi method for optimizing multi-response simulation problems*. *0273*(May). https://doi.org/10.1080/03052150701857645

Leng, Y., & Wiley, J. (n.d.). *MATERIALS CHARACTERIZATION Introduction to Microscopic and Spectroscopic Methods*.

Lin, H. (2012). *The use of the Taguchi method with grey relational analysis and a neural network to optimize a novel GMA welding process*. 1671–1680. https://doi.org/10.1007/s10845-010-0468-2

Liu, Q., Wu, C., Zhan, L., Liu, W., Yao, S., Wang, J., & Ma, Y. (2023). Effect of residual carbon on the phase transformation and microstructure evolution of alumina-mullite fibers prepared by sol-gel method. *Journal of the European Ceramic Society*, *43*(3), 1039–1050. https://doi.org/10.1016/J.JEURCERAMSOC.2022.10.069

Maazinejad, B., Mohammadnia, O., Ali, G. A. M., Makhlouf, A. S. H., Nadagouda, M. N., Sillanpää, M., Asiri, A. M., Agarwal, S., Gupta, V. K., & Sadegh, H. (2020). Taguchi L9 (34) orthogonal array study based on methylene blue removal by single-walled carbon nanotubes-amine: Adsorption optimization using the experimental design method, kinetics, equilibrium and thermodynamics. *Journal of Molecular Liquids*, *298*, 112001. https://doi.org/10.1016/J.MOLLIQ.2019.112001

Madfa, A. A., Al-Sanabani, F. A., Al-Qudaimi, N. H., & Al-Qudaimi Alumina, N. H. (2014).) Ceramic for Dental Applications: A Review Article. In *American Journal of Materials Research American Journal of Materials Research* (Vol. 1, Issue 1). http://www.aascit.org/journal/ajmr

Mahdi SIAHPOOSH, S., Salahi, E., & Alikhani HESSARI, F. (2016). Synthesis of γ-Alumina Nanoparticles with High-Surface-Area via Sol-Gel Method and their Performance for the Removal of Nickel from Aqueous Solution. *Bulletin de La Société Royale Des Sciences de Liège*, *85*, 912–934.

Marlina Ginting, E., & Bukit, N. (2015). SYNTHESIS AND CHARACTERIZATION OF ALUMINA PRECURSORS DERIVED FROM ALUMINUM METAL THROUGH ELECTROCHEMICAL METHOD. In *Indones. J. Chem* (Vol. 15, Issue 2).

Mejid, N., Elsiti, I., Handawi, M., & Elmunafi, S. (2023). *Optimization of machining parameters for turning process by using grey relational analysis*. 1–6.

Mgal, O., & Growth, S. B. (2017). *PA Pajaczkowska, Institute of Electronic Materials Technology, Warsaw, Poland P Reiche and D Klimm, Institute of Crystal Growth, Berlin, Germany G Majumdar, Jadavpur University, Kolkata, India*. *July 2015*, 803581. https://doi.org/10.1016/B978-0-12-803581-8.09230-4

Milani, S. S., Kakroudi, M. G., Vafa, N. P., Mokhayer, M. M., & Gharamaleki, S. H. (2020). Properties of alumina sol prepared via inorganic route. *Ceramics International*, *46*(7), 9492–9497. https://doi.org/10.1016/J.CERAMINT.2019.12.210

Mirjavadi, S. S., Alipour, M., Hamouda, A. M. S., Kord, S., Koppad, P. G., Abuzin, Y. A., & Keshavamurthy, R. (2018). Effect of hot extrusion and T6 heat treatment on microstructure and mechanical properties of Al-10Zn-3.5Mg-2.5Cu nanocomposite reinforced with graphene nanoplatelets. *Journal of Manufacturing Processes*, *36*, 264–271. https://doi.org/10.1016/j.jmapro.2018.10.026

Mota, M. F., Santos, A. M. C., Farias, R. M. C., Neves, G. A., & Menezes, R. R. (2019). Synthesis and characterization of alumina fibers using solution blow spinning. *Ceramica*, *65*(374), 190–193. https://doi.org/10.1590/0366-69132019653742618

Nampi, P. P., Ghosh, S., & Warrier, K. G. (2011). Calcination and associated structural modifications in boehmite and their influence on high temperature densification of alumina. *Ceramics International*, *37*(8), 3329–3334. https://doi.org/10.1016/J.CERAMINT.2011.04.129

Narayanan, M. V., & Rakesh, S. G. (2018). Synthesis of colloidal alumina nanoparticles using green method. *IOP Conference Series: Materials Science and Engineering*, *402*(1). https://doi.org/10.1088/1757-899X/402/1/012150

Niero, D. F., Montedo, O. R. K., & Bernardin, A. M. (2022). Synthesis and characterization of nano α-alumina by an inorganic sol–gel method. *Materials Science and Engineering: B*, *280*, 115690. https://doi.org/10.1016/J.MSEB.2022.115690

Nikiforov, S. V, Ananchenko, D. V, Ramazanova, G. R., Shtang, T. V, Ishchenko, A. V, & Yakovlev, G. A. (2023). *The effect of annealing temperature on the change in the structure , luminescent and dosimetric properties of ultrafine α -Al 2 O 3 ceramics*. *166*(April), 106981.

Northwest, P., Molecular, E., & Northwest, P. (n.d.). *Version of Record: https://www.sciencedirect.com/science/article/pii/S0021951720304152*.

Okada, K., Nagashima, T., Kameshima, Y., & Yasumori, A. (2003). Effect of crystallite size of boehmite on sinterability of alumina ceramics. *Ceramics International*, *29*(5), 533–537. https://doi.org/10.1016/S0272-8842(02)00198-0

Panda, A., Sahoo, A. K., & Rout, A. K. (2016). *Multi-attribute decision making parametric optimization and modeling in hard turning using ceramic insert through grey relational analysis : A case study*. *5*, 581–592. https://doi.org/10.5267/j.dsl.2016.3.001

Pourmadadi, M., Farokh, A., Rahmani, E., Shamsabadipour, A., Eshaghi, M. M., Rahdar, A., & Ferreira, L. F. R. (2022). Porous alumina as potential nanostructures for drug delivery applications, synthesis and characteristics. *Journal of Drug Delivery Science and Technology*, *77*, 103877. https://doi.org/10.1016/J.JDDST.2022.103877

Process, S. (n.d.). *An Integrated Approach of GRA Coupled with Principal Component Analysis for Multi-Optimization of Shielded Metal Arc Welding*.

Rabia, A. R., Ibrahim, A. H., & Zulkepli, N. N. (2018). Activated alumina preparation and

characterization: The review on recent advancement. *E3S Web of Conferences*, *34*. https://doi.org/10.1051/e3sconf/20183402049

Rogojan, R., Andronescu, E., Ghiţulică, C., Vasile, B. Ş., & Ştefan Vasile, B. (2011). SYNTHESIS AND CHARACTERIZATION OF ALUMINA NANO-POWDER OBTAINED BY SOL-GEL METHOD. *Bull., Series B*, *73*(2).

Romero Toledo, R., Ruíz Santoyo, V., Moncada Sánchez, D., Martínez Rosales, M., Romero Toledo, R., Ruíz Santoyo, V., Moncada Sánchez, D., & Martínez Rosales, M. (2018). Effect of aluminum precursor on physicochemical properties of Al2O3 by hydrolysis/precipitation method. *Nova Scientia*, *10*(20), 83–99. https://doi.org/10.21640/NS.V10I20.1217

Sadabadi, H., Aftabtalab, A., Zafarian, S., Shaker, S., Ahmadipour, M., & Rao, K. V. (2013). High purity Alpha Alumina nanoparticle: Synthesis and characterization. *Article in International Journal of Scientific and Engineering Research*, *4*(4). http://www.ijser.org

Saeheaw, T. (2022). Heliyon Application of integrated CRITIC and GRA-based Taguchi method for multiple quality characteristics optimization in laser-welded blanks. *Heliyon*, *8*(October), e11349. https://doi.org/10.1016/j.heliyon.2022.e11349

Series, C. (2024). *The sintering temperature effect of Alumina The sintering temperature effect of Alumina (Al 2 O 3) ceramic using the sol-gel method*. https://doi.org/10.1088/1742-6596/2900/1/012044

Shahraki, A., Malek Khachatourian, A., Rezaei, B., & Nemati, A. (2025). Influence of calcination temperatures on the structural, microstructural, and thermal characteristics of electrospun alumina nanofibers. *Ceramics International*. https://doi.org/10.1016/J.CERAMINT.2025.01.275

Sigmund, W. M., & Bell, N. S. (2000). *Novel Powder-Processing Methods for Advanced Ceramics*. *74*, 1557–1574.

Singh, A. K., & Sarkar, R. (2015). Synthesis and Characterization of Alumina Sol and Its Use as Binder in No Cement High-Alumina Refractory Castables. *International Journal of Applied Ceramic Technology*, *12*, E54–E60. https://doi.org/10.1111/ijac.12368

Souza, F. De, & Braganc, S. R. (2017). *Extraction and characterization of humic acid from coal for the application as dispersant of ceramic powders*. *7*(3), 254–260. https://doi.org/10.1016/j.jmrt.2017.08.008

Spear. (n.d.). *Synthesis of alumina nanoparticles by sol-gel method and their applications in the removal of copper ions (Cu 2+) from the solution*. https://doi.org/10.1088/1757-899X/701/1/012034

Su, J., Liu, Y., Peng, X., Sun, G., & Jiang, X. (2023). Preparation of α-Al2O3 by low-temperature calcining γ-Al2O3 with α-phase seed in-situ obtained by ball milling. *Materials Today Communications*, *36*, 106681. https://doi.org/10.1016/J.MTCOMM.2023.106681

Vignesh Raj, S., Rajkumar, M., Meenakshi Sundaram, N., & Kandaswamy, A. (2018). Synthesis and characterization of hydroxyapatite/alumina ceramic nanocomposites for

biomedical applications. *Bulletin of Materials Science*, *41*(4). https://doi.org/10.1007/s12034-018-1612-4

Vural, S., & Sari, Ö. (2019). Synthesis and characterization of SDS assistant α-alumina structures and investigation of the effect of the calcination time on the morphology. *Colloid and Polymer Science*, *297*(1), 107–114. https://doi.org/10.1007/s00396-018-4442-4

Wang, C. C., & Lin, T. (2007). *Optimizing the rapid prototyping process by integrating the Taguchi method with the Gray relational analysis*. *5*(March), 304–315. https://doi.org/10.1108/13552540710824814

Yang, Y., Wang, N., Pang, X., Yasinskiy, A., Tan, Y., Yu, J., Wang, Z., & Shi, Z. (2021). Thermodynamics of the decomposition of aluminum chloride hexahydrate to prepare alumina. *Journal of Materials Research and Technology*, *15*, 6640–6646. https://doi.org/10.1016/j.jmrt.2021.11.099

Yao, Z., Peng, Y., Xia, C., Yi, X., Mao, S., & Zhang, M. (2020). The effect of calcination temperature on microstructure and properties of FeNiMo@Al2O3 soft magnetic composites prepared by sol-gel method. *Journal of Alloys and Compounds*, *827*, 154345. https://doi.org/10.1016/J.JALLCOM.2020.154345

Yaqoob, S., Ghani, J. A., Jouini, N., Juri, A. Z., Hassan, C., & Haron, C. (2024). *Multi-objective optimization using Grey Relational Analysis (GRA) for the high-speed orthogonal turning of heat-treated alloy steel*. *43*(July), 1–16.

Young, S. K. (2002). Overview of Sol-Gel Science and Technology. *Army Research Laboratory*.